## Title

NUCLEAR ORIENTATION STUDIES ON SOME HIGH SPIN ISOMERS IN FERROMAGNETIC AND NON-FERROMAGNETIC LATTICES



## Author

Bacon, Frederick.

## Publication Date

1972-09-01

LBL-1271

# NUCLEAR ORIENTATION STUDIES ON SOME HIGH SPIN ISOMERS IN FERROMAGNETIC AND NON-FERROMAGNETIC LATTICES

Fredrick Bacon
(Ph. D. Thesis)

September 1972

Prepared for the U.S. Atomic Energy Commission under Contract W-7405-ENG-48




LBL-1271

## DISCLAIMER

NUCLEAR ORIENTATION STUDIES ON SOME HIGH SPIN ISOMERS IN FERROMAGNETIC AND NON-FERROMAGNETIC LATTICES

Contents

LIST OF FIGURES

# NUCLEAR ORIENTATION STUDIES ON SOME HIGH SPIN ISOMERS IN FERROMAGNETIC AND NON-FERROMAGNETIC LATTICES

Fredrick Bacon

Department of Chemistry and
Lawrence Berkeley Laboratory
University of California
Berkeley, California 94720

September 1972

## ABSTRACT

The methods of nuclear orientation and magnetic resonance on oriented nuclei have been applied to study the magnetic hyperfine interactions of some spin isomers in the $g_{9/2}$, $h_{11/2}$, and $i_{13/2}$ shell closure regions. It is demonstrated that from a nuclear orientation experiment alone only the magnetic hyperfine interaction constant can be determined unambiguously and that from the combined data of an orientation experiment and a magnetic resonance experiment on oriented nuclei the spin of the parent level can be determined. The nuclear magnetic dipole moments of the $12^-$ levels of $^{196}$Au, $^{198}$Au, and $^{200}$Au were determined. From a magnetic resonance experiment on the oriented ground states of $^{196}$Au and $^{198}$Au the induced hyperfine fields in nickel for these nuclei were determined. The hyperfine anomalies between $^{196,198}$Au and $^{197}$Au were derived. A comparison of these derived anomalies and the one measured by the spin echo method is made and from this comparison a discussion of the non-contact contribution to the induced nickel field is presented. The spins, nuclear magnetic dipole moments and magnetic resonance frequencies were determined for $^{200m}$Au, $^{195m}$Pt, and $^{93m}$Mo and E2/M1 mixing ratio for the 99 keV gamma of $^{195m}$Pt

was measured. A brute force polarization of $^{93m}$Mo in niobium was demonstrated and the possibility of obtaining the single level hyperfine anomaly from a combined brute force and ferromagnetic polarization experiment is discussed. The magnetic hyperfine interaction constants for $^{101m}$Rh in nickel and iron were determined and the magnetic resonance frequency for this isotope in nickel was observed.

## INTRODUCTION

A nuclear ordering, be it ever so small, will result whenever the spins of a nuclear system are oriented with respect to some space-fixed axis. For radioactive nuclei, since there exist a directional correlation between the nuclear spin axis and the axis of the emitted gamma radiation, anisotropic phenomena will accompany the nuclear ordering. Thus, nuclear orientation, as this ordering is commonly called, was historically developed as a tool for studying nuclear properties, e.g. the spin, and logically so, since it is one of the more elegant applications of angular momentum theory.

Because the nuclear substate splittings are energetically very small ($\sim 10^{-18}$ eV or $\sim 0.01$ K) and sizable population differences are required, many of the static methods for achieving nuclear orientation, including those of interest here, are low temperature methods. Of the proposed methods, however, the ones which gained immediate success were those not requiring large magnetic fields. These include the two magnetic hyperfine structure interaction methods. The first was suggested by Gorter[1] and independently by Rose.[2] The second is due to Bleaney.[3] Also included is the electric hfs method of Pound.[4] All these methods, though, were applied to ionic crystalline lattices. It was not until later that a fourth hfs method for achieving nuclear orientation in ferromagnetic lattices--based on a large nuclear Zeeman type interaction--was successful. Making use of the induced hyperfine field at gold atoms in iron, Samoilov, Sklyarevskii, and Stepanov[5] demonstrated this modification of the direct method.[6] In what followed, many isotopes were oriented in ferromagnetic lattices,[7] and nuclear orientation became the sole tool for measuring induced hyperfine fields of solute impurities at very low temperatures.

In 1966, Matthias and Holliday,[8] following the suggestion of Bloembergen and Temmer,[9] were able to carry out a nuclear magnetic resonance experiment on thermally oriented $^{60}$Co in iron. Shortly thereafter, magnetic resonances on several isotopes oriented in iron or nickel were done with increased emphasis on measurements of nuclear spin-lattice relaxation times. The solid state physics shift of nuclear orientation continued through the work of Brewer, Shirley, and Templeton[10] who first observed the low temperature independence of nuclear spin-lattice relaxation times for $^{60}$Co(Fe). A recent publication by Bacon, Barclay, Brewer, Shirley, and Templeton[11] has given theoretical details explains the experimentally observed low temperature independence of nuclear relaxation times.

The present thesis undertakes an experimental investigation of the nuclear magnetic moments and magnetic hyperfine interactions of several high spin levels of isotopes embedded in ferromagnetic and non-ferromagnetic lattices via the method of nuclear magnetic resonance on oriented nuclei, hereafter abbreviated NMR/ON. From the combination of the two techniques, one gets the advantages of both methods. A nuclear orientation (ON) experiment on radioactive nuclei requires only trace amounts ($\sim 10^{10}$) of the solute nuclei because essentially one decay at a time is observed. In this method, for interactions of interest here, the absolute value of the hyperfine interaction constant is obtained as a product of the magnetic moment, $\mu$, and the magnetic field, H, $|\mu H|$ only. It should be born in mind that this is the only unambiguous datum obtained in a nuclear orientation experiment because the other angular momentum coefficients on which the anisotropy depends are often too insensitive to allow, say, spin

determinations. The accuracy of NMR is carried over into the combined technique since one still measures a resonant frequency but with a different response function. Furthermore, the resonance technique allows a determination of the magnetic hyperfine splitting; i.e., $|\mu H/Ih|$ or $|\gamma H|$ where $\gamma$ is the gyromagnetic ratio and I the total spin angular momentum. It is therefore clear that from two separate experiments--an orientation experiment yielding $|\mu H|$ and a resonance experiment yielding $|\mu H/Ih|$--a value of the spin for the parent state can be determined from the ratio

$$|\mu H|_{ON} \Big/ |\gamma H|_{NMR} = Ih$$

where h is Planck's constant.

Many practical advancements, including the NMR/ON technique, have aided materially the accuracy of orientation measurements and have permitted wider use of this field. The experimental and technological advances would include the extensive compilations of induced hyperfine fields at solute nuclei,[12] the use of cerium magnesium nitrate (CMN) as a major cooling salt (thus allowing lower temperatures to be reached), the use of gamma ray thermometry, the development of high field superconducting magnets, and improved dewar and cryostat designs. Accordingly, the magnetic moment of a nuclear state can now be determined with an accuracy of the order of one percent. In addition, for those cases where the magnetic moment is known, the NMR/ON technique provides an accurate tool for studying the hyperfine anomaly in ferromagnetic lattices. Also, the study of single level hyperfine anomalies is afforded by the direct interaction of the nuclear moment with a uniform external magnetic field.

The relevant theoretical aspects of spin isomers, nuclear moments and the NMR/ON technique are presented in Chapters 1 and 2 followed by a chapter on gamma ray thermometry. Chapters 4, 5, and 7 treat the experimental aspects with discussions of the gold isotopes $^{196m}$Au, $^{198m}$Au, $^{200m}$Au, the ground states of $^{196}$Au and $^{198}$Au followed by discussions of the 13/2 state of $^{195}$Pt and $^{101m}$Rh. Chapter 6 is devoted to the brute force and ferromagnetic polarizations of $^{93m}$Mo.

# THEORY

## I. High Spin Isomers

There is no formal theory, per se, of high spin isomers, and, in actuality, the name is more generic and serves to distinguish spin isomerism from other types of nuclear isomerism, for example, that due to K forbiddenness. Their existence can be explained, however, within the framework of the shell model of the nucleus and, for the isotopes here investigated--all with nucleon configurations close to major shell closures--the states should be adequately described by this model. In high spin cases, the long lifetime is due mainly to the large multipolarity of the transition to a lower energy state; the shell-model gamma transition rates, though, are frequently incorrect.[13]

The single particle model of the nucleus is well established as a major theory for correlating and predicting nuclear phenomena and the interested reader is referred to the literature for greater details.[13-15] Only those points of immediate concern will be mentioned here.

The shell model, implying an isotropic nuclear potential, as originally conceived assumed either a square well or harmonic oscillator potential in which the nucleons moved independently of one another. Here, assuming the harmonic oscillator potential, the eigenvalues E of the Schrödinger equation are

$$E = \hbar\omega\ (3/2 + N)$$

where $\omega$ is similar to the classical oscillator frequency and N, the principal quantum number, is given by

$$N = 2n - 2 + \ell \quad .$$

The orbital angular momentum quantum number $\ell$ can have values from zero up to the maximum allowed by the eigenvalue equation and n is equal to the number of nodes, including the one at zero, in the radial wave function minus $\ell$. Corresponding to any given eigenvalue E, there are a number of degenerate eigenfunctions classified by their $\ell$ values; i.e.,

for N even $\quad \ell = 0, 2, 4. \ . \ . N$

for N odd $\quad \ell = 1, 3, 5. \ . \ . N$

Thus, the sequence of single particle levels for the harmonic oscillator will consist of bands of degenerate levels which can be labeled by their quantum numbers $(n,\ell)$:

1s; 1p; 2s, 1d; 2p, 1f; . . . 3p, 2f, 1h. . . .

The usual atomic spectroscopic notation has been used.

The total degeneracy of each energy state for each type of nucleon is $(N + 1)(N + 2)$, and the magic numbers (corresponding to shell closures) 2, 8, 20, 28, 50, 82, and 126 are reproduced by considering an attractive spin-orbit type interaction

$$U(r)\cdot(\vec{S}\cdot\vec{\ell}) \quad .$$

The $\vec{S}$ is the intrinsic particle spin operator and $U(r)$ is a function of radial distance. This type of force removes the spin degeneracy in each single particle level and gives rise to a total angular momentum quantum number

$$I^{*} = \ell \pm 1/2 \quad .$$

Evaluating the scalar product $(\vec{s}\cdot\vec{\ell})$ as usual,[13] it can be seen that the spin-orbit force leads to a depression of the $j = \ell + 1/2$ component of an $\ell$-orbit by

$$-1/2\ \ell\ \xi_{n\ell} \quad ,$$

and an elevation of the $j = \ell - 1/2$ component by

$$1/2\ (\ell + 1)\ \xi_{n\ell} \quad .$$

The total splitting for the two components is

$$1/2\ (2\ell + 1)\ \xi_{n\ell}$$

where $\xi_{n\ell}$ is the strength of the spin orbit force.

Spin-orbit coupling plays a similar role in electronic energy states but for the nuclear case it is stronger and of the opposite sign; i.e., states with $\ell + 1/2$ are more tightly bound than states with $\ell - 1/2$. The coupling is largest for high angular momentum values and, therefore, it tends to depress certain high spin levels from one shell to a lower shell, changing the harmonic oscillator occupation numbers. For example, the $1g_{9/2}$ level of the fourth oscillator shell is depressed close to the

---

*Here, upper case I (or J) will be used to represent the total spin angular momentum of all of the one or more nucleons; lower case j will represent the orbit of a single nucleon, or correspondingly its total angular momentum.

preceding oscillator shell group and a large energy gap is produced after occupation number 50. A similar state of affairs exists for the $5h_{11/2}$ level (shell closure at 82) and the $6i_{13/2}$ level (closure at 126). Indicating shell closure by brackets, [ ], and labeling levels by their (nlj) quantum numbers, the spectrum can be rewritten

$$[\ldots 2p_{1/2}\ 1g_{9/2}][1g_{9/2}\ 2d_{5/2}\ldots 3s_{1/2}\ 1h_{11/2}][5h_{9/2}\ldots 3p_{3/2}\ 3p_{1/2}\ 1i_{13/2}]\ldots$$

This notation, however, does not imply the level ordering within each shell, which must be experimentally determined.

The fundamental assumption of this model is that the nucleons in any odd nucleus can be regarded as filling the single particle levels in such a way that all of them except the last (top-most) odd nucleon pair off to form an "inert" core. This core contributes neither to the angular momentum of the nucleus nor to its nuclear magnetic or quadrupole moments. For odd-odd nuclei, a similar statement can be made. Here, each nucleon fills its own proton or neutron shell and, assuming the particles do not interact, a group of degenerate states is formed with all spins from $|I - I'|$ to $|I + I'|$. It further assumes, to agree with observed spins, that there are large pairing energies for large $\ell$ values so that large total angular momentum, e.g. 11/2, do not appear in nuclear ground states.

An important feature of the single particle model level sequence, with regard to spin isomerism, is the large depression of the $j = \ell + 1/2$ member for the orbits of high $\ell$-value. These are depressed into the low spin levels of the major shell of opposite parity and become a part of that shell. The big spin changes between adjacent levels provide a

necessary condition for the occurrence of isomeric states which can decay only by the emission of radiation of high multipole order.

## II. Single Particle Model of Nuclear Magnetic Moments

### A. Odd Mass Nuclei

The nuclear magnetic moment provides a sensitive test of the nuclear coupling scheme because of the great difference between the g factors associated with the various components--orbital and spin angular moments of the nucleon--of the total nuclear angular momentum.

For a proton moving within the nucleus there will be two contributions to its magnetic moment:

1) one from currents generated by its motion--the orbital contribution $g_\ell$

2) one from its intrinsic spin--the spin contribution $g_s$.

The neutron, being without a charge, has only the intrinsic spin component. Therefore, the magnetic moment operator for a single nucleon can be written in terms of the orbital and spin g factors as

$$\vec{\mu} = g_\ell \vec{\ell} + g_s \vec{S}$$

where

$$g_\ell = \begin{cases} 1 \\ 0 \end{cases} \qquad g_s = \begin{cases} 5.58 \text{ proton} \\ -3.82 \text{ neutron} \end{cases}$$

in Bohr magneton units, eh/2Mc. The $\vec{\ell}$ and $\vec{S}$ are the orbital angular momentum and spin angular momentum operators. In the nuclear case, the total angular momentum $j = \ell \pm 1/2$ is a good quantum number and the magnetic moment is

defined as the expectation value of the z component of $\mu_{op}$ taken in the nuclear substate with the z component, m, of j equal to j

$$\mu = \langle j,m = j|\mu_z|j,m = j \rangle \quad .$$

Using the normal identities between $j = \ell + S$, the expectation value of $\mu$ may be evaluated as

$$\mu = (j - 1/2)g_\ell + 1/2\ g_s \qquad \text{for } j = \ell + 1/2$$

and

$$\mu = \frac{j}{j + 1}\left[(j + 3/2)g_\ell - 1/2\ g_s\right] \text{ for } j = \ell - 1/2 \quad .$$

The above equations may be combined resulting in Eq. (1)

$$\mu_{sp} = j\left\{g_\ell \pm (g_s - g_\ell)\frac{1}{2\ell + 1}\right\} \quad \text{for } j = \ell \pm 1/2 \quad .$$

This equation gives the single particle moment $\mu_{sp}$ and is applicable to odd mass nuclei, or it can be used to calculate the moment of a single nucleon.

## B. Even Mass Nuclei

Here, consider the coupling of two particles in different orbits, e.g., a proton in orbit $(\ell,j)$ and a neutron in orbit $(\ell',j')$. Generally, in treating odd-odd nuclei, it is assumed that the effective interaction strength between the two nucleons in orbits $\ell$ and $\ell'$ is weaker than the spin-orbit force (allowing j-j coupling) and also weaker than the

interaction between nucleons in the same orbit.[13] With these assumptions, each total state wave function, representing the coupled proton and neutron, can be regarded as a simple vector-coupled product of the internal wave functions of the two particles. Assuming further that the lowest state of an odd-odd nuclear system can be written as a vector coupled product of the lowest state of the proton (referred to by $\pi$) group of spin $J = j_\pi$, moment $(g_j \vec{j})_\pi$ and that the lowest state of the neutron (referred to by $\nu$) group of spin $J = j_\nu$, moment $(g_j \vec{j})_\nu$ then the magnetic moment operator for the total system is

$$\vec{\mu} = (g_j \vec{j})_\pi + (g_j \vec{j})_\nu \quad .$$

The magnetic dipole moment of the state of the total system spin $j_\pi + j_\nu = J$ can be expressed as[13]

$$\mu = \langle J, M = J | \vec{\mu} \cdot \vec{J} | J, M = J \rangle / (J + 1) \quad .$$

This equation can be evaluated to give the single particle value of the magnetic dipole moment for two coupled nucleons 1 and 2. The results, expressed in terms of the g factor, is Eq. (2)

$$g = (g_1 + g_2)\, 1/2 + (g_1 - g_2) \left\{ \frac{j_1(j_1 + 1) - j_2(j_2 + 1)}{2J(J + 1)} \right\} \quad ,$$

where $J = j_1 + j_2$.

# THEORY OF NUCLEAR MAGNETIC RESONANCE ON ORIENTED NUCLEI

## I. A Thermally Oriented Ensemble Defined

The theory of nuclear orientation is well established and the reader is referred to a thorough article of Blin-Stoyle and Grace[16] and references therein for greater details.

An ensemble of nuclei is said to be thermally oriented if

1) the nuclear spins of the ensemble are coupled to a fixed spatial axis

2) the ensemble is in thermal equilibrium with a bath at temperature T.

For magnetic Zeeman interactions, application of a magnetic field H defines the fixed axis, or quantization axis, for the system and the Hamiltonian is

$$\vec{\mathcal{H}} = -\vec{\mu} \cdot \vec{H} \quad .$$

The 2I + 1 spin degeneracy is lifted completely and the magnetic substates, distinguished by quantum numbers m = -I...+I in unit steps, have energy

$$E = -mg_N \mu_N H \quad .$$

The probability P(m) of a given m substate being occupied for an ensemble in contact with a thermal bath is given by the Boltzmann distribution function

$$P(m) = \frac{\exp - (mg_N \mu H/kT)}{\sum_m \exp - (mg_N H/kT)} \quad .$$

As the observation of anisotropic phenomena associated with nuclear processes requires population differences $\geq 1\%$, the argument of the exponent must be of order unity. This occurs when kT is approximately equal to the hyperfine

interaction energy, i.e. $T \sim 0.01$ K. Because appreciable population differences are required and since the spin degeneracy is completely lifted ($E_{-m} \neq E_{+m}$), the following relationship holds

$$P(-m) \neq P(+m) \quad .$$

Therefore nuclear polarization results as opposed to nuclear alignment where $P(-m) = P(+m)$ holds.

## A. The Angular Distribution Function

The $\gamma$-ray angular distribution function for an ensemble of thermally oriented nuclei possessing cylindrical symmetry about the orientation axis is given by $W(\theta)$ Eq. (3)

$$W(\theta) = 1 + \sum_{k=\text{even}} Q_k \, U_k \, F_k \, B_k \, P_k \, (\cos \theta) \quad ,$$

where $\theta$ is the angle between the quantization axis and the direction of the emitted radiation. The sum is over the even terms because a parity conserving interaction, gamma radiation, is observed. The Legendre polynomial $P_k(\cos \theta)$ embodies the spatial anisotropy of the emitted gamma radiation.

The orientation parameter $B_k$[16] is proportional to the $P(m)$ mentioned earlier and is implicit in the hyperfine interaction constants. It has the general form

$$B_k = [(2I + 1)(2k + 1)]^{1/2} \sum_m (-1)^{I-m} \begin{pmatrix} I & I & k \\ m & -m & 0 \end{pmatrix} P(m)$$

The value of k is restricted to $k \leq 2I$; for $k > 2I$, $B_k = 0$. Although not apparent from its defining equation, the $B_k$'s, apart from normalization, are equal to the statistical moments of the spin distribution. For low degrees of orientation, the value of this parameter decreases with increasing k as $(E/kT)^k$.

The remaining terms in the angular distribution function, except for $Q_k$, are angular momentum coefficients and depend implicitly on the spin momenta I of the parent nuclei and daughter levels, the multipole order L of the transition, the multipolarity mixing $\delta$ and the rank k in the summation. The $F_k$ refers to the angular momenta coupling of the observed gamma transition $I_1 \xrightarrow{L} I_2$ and is given by

$$F_k = (-1)^{I_2 + I_1 - 1} [(2I_1 + 1)(2k + 1)]^{1/2}(2L + 1)\begin{pmatrix} L & L & k \\ 1 & -1 & 0 \end{pmatrix}\begin{Bmatrix} L & L & k \\ I_1 & I_1 & I_2 \end{Bmatrix}$$

for pure or unmixed transitions. According to Ferentz and Rosenzweig's tabulations,[17]

$$F_k = [F_k(L\ I_1\ I_2) + \delta^2\ F_k(L'\ I_1\ I_2) + 2\delta\ F_k(L\ L'\ I_1\ I_2)]/(1 + \delta^2) \quad ,$$

for mixed transitions of multipolarity L and L'. The restrictions on $F_k$ are $|L' - L| \leq k \leq |\min 2I_1 \text{ or } L + L'|$ where min means the smaller of the two, and $F_k = 0$ otherwise. Hence, for most observed transitions, with typical multipole order $L \leq 2$, the summation is ended after the $k = 4$ term.

The reorientation parameter $U_k$ is associated with the angular momenta (now indicated I' and L') of the transitions preceding the observed one. In terms of 6j symbols it is defined by

$$U_k = [2I_1' + 1)(2I' + 1)]^{1/2}(-1)^{I_1' + I' - L'} \begin{Bmatrix} I_1' & I_1' & k \\ I' & I' & L' \end{Bmatrix} .$$

This term is solely geometrical in nature and results from the coupling of three angular momenta in one scheme to a different coupling in another. If the observed transition is preceded by several unobserved transitions the net attenuation is the product of the $U_k$'s. For admixed transitions this coefficient is

$$U_k(LL') = [U_k(L) + \delta^2 U_k(L')]/(1 + \delta^2) .$$

Since the radiation detector subtends a finite solid angle of the radiation pattern, the observed anisotropy is further attenuated by solid angle corrections terms $Q_k$. The corrections, which result from integrating the $P_k(\cos\theta)$ term over the solid angles of the detector, are tabulated[18,19] for both solid state and Na(I) detectors.

As can be seen from their defining equations, these coefficients can be calculated exactly provided, of course, the angular momenta are known. In addition, from their implicit dependence on the hyperfine interaction constants, spins of parent and daughter levels, and mixing ratios, one can, in theory, derive a value for any one of the three. In actuality, as will be demonstrated below, only the magnetic hyperfine interaction constant can be derived from a nuclear orientation experiment. The coupling coefficients $U_k F_k$ are too insensitive to spin values, particularly so for spin sizes considered here, to allow unambiguous spin determinations.

B. Polarization Via Magnetic Zeeman Interaction

Two methods were used for obtaining nuclear polarization in the present work. Formally, these methods are identical and both can be described by the Hamiltonian

$$\mathcal{H} = - \vec{\mu} \cdot \vec{H}_{eff} \quad .$$

In one case, called the brute force method, the nuclear moments couple directly to an externally applied magnetic field. For this method, $H_{eff}$ is

$$H_{eff} = H_o \quad .$$

Clearly, large laboratory fields ($\sim 10^5$ Oe) are required and the lattices of the oriented nuclei must be non-ferromagnetic. At the present technological state, favorable nuclei for brute force polarization should have

1) large nuclear moments $\gtrsim 5$ nm

and/or

2) large gamma ray anisotropies.

In theory, however, this appears to be the most important method for orienting nuclei since it depends only on a finite nuclear moment without additional lattice requirements.

In the second method, the polarization is achieved via the interaction of the nuclear magnetic moment with the induced hyperfine field of a ferromagnet. One then need only apply an external field ($\sim$ one KOe) to align the electronic spins responsible for the induced field. The field of a solute nucleus in a ferromagnet will be proportional to an algebraic sum of the fields of the lattice and can be written

$$H_{eff} = H_{hf}^{o} + H_L + H_o - DM \quad .$$

The $H_o$ is the externally applied dc field and -DM is the demagnetizing factor times the magnetization. The magnetizing field inside the sample, however, is not $H_o$ but $H_o$ - DM, and it is important to minimize the effects of the demagnetizing field since it can be of order $H_o$.[20] The demagnetizing term can be made very small by using thin foils and by applying the dc field parallel to the plane of the foil where the demagnetizing factor is smaller. The local nucleus-electron interaction gives rise to the hyperfine field $H_{hf}^{o}$, and $H_L$ is the Lorentz field plus fields arising from dipoles in the Lorentz cavity. The sum of these two terms is experimentally invariant for a given case and the effective hyperfine field is

$$H_{hf}^{eff} = H_{hf}^{o} + H_L \quad .$$

This term is responsible for orienting solute nuclei and it is the generally reported hyperfine field.

## II. Nuclear Magnetic Resonance on Oriented Nuclei

The theory of magnetic resonance on oriented nuclei is fully described in the literature.[21-22] Accordingly, only a descriptive and requisite treatment will be given here.

There are three conditions, discussed by Abragam and Pound,[23] necessary for a successful resonance experiment on oriented nuclei; namely, a) the magnetic substate splitting must be large compared with the natural linewidth, b) the amplitude of the rf field must be sufficiently large to

induce transitions in each nucleus in times of order the effective nuclear lifetime and c) other time-dependent interactions should be minimal so that the nuclear spin-correlation time is of the order of or exceeds the nuclear lifetime. For nuclear orientation, where resonance is observed on the parent level ($t_{1/2} \sim$ hours), condition a) is satisfied. Condition b) can be met through use of the ferromagnetic enhancement of the rf field. This condition will be discussed more fully below. With regard to c), other time dependent interactions affecting nuclear orientation have been studied in some detail (see Ref. 7). The major one of concern would be the transient non-equilibrium electronic configuration of the daughter nucleus following beta decay. Very large time dependent fields can exist during this time which can, in fact, partly destroy the orientation. In ferromagnets, though, this effect is negligible since the exchange field keeps the Hamiltonian diagonal and the conduction electrons of the lattice act as reducing agents. Condition c) then is satisfied in the present cases.

Magnetic resonance on the oriented ensemble can be described as usual.[24] Consider a nucleus of the ensemble with magnetic moment $\mu$ in the state $|m\rangle$. In a magnetic field $H_o$ defining the quantization axis, the moment will precess about $H_o$ according to the torque equation

$$\frac{d\vec{\mu}}{dt} = \gamma\vec{\mu} \times \vec{H}_o \quad ,$$

with the Larmor frequency $\nu_L = \gamma H_o$. Resonance at a frequency $\nu$ is achieved by applying an oscillatory field $H(t) = 2H_1 \cos 2\pi\nu t$ perpendicular to the $H_o$ axis. Transforming into a frame rotating about $H_o$ with frequency $\nu_L$

the magnetic moment no longer precesses about $H_o$. The oscillatory field can be resolved into its left and right circularly polarized components and only one--the one with the correct sense--will survive the transformation. This component is perpendicular to $H_o$ and is time independent. The resonance process can be understood as a precession about this $H_1$ field

$$\frac{d\vec{\mu}}{dt} = \gamma\vec{\mu} \times H_1 \quad ,$$

where, now, $\nu_1 = \gamma H_1$. Resonance occurs when the precessional angle about $H_1$ is $\sim \pi/2$ radians. The orientation of the moment in the laboratory frame is now given by a different quantum number $|m'\rangle$. Thus the orientation of the ensemble is destroyed (though not completely) upon resonance--a process often called resonant destruction of the anisotropy.[21] Physically, this is observed through a change in the counting rate in a given direction; i.e., one monitors the count rate as a function of the applied rf frequency.

The resonance process is identical to conventional NMR; however, there are some salient differences. Firstly, only trace amounts of the solute nuclei ($\sim 10^{10}$) are required. Secondly, tensors of rank greater than one are observed; in the present work, for example, second and fourth rank tensors are of interest. Also, a response function different from the magnetic susceptibility is required for oriented nuclei. This may be written

$$B_k(2\pi\nu, t = \infty) = G_k(2\pi\nu, t = \infty)\, B_k(0) \quad .$$

The rf perturbation is contained in the $G_k(2\pi\nu,t)$ function analogous to the one given by Frauenfelder and Steffen.[25] Here, $B_k(0)$ is the unperturbed

equilibrium value of $B_k$. The perturbation factors are discussed at length in Ref. 26. A simple description of the effect of the perturbation on the distribution function $W(\theta)$ can be given under certain conditions. At resonance in the Larmor frame the distribution precesses about $H_1$ in the yz plane around the x axis. At saturation, detectors in this frame would register a time-integrated intensity proportional to $[P_k(\cos \pi/2)]^2$ in the yz plane. In the laboratory frame at resonance for $\theta = 0$, however, the laboratory and Larmor frames coincide and the time average of the $G_k$ can be shown to be $[P_k(\cos \pi/2)]^2$ also for observations along the z axis. That is, the distribution function is $W(\theta) = \sum_k Q_k U_k F_k [P_k(\cos \pi/2)]^2$ in the laboratory frame. There thus exist non-zero hard core values for the even rank tensors at resonance and complete resonant destruction of the anisotropy is impossible. This holds, however, only in the limit of infinite correlation times and at saturation.

To date, all of the reported resonances were observed in ferromagnetic lattices with linewidths of order magacycles, far exceeding the expected natural linewidths. The widths have been attributed to inhomogeneous broadening[27] whereby the rf power is absorbed only by those nuclei whose surrounding fields satisfy the resonance condition. Generally, in this case spin-spin interactions times ($T_2$) will be comparable to spin-lattice interactions times ($T_1$) and one can explain the observed linewidths as a superposition of several spin packets of width $1/T_2$. Because the local field distribution is random, the resulting line shape will be gaussian. Inhomogeneous broadening can be due to several factors: hyperfine interactions, dipolar interactions between unlike spins, inhomogeneities in the applied field, lattice strains, vacancies and dislocations.

Because of the inhomogeneously broadened lines, one must frequency modulate the applied rf field to observe resonance on oriented nuclei in ferromagnetic lattices. Modulation with a triangular wave is preferred since it transforms linearly in the Larmor frame. Physically, this corresponds to spending equal times at all satellite frequencies; a sinusoidal wave spends more time at crest and through frequencies. Also the frequency must be modulated over a bandwidth of many spin packets of widths $1/T_2$ ($\sim \pm 500$ KHz) to enhance the effect.

The power requirement for resonance on oriented nuclei was alluded to by condition b) above. It is required that each nucleus precess by about one radian about $H_1$ before decaying or relaxing. In nuclear orientation $t_{1/2} \sim$ hours, and nuclear decay does not compete with relaxation $T_1$. The condition for resonance can be written as

$$\gamma H_1 T_1/h \geqslant 1 \quad .$$

This relation assumes a natural linewidth $\Delta\nu \sim 1/T_2$. For inhomogeneously broadened lines of width $\Gamma$ this relation must be altered. In this case, the applied rf field $H_1^{app}$ must be larger,

$$H_1^{app} = (\Gamma/\Delta\nu)\, H_1 \quad .$$

Combining this condition with the above relation, one gets the power requirement for the observed linewidths

$$\gamma H_1^{app} = h\Gamma\, T_2/T_1 \quad ,$$

with $\Delta\nu$ set equal to $1/T_2$.

In a ferromagnet, however, an $H_1$ field of this magnitude is not necessary because of ferromagnetic enhancement. As mentioned earlier the hyperfine field at the nucleus is in part due to the electronic magnetization of the lattice. The action of the rf field on the electronic magnetization causes a transverse component, say $M_x$, on the lattice magnetization, which in turn, through contact interactions, produces a transverse magnetization at the nucleus. This is possible because nuclear frequencies are much lower than electronic frequencies. The saturation enhancement factor may be written

$$F = (1 + H_{hf}/H_o^{app}) \quad ,$$

and the $H_1^{app}$ field is increased accordingly such that

$$H_1 = F\, H_1^{app} = (1 + H_{hf}/H_o^{app})\, H_1^{app} \quad .$$

An identical enhancement applies also for the dc field provided it is much larger than the anisotropy field.

## GAMMA RAY THERMOMETRY

### I. Theoretical Considerations

The ultimate accuracy of hyperfine interaction constants measured by nuclear orientation often depends heavily on the temperature measurements. The method used in the present work is based on the anisotropic distribution of gamma rays and is commonly known as gamma-ray thermometry.[7] This method is especially good in the range below 0.1 K. There are three theoretical bases for gamma ray thermometry:

1) Given the nuclear spin Hamiltonian and its constants, the eigenstates and eigenvalues can be calculated.

2) Each $B_k$ is a single-valued function of the thermodynamic temperature T of the spin system for a specific Hamiltonian.

3) Measurement of the gamma ray distribution gives the $B_k$ parameters and hence T.

For the present work, the angular distributions of the 1172 keV and 1332 keV of $^{60}Co$ (see Fig. 1) in iron or nickel were used for temperature measurements. The Hamiltonian is again given by

$$\mathcal{H} = - \vec{\mu} \cdot \vec{H}_{eff}$$

with eigenvalues

$$E = - m \, g_N \mu_N H_{hf} \quad .$$

The relevant parameters for $^{60}Co$ in iron and nickel are given in Table 1. The hyperfine splitting $g\mu_N H_{hf}$ is also given in units of millidegrees K.

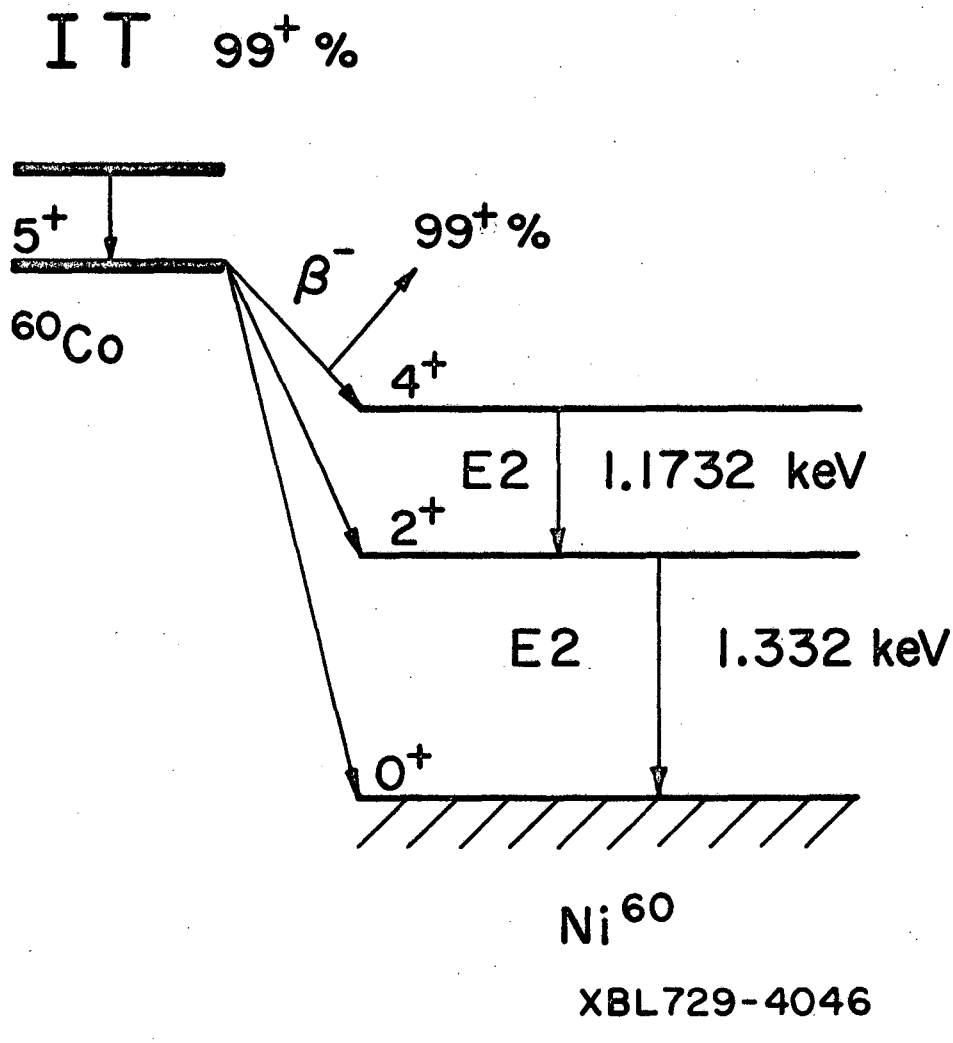


Fig. 1. Decay scheme of $^{60}Co$.

Table 1. Parameters for $^{60}Co$

$\mu = 3.754$ nm[a]

| Host | $H_{hf}$(KOe) | Hyperfine Splitting (mK) |
|---|---|---|
| Fe | -287.7[b] | 7.96 |
| Ni | -120.0[b] | 3.29 |

[a]Ref. 37.

[b]Ref. 12.

The $U_k F_k (k = 2,4)$ coefficients for $^{60}Co$ are exactly calculable:

$$U_2F_2 = -0.42056 \qquad U_4F_4 = -0.24280$$

From angular momentum considerations it can be shown that the distribution patterns of the two gamma rays are identical; therefore they have identical $U_k F_k$ coefficients.

From these known parameters together with appropriate solid angle corrections, theoretical anisotropy vs. reciprocal temperature curves for $^{60}Co$ in iron and nickel were calculated by means of one of the nuclear orientation data analyses programs (NODA3).[28] The output not only included a plot but also the calculated temperatures and anisotropies in adjustable stepwidths. Thus from the observed anisotropy, here defined as

$$A = 1 - W(0^\circ)$$

$$= 1 - (\text{number of cold counts})/(\text{number of warm counts})$$

the temperature was determined from the printout. On account of the saturation behavior of the ninety degree anisotropy, no temperature determinations were made from this set of data.

The statistical error, of course, depends on the number of counts N obtained during a counting interval. For N pulses the error is

$$\sqrt{N} = (N_B + N_o W)^{1/2} \quad ,$$

where $N_B$ is the background number of counts and $N_o$ the number of counts for the system of unoriented nuclei. W is the anistropy at a given temperature $W(\theta,T)$. The resulting error in the anisotropy is approximately

$$\Delta W(\theta,T) \cong [N_B + N_o W(\theta,T)]^{1/2} \quad ,$$

and the temperature errors used in fitting the data was

$$\Delta\, 1/T = (1/T_h + 1/T_\ell)/2 \quad ,$$

where $T_h$ and $T_\ell$ refer to the upper and lower error limits in the $^{60}Co$ anisotropy.

II. $^{60}Co$ Thermometer Preparation

The $^{60}Co$ activity was obtained as $CoCl_2$ in a solution of 1 N HCl from New England Nuclear. It was made by $^{59}Co(n,\gamma)^{60}Co$. To save time, the thermometers were made beforehand. The chemical preparation is outlined below.

a) Possible iron and nickel contaminants were removed by ion exchange with a Dowex-1 anion exchange column equilibrated at pH = 8.

b) The active solution was deposited onto a minimum mass ($\lesssim$ 50 mg) of 99.999% iron or nickel and evaporated to dryness. This process was repeated until activity was typically 50 mr @ 3 inches.

c) The $^{60}Co$ was thereafter hydrogen reduced at T $\sim$ 600 - 700°C for about three hours.

d) The active foil was then torch-melted.

Subsequent rolling and annealing produced foils of approximately 10 $cm^2$ area. To minimize the background in an orientation experiment, about 3000 cts/min @ 4-1/2 inches in the 1172 keV gamma transition was used. Therefore, only a small portion of the foil was required and typical $^{60}Co$(Fe) or (Ni) concentrations were less than 1 at. % Co.

NUCLEAR ORIENTATION STUDIES ON THE EVEN MASS GOLD ISOTOPES A = 196, 198, 200

From nuclear systematics, high spin isomers are expected to exist in many even mass gold isotopes. That is, because of the low excitation energies of the $11/2^-$ proton state in odd mass gold isotopes and the $13/2^+$ neutron states in odd mass isotopes of platinum and mercury one expects a low lying $12^-$ state from the proton-neutron coupling in the neighboring even mass gold isotopes. The expected large moment of these two particle states and the large induced hyperfine field for Au(Fe)[12] make nuclear polarization easily realized. Furthermore, the high saturation of the nuclear polarization reached allows determination of the magnetic hyperfine interaction from the temperature dependence of the gamma ray anisotropy alone without reliance on factors possibly influencing the absolute magnitude of the anisotropy. This is a significant advantage because accurate measurements of the nuclear moment can be obtained from a nuclear orientation experiment alone--a fact borne out by subsequent magnetic resonance experiments on many of the isotopes studied.

## I. Experimental

### A. Activity Production and Chemical Preparations

Since all of the gold isotopes studied had similar production and chemistry they will be treated collectively. The active isotopes were produced at the 88" Cyclotron of LBL by either one of two methods: enriched $^{196}$Pt(d,2n) reaction or enriched $^{198}$Pt($\alpha$,pn) reaction. The enriched platinum was supplied by the Oak Ridge National Lab with isotopic abundances for the $^{196}$Pt of 13.8% $^{194}$Pt, 38.2% $^{195}$Pt, 45.8% $^{196}$Pt,

2.3% $^{198}$Pt and abundances 5.8% $^{194}$Pt, 13.6 $^{195}$Pt, 36.2% $^{196}$Pt, 44.4% $^{198}$Pt for the enriched $^{198}$Pt. Irradiation of the foils with 18 MeV deuterons produced mainly $^{196m}$Au, $^{196}$Au, $^{198m}$Au, and $^{200m}$Au whereas the 35 MeV alpha irradiation produced mainly $^{198m}$Au, $^{198}$Au, and $^{200m}$Au. The gamma ray spectrum for the alpha irradiation is shown in Fig. 2 together with the $^{60}$Co gammas.

The carrier free activity was obtained by the standard HCl--ethyl-acetate solvent extraction procedure[29] outlined here. The bombarded foil was dissolved in aqua regia. Thereafter, the solution was evaporated to dryness and taken up with 6 M HCl followed by ethyl acetate extraction of the gold. After evaporating the gold rich phase to dryness, it was taken up with 1 M KCN electroplating solution. Trace amounts of gold were subsequently electroplated onto either iron or nickel foils (99.999% purity) under the following conditions: T $\sim$ 55 - 70°C, 2 to 3 volts at 3 milliamps. The elevated temperatures are quite necessary for plating on iron, whereas for nickel room temperature plating proceeded at reasonable rates--usually 50 mr @ 2" to 3" within one hour. For the nuclear orientation experiments, the Au(Fe)/(Ni) foil was torch melted with the thermometer foil under a hydrogen atmosphere at least three times to insure a homogeneous mixture. Afterward, the foil was alternately annealed and cold rolled, by means described in Ref. 30, to a typical thickness $\sim$ 0.003 inch. For the NMR/ON experiments, a similar cold rolling and annealing procedure was followed until the foil thickness was of the order of the radiofrequency skin depth,[31] which, for these cases, was estimated as from 10000 Å to 20000 Å.

Because of the many highly converted transitions, the gold activities--$^{196m}$Au, $^{198m}$Au, and $^{200m}$Au--were adjusted to minimize self heating and thereby

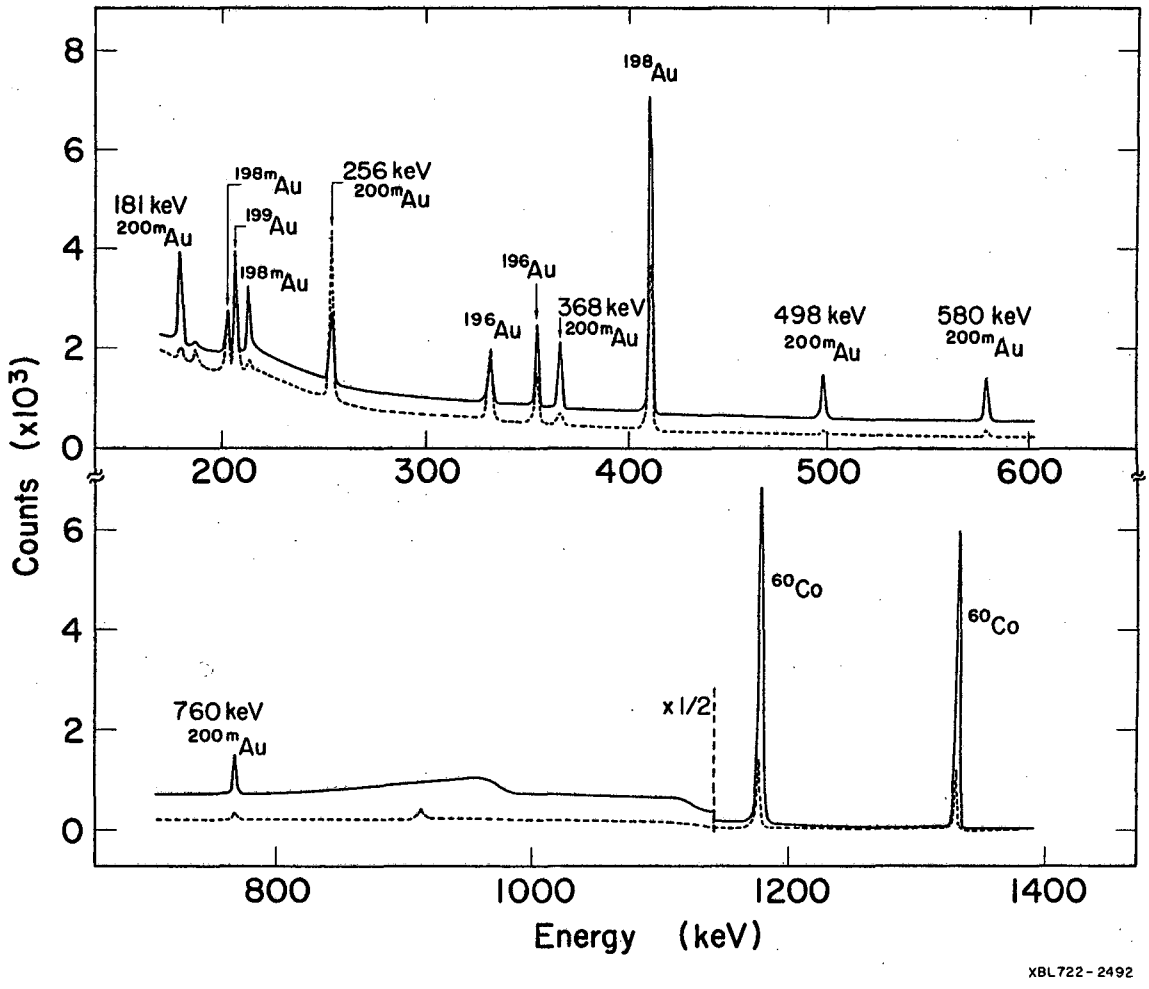


Fig. 2. The gamma ray spectrum resulting from an (α,pn) reaction on enriched $^{198}Pt$ foils. The $^{60}Co$ gamma lines are also shown. The solid curves indicate the isotropic intensities and the dashed curves indicate the anisotropic intensities at zero degree.

reach lower temperatures. The standard gamma ray activity adjustment was approximately 4000 cts./min @ 4-1/2 inches for the 412 keV gamma ray of $^{198}Au$. In addition, to facilitate handling and soldering of the very thin resonance foils, copper was vapor deposited on to one side according to the recipe: 15 mg of copper at a copper-substrate distance of 4-1/2 inches and pressure $\sim 10^{-6}$ mm. The deposited layer seldom came off.

## B. Apparatus Description

The magnetic cooling apparatus used for the gold, platinum and rhodium experiments was similar to the one described in Ref. 30 and differed only in a few respects detailed below. Figure 3 shows the apparatus. The new superconducting polarizing magnet has a coil constant of 253 gauss/ampere.

### 1. Salt Pill

The paramagnetic salts used were cerium magnesium nitrate $Ce_2Mg_3(NO_3)_{12}\cdot 24H_2O$ for the main cooling salt and chromium potassium alum $CrK(SO_4)_2\cdot 12H_2O$ (hereafter referred to as CA) as a thermal guard pill. The salt slurries were prepared in identical fashions to those of Ref. 32. The CMN container was made from 0.005 inch thick electrolytic grade copper into a 2 inch diameter by 3-1/2 inch high cylinder. Two 1/4 inch thick fibreglass discs served as the bottom and top covers. (To insure leak tight constructions, all walls and bottom fibreglass discs were epoxied with Shell Epon 828 (or 826) resin and Versamid 125 catalyst.) Approximately 16 copper fins submerged into the CMN and tapered to a silver soldered

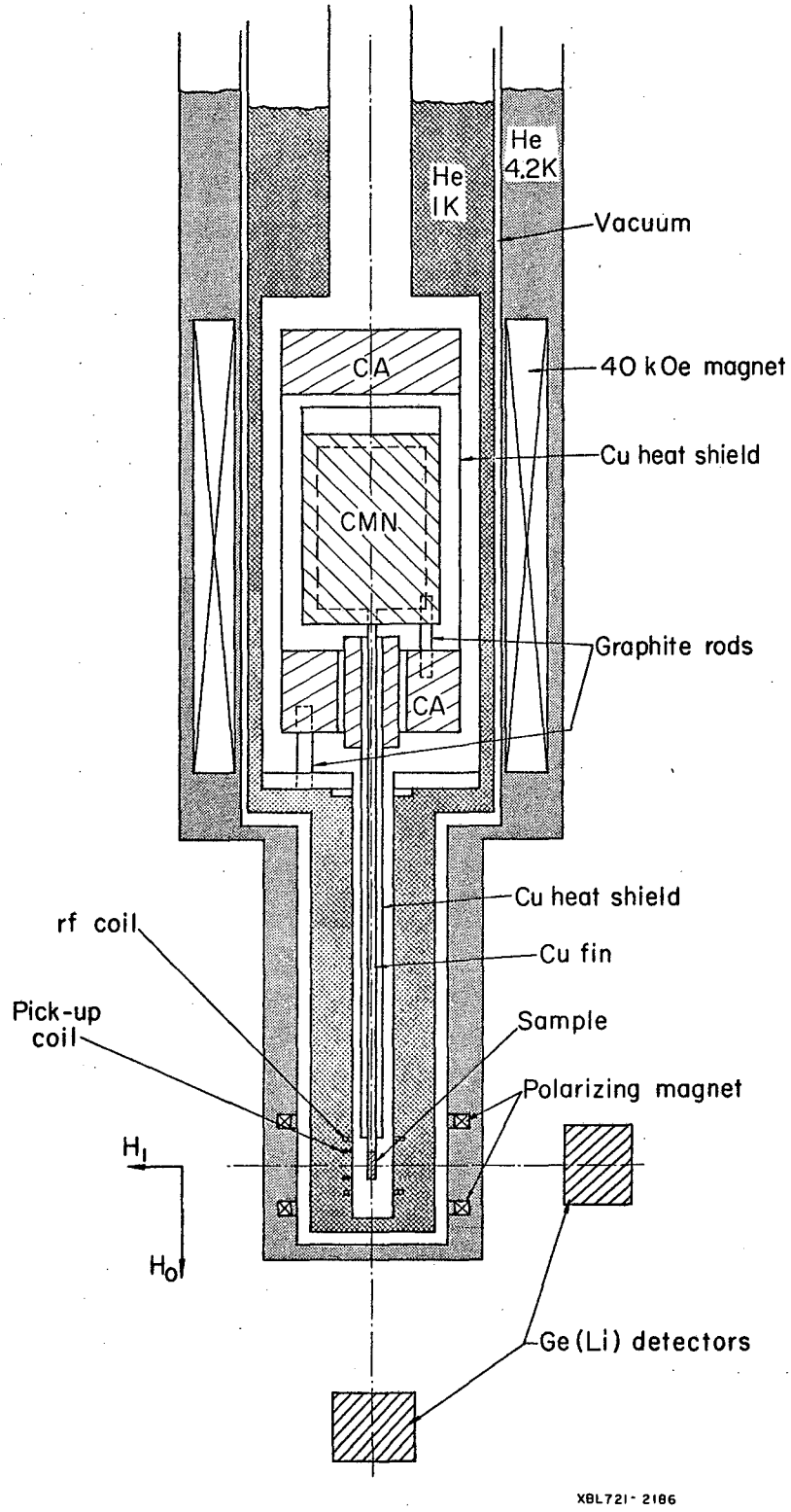


Fig. 3. The magnetic cooling apparatus used for the nuclear orientation experiments in ferromagnetic lattices and the magnetic resonance experiments on oriented nuclei.

copper stalk provided the thermal contact for indirect cooling of the sample foils. The total contact area within the CMN was about 1600 $cm^2$. A copper cylinder in contact with 80 $cm^3$ of CA provided a heat shield for the CMN container. The main cooling pill was thermally insulated by pitch bonded graphite rods from the bottom CA container with an approximately equal volume of CA as the top container. This bottom CA container functioned mainly as a one degree heat sink since it sat in contact with the cryostat insulated, though, by pitch bonded graphite rods and fibreglass. Within this container and thermally isolated from it, a fibreglass cylinder with about 12 $cm^3$ of CA served as thermal contact for the heat shield surrounding the cooling stalk.

2. The Cryostat

The cryostat is a 0.035 inch thick 10 inches long tube (for holding the salt pill) attached to a 1-1/2 inch O.D. stainless steel pumping tube. All joints are made with either silver solder or BiCd eutectic (40% wt. Cd, 60% wt. Bi) solder. The BiCd is superconducting but has a low critical field of about 30 Oe at 0.54 K[33] compared with the 60 Oe dipolar field of CMN.[34] The superconducting PbSn (50-50% wt.) solder was also used without any apparent effects on the salts. The cryostat tail is a glass-to-stainless steel housekeeper seal and is attached to the main body of the cryostat via an indium O-ring seal. No super leaks were ever encountered with this seal and it is much more convenient than the indium coated copper gaskets needed for the Varian seals.

3. The Radiofrequency Leads

The rf leads were 9/64 inch diameter stainless steel coaxial leads (Uniform Tube Company) with either stainless steel or copper conductor insulated from the outer ground tube by teflon. The electrical connection was made by the BNT type connector and the leads exterior to the apparatus were the high frequency 1/2 inch Superflexible Heliax cable Type FSJ4-50 (Andrew Corporation) as opposed to the standard 50 ohm coaxial cables. These leads worked exceedingly well. The rf coil was a Helmholtz pair with one turn of copper on each ear. The pick up coil had one turn of copper.

4. The 1 K Dewar

The 1 K dewar differs only slightly from the original one for this apparatus as described in Ref. 30. The present dewar has the bottom of the tapered section made from two one millimeter thick pieces of beryllium--one for each wall of the dewar. To prevent deterioration of the windows with thermal cycling, the apparatus was kept at LN temperatures. These low Z windows provided minimal radiation attenuation needed for the present work.

## C. Electronics

For the nuclear orientation experiments, lithium drifted germanium detectors were used for counting at zero and ninety degrees relative to the polarizing field. (Specifications for the detectors are listed in the Appendix (V).) A schematic of the associated electronics is given in Fig. 4 for the zero degree detector, with an identical setup being used

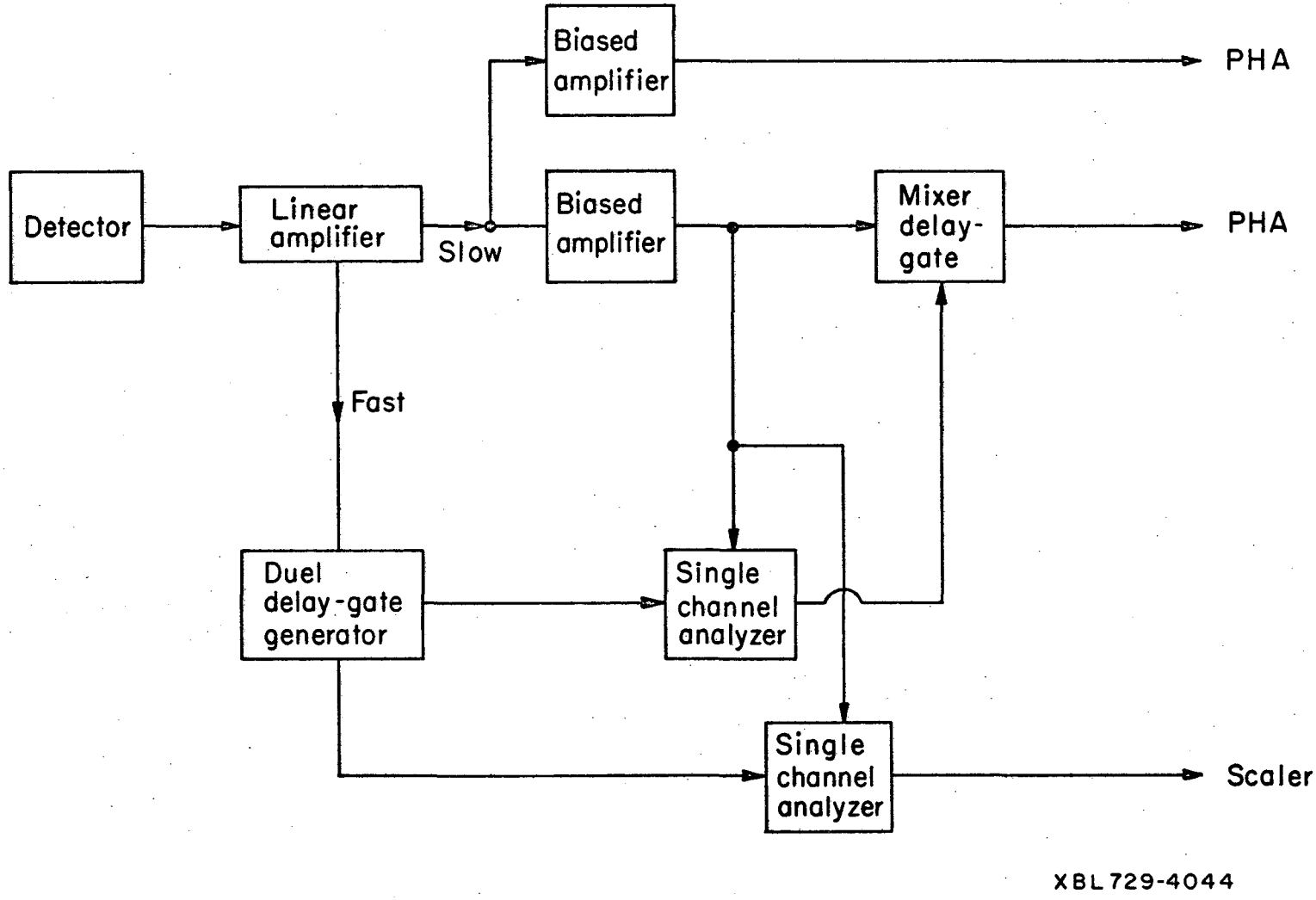


Fig. 4. The schematic of the electronic counting equipment used for data taking.

for the ninety degree detector. Through one of the biased amplifiers low energy gamma spectra were taken, and high energy gammas and the $^{60}Co$ gamma spectra were taken with the other or with the mixer delay gate. The output of the amplifiers were fed into either the 1600 channel Scipp analyzer or the PDP-7 computer and the data in both cases were recorded on magnetic tape. The single channel analyzer outputs were fed into a 400 channel analyzer equipped with a 4-Channel Multiscaler unit operating in the Multi-Sweep mode. The data here accumulated and displayed served to monitor the temperature and warm-up rate of the foils.

For higher counting rates, a sodium iodide detector at zero degrees was used for counting in the resonance experiments. In these experiments, the single channel analyzer outputs were fed into the 4-Channel Multiscaler unit now operating in the Multi-Sweep Sequential $\Delta$ T1 - $\Delta$ T2 mode. This mode allows counting for a preset time $\Delta$ T1 and stopping for a preset time $\Delta$ T2 during which the frequency could be changed.

The radiofrequency field was supplied by a Model 610B Wiltron oscillator equipped with internal sawtooth frequency modulation. A Type 874-TPD coaxial power divider (General Radio Company) was used to send equal rf amplitudes to the coil and a 5245L Model Hewlett Packard frequency counter for frequency measurements. Attenuation or amplification of the rf power leading to the coil was achieved by using either a 20 db attenuator (Lecroy Research Systems Corporation) or a IFI Model 510 wide-band amplifier. The signal from the pickup coil was displayed with a Type 661 sampling oscilloscope.

## D. Data Taking and Processing

The data of the nuclear orientation experiments were accumulated continuously for fifteen minute periods until the anisotropies disappeared--typically over a ten hour time span. The corrected gamma line intensities were arrived at through use of the PDP-7 computer which fitted the background to a third order polynomial. All subsequent data processing was achieved by a series of fit programs for the LBL CDC 6600 computer. These programs are dubbed NODA1, NODA2, and NODA3, short for nuclear orientation data analyses, and assume a magnetic hyperfine interaction Hamiltonian of the form $\mathcal{H} = -\vec{\mu} \cdot \vec{H}$. The NODA2 program corrects the line intensities for decay and gives the anisotropies as either $(1 - W(\theta))$ or $(W(\theta) - 1)$ for each gamma line. The errors are either the linear projection of the difference in the independent variable on the difference in the dependent variable or mean square root. These anisotropies can then be fitted by least squares method to the angular distribution function vs. reciprocal temperature (from the $^{60}Co$ anisotropies) by the NODA1 program. The data are generally fitted using two parameters: $|\mu H|$ and an amplitude factor or multipole mixing ratio. The amplitude factor becomes important only if saturation of the anisotropy is reached. In some cases, say if $|\mu H|$ is known, a third parameter $F_k U_k$ $(k = 2,4)$ can be fitted after appropriate changes; the errors can be selected as above.

The magnetic resonance data are treated almost similarly but by different means. Since with the 4-channel Multi-Scalar the total gamma line intensity is counted, there are no background corrected intensities. The total intensities are corrected for decay, however, and the resonance curve fitted with a least squares gaussian plus straight line background

fit by a subprogram of NODA1. The subprogram is a five parameter fit: the resonance frequency, the amplitude, the half width at half maximum HWHM, the line slope and intercept. The errors can be also selected as in the NODA2 program.

## E. Results

### 1. $^{196m}$Au

The 9.7 h lived $12^-$ isomer of $^{196}$Au has been assigned the shell model configuration $[\pi h_{11/2}, \nu i_{13/2}]12^-$.[35] Nuclear orientation experiments were performed on this state to measure the magnetic moment and, thus, test the validity of this assignment. The energy level scheme for the isomeric decay of $^{196m}$Au is well known and is shown in Fig. 5. The gamma transitions of interest are a pure E2 at 148 keV and 188 keV transition with an unknown M1/E2 mixing ratio.

The $^{196m}$Au:$^{60}$Co(Fe) or (Ni) foil was attached to the copper fins of the magnetic cooling apparatus with Bi-Cd solder using stainless steel Rotomex flux. The cooling magnet was operated at 30 KOe field and a field of 4 KOe was applied parallel to the plane of the foil by the polarizing magnet. The final temperatures for these runs were about 8 mK.

Figure 6 shows the temperature dependence of the anisotropy for the 148 keV gamma line. The circles are for the iron lattice and the squares for the nickel lattice. The solid curve is a result of the fit of the $W(\theta)$ function to the $^{196m}$Au(Fe) data and the dashed curve a fit to the $^{196m}$Au(Ni) data. The iron lattice anisotropies were fitted using the hyperfine interaction constant $|\mu H|$ and an amplitude factor as free

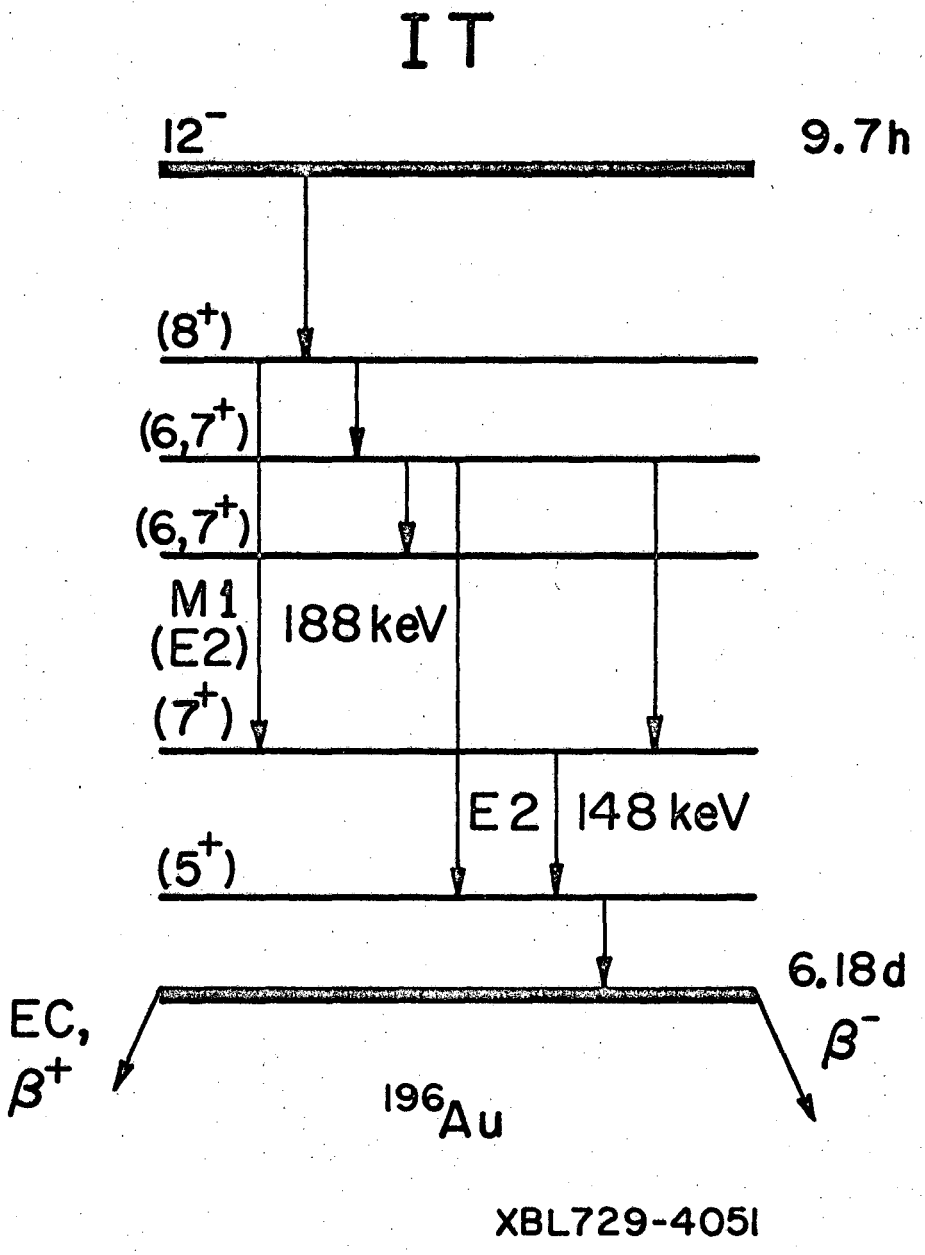


Fig. 5. Decay scheme of $^{196m}$Au.

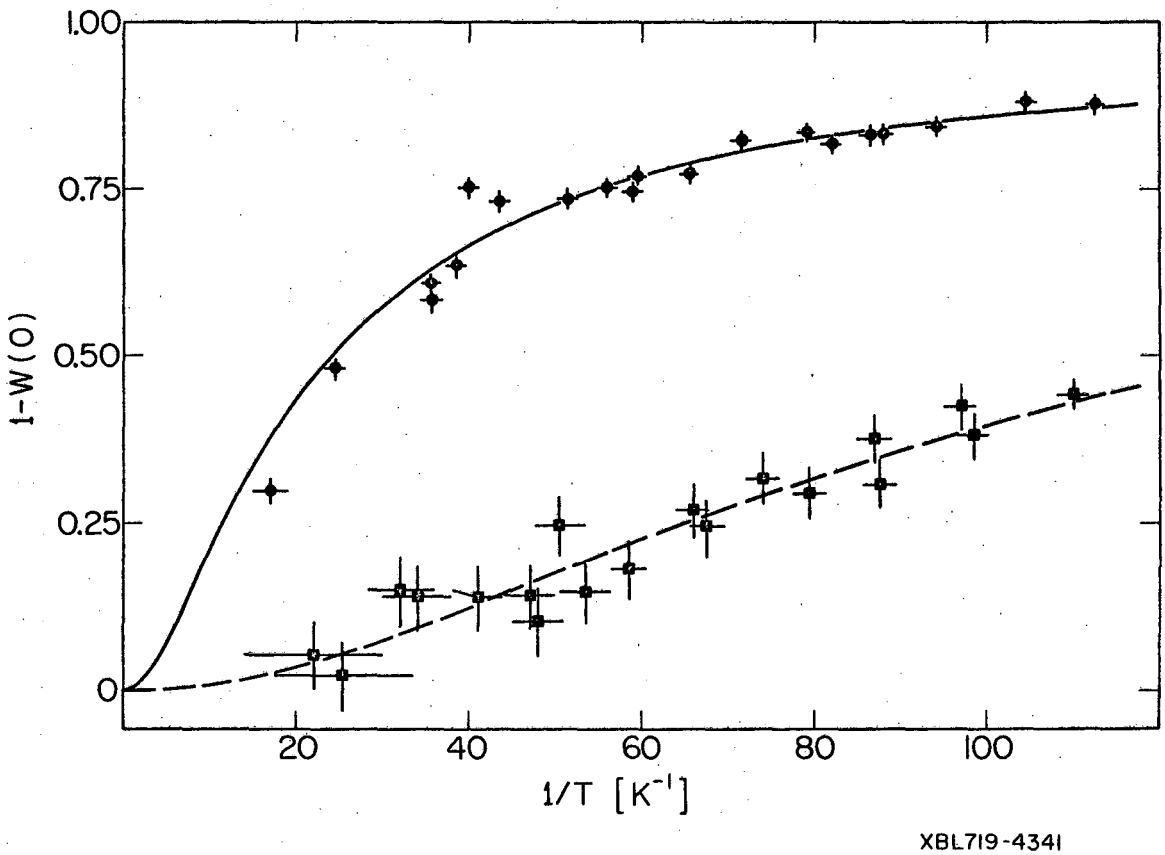


Fig. 6. The zero degree anisotropies vs. 1/T curves for the 148 keV gamma of $^{196m}$Au. The circles are the $^{196m}$Au(Fe) results and the squares are $^{196m}$Au(Ni) results. The solid and the dashed curves are the results of a theoretical fit of the data to the distribution function for the iron and nickel lattices, respectively.

parameters. The saturation value of $W(0°)$ agrees within error limits with the theoretical one calculated from the $^{196m}$Au decay scheme.[7] Because saturation was not reached in the nickel lattice, these data were fitted with a single parameter, $|\mu H|$, with the amplitude factor fixed from the iron fit. The importance of reaching saturation is therefore demonstrated.

The final and uncorrected results for the magnetic hyperfine constants are summarized in Table 2. Their ratio agrees within error with the ratio of the hyperfine fields of $^{197}$Au in iron and nickel.[12] Since the mixing ratio of the 188 keV gamma transition is not known (nor could it be determined from these experiments) the above results were based on the 148 keV gamma line alone.

An attempt to find the resonance frequency in iron was unsuccessful. Failure was due mainly to the decay of $^{196m}$Au with the growing background from the 6.18 day lived $^{196}$Au ground state. Through off resonance rf heating, however, the nuclear spin-lattice relaxation time was estimated to be less than 10 seconds.

2. $^{198m}$Au

The decay of the assumed $12^-$ state of $^{198}$Au was first observed during the course of this work and later reported by Cunnane and Daly.[36] It too should have the shell model configuration $[\pi h_{11/2}, \nu i_{13/2}]12^-$. The magnetic moment and halflife were determined. Nuclear orientation experiments were done on $^{198m}$Au: $^{60}$Co(Fe) and (Ni) foils in the temperature range of 4 mK as described for $^{196m}$Au.

Table 2. Summary of experimental results for $^{196m}Au$

| Host | θ | $\lvert\mu H\rvert$ ($10^{-18}$ erg) | $\lvert\mu H\rvert_{AVG}$ ($10^{-18}$ erg) |
|---|---|---|---|
| Fe | 0° 1) | 31.8 ± 1.6 | |
| Fe | 90° 1) | 27.3 ± 3.1 | |
| Fe | 0° 2) | 30.0 ± 2.4 | |
| | | | 30.6 ± 1.2 |
| Ni | 0° | 6.0 ± 0.4 | |
| Ni | 0° | 7.4 ± 0.7 | |
| | | | 6.4 ± 0.4 |

The 1) and 2) refer to two different samples.

The gold activity spectrum, Fig. 7, clearly shows the presence of a longer lived isomeric state; spectrum c) was taken after several $^{196m}$Au and $^{200m}$Au halflives. Cunnane and Daly similarly have assigned the 181-, 203-, and 214 keV transitions to $^{198m}$Au. Because of other interfering transitions, however, quantitative measurements were made only for the 203- and 214 keV transitions. Following the decay of the 214 keV line for several days, the halflife of this isomeric state was determined to be $t_{1/2} = 49 \pm 2$ h in agreement with the halflife measurement of Ref. 36 of $t_{1/2} = 2.3$ day. Figure 8 shows the decay curve.

Zero and ninety degree data were fitted simultaneously for the 214 keV gamma line with $|\mu H|$, $U_2F_2$, $U_4F_4$ as free parameters and assuming a spin of 12. The simultaneous fit procedure was necessary because of incomplete knowledge of the decay scheme. Figure 9 shows the temperature dependence of the anisotropy for the $^{198m}$Au(Fe) parallel and perpendicular to the polarizing field axis.

As can be seen from the gold spectrum (Fig. 7), the 203 keV line is barely separated from the 208 keV line of $^{199}$Au. This spectrum was taken with the zero degree detector; however, the energy resolution is worse for the ninety degree detector and the two lines coalesce. For this reason, only the zero degree data were analyzed for the 203 keV transition. Furthermore, because of the difficult and uncertain background corrections for this line, only the $^{198m}$Au(Ni) data were fitted. In this lattice the nuclear polarization of the $^{199}$Au ($\mu = 0.26$ nm[37]) is negligible, and thus an uncorrected contribution for the 208 keV line tail should not significantly influence the anisotropy determination. The results of a least squares fit are presented in Table 3.

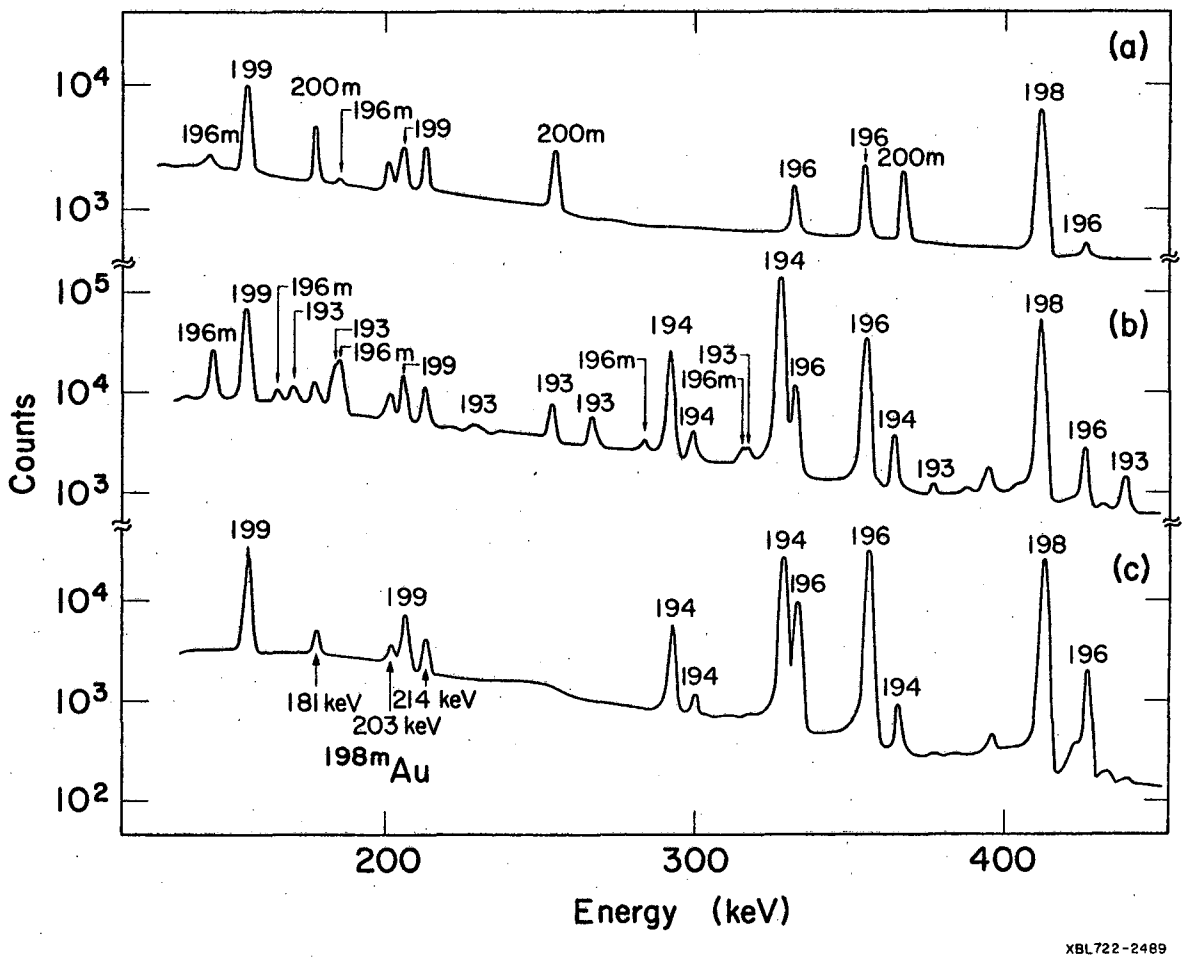


Fig. 7. Gamma ray spectrum showing the evidence of the $^{198m}$Au activity. Spectrum (a) resulted from alpha irradiation of the enriched $^{198}$Pt foil. Spectra (b) and (c) resulted from deuteron irradiation of the enriched $^{198}$Pt foil. Spectrum (b) was taken immediately following source preparations whereas spectrum (c) was taken four days later.

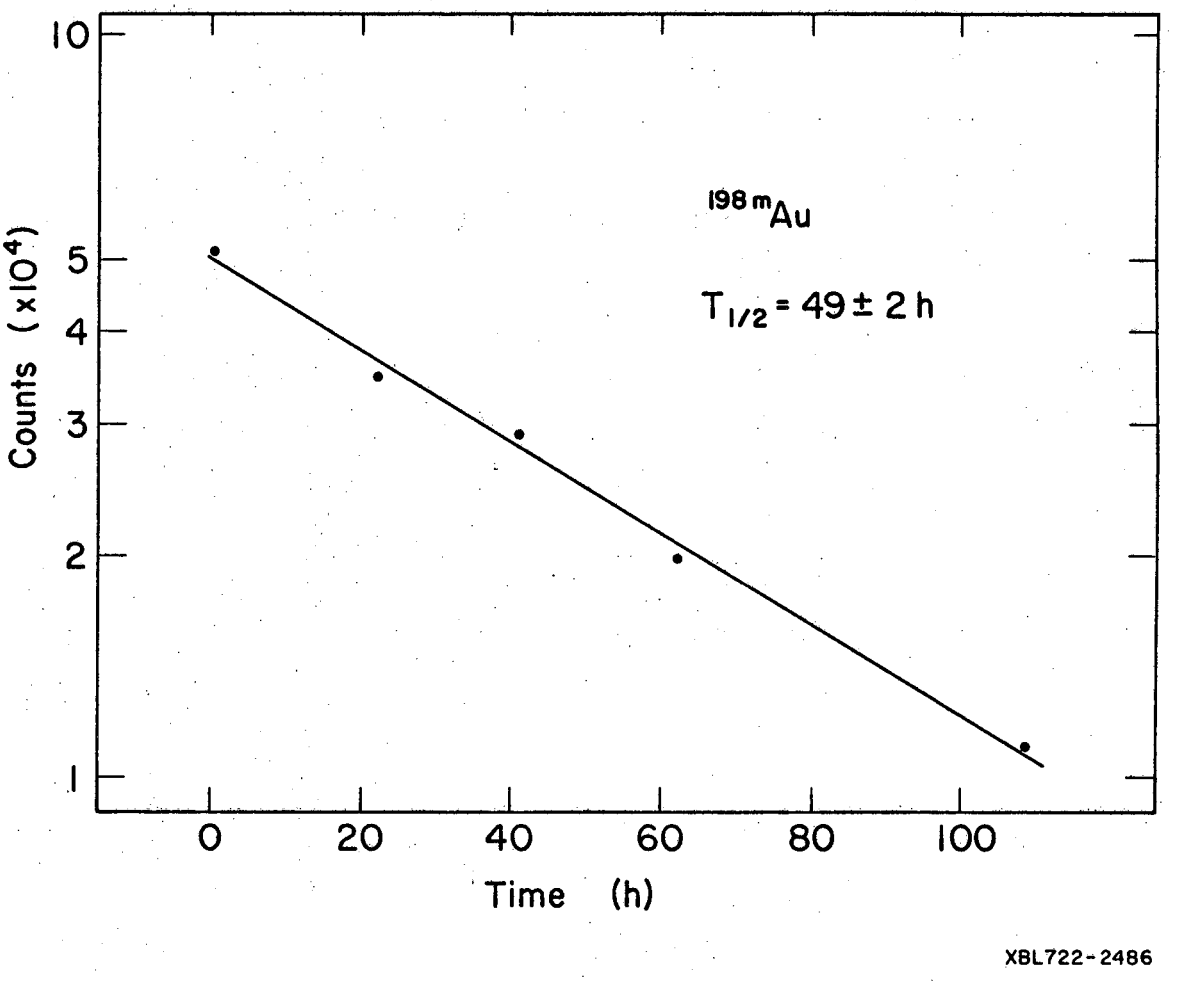


Fig. 8. Decay curve for $^{198m}$Au. This curve was obtained by following the decay of the 214 keV line from this isotope for several days.

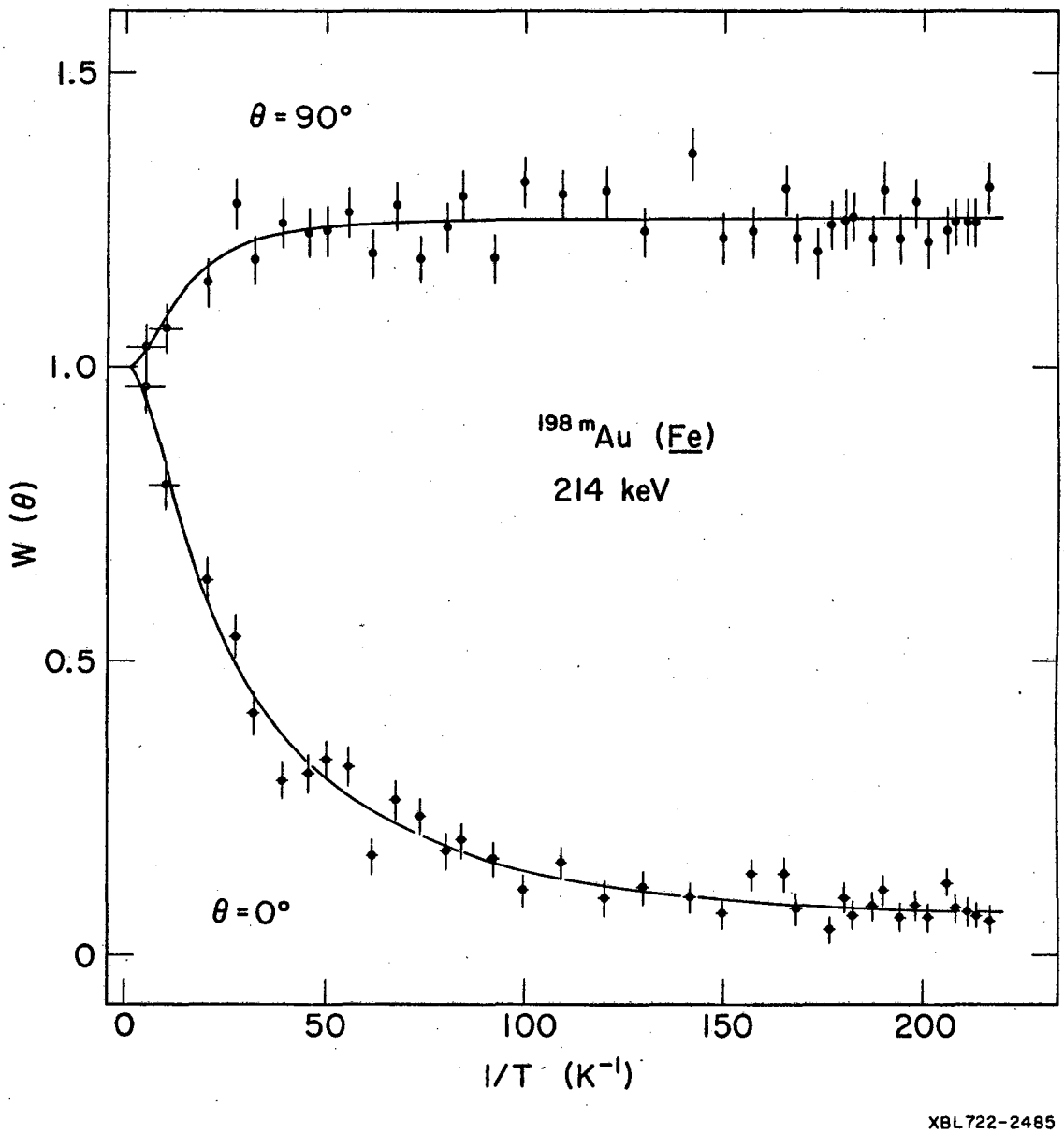


Fig. 9. The gamma ray anisotropies vs. 1/T curve for the 214 keV gamma of $^{198m}$Au in iron. This curve results from a simultaneous fit of the zero and ninety degree data to the distribution function.

Table 3. Summary of experimental results for $^{198m}Au$

| Host | $\lvert\mu H\rvert$ ($10^{-18}$ erg) |
|---|---|
| Fe | 30.4 (12) |
| Ni | 7.9 (6) |
| Ni | 6.5 (10) |

Values for the products of the angular momentum coefficients were obtained from the simultaneous fits. For the 214 keV gamma line they are

$$U_2F_2 = -0.33(3)$$

$$U_4F_4 = -0.15(7)$$

These values imply quadrupolar transitions with $I_i - I_f = 2$. The positive anisotropy observed for the 203 keV gamma line with

$$U_2F_2 = +0.4(1)$$

$$U_4F_4 = +0.0(1)$$

indicates a likely multipole order of M1 with E2 admixture and a negative mixing ratio.

As a check of this simultaneous fit procedure, the anisotropy of the 412 keV gamma of $^{198}$Au ground state was analyzed with a simultaneous fit. The derived hyperfine interactions constants agreed within 3% of the known values for $^{198}$Au(Ni). These results are given in Table 4.

3. $^{200m}$Au

Another very similar high spin gold state, $^{200m}$Au ($t_{1/2}$ = 18.7 h),[38] was also investigated. It too has an assumed spin and parity of $12^-$ with shell model configuration $[\pi h_{11/2}, \nu i_{13/2}]12^-$. For this isotope, both nuclear orientation and NMR/ON experiments were performed in both iron and nickel lattices for the former and only nickel for the latter experiment. The results of each are detailed separately below.

Table 4. Results of the simultaneous fit of the anisotropy curves for the 412 keV gamma ray of $^{198}$Au(Fe) in comparison with known values

| ($10^{-18}$ erg) | $U_2$ | $U_4$ | |
|---|---|---|---|
| 3.50(6) | 0.797(22) | 0.261(58) | this work |
| 3.437 | 0.795(7) | 0.347(30) | Ref. 42 |

a. Nuclear Orientation Results. There are six major gamma lines following the beta decay of $^{200m}$Au to $^{200m}$Hg. (See Fig. 10.) Of these six lines, only the 256 keV transition showed a positive anisotropy--an increase in intensity along the axis of orientation--whereas the 368-, 498-, 580-, and 760 keV transitions showed sizable negative anisotropies. The remaining 181 keV line showed a different decay time, later found to be from the $^{198m}$Au, and was not analyzed.

Figure 11 shows the temperature dependence of the anisotropy for the 368 keV gamma ray for the $^{200m}$Au(Fe) sample. The solid curve is a result of a simultaneous fit of the zero and ninety degree data to $W(\theta)$ using $|\mu H|$, $U_k F_k$ ($k = 2,4$) and an amplitude factor as free parameters. In this case the amplitude factor corrects for possible differences existing between the background corrections for the zero and ninety degree data. (Reference to the drawing of the apparatus (Fig. 3) reveals that the ninety degree data will in general suffer more from scattering and intensity loss than the zero degree data therefore their respective backgrounds are affected differently.)

A similar fit was applied to the $^{200m}$Au(Ni) data assuming various spins for the isomeric state. Here, the $|\mu H|$ obtained from the resonance work, discussed below, was held constant. The hyperfine interaction constants derived therefrom are given in Table 5a. It turned out that the $|\mu H|$'s derived were essentially independent of the assumed spins. This fact supports the statement made earlier that from an orientation experiment only $|\mu H|$ is determined. Agreement with the NMR/ON results, however, was reached only for a spin of 12. This result is shown in Column 3 of Table 5a. Because of the larger spin, the sensitivity of this method is less than that for a similar case, $^{195m}$Pt with $I = 13/2$ discussed below, to which this method was applied.

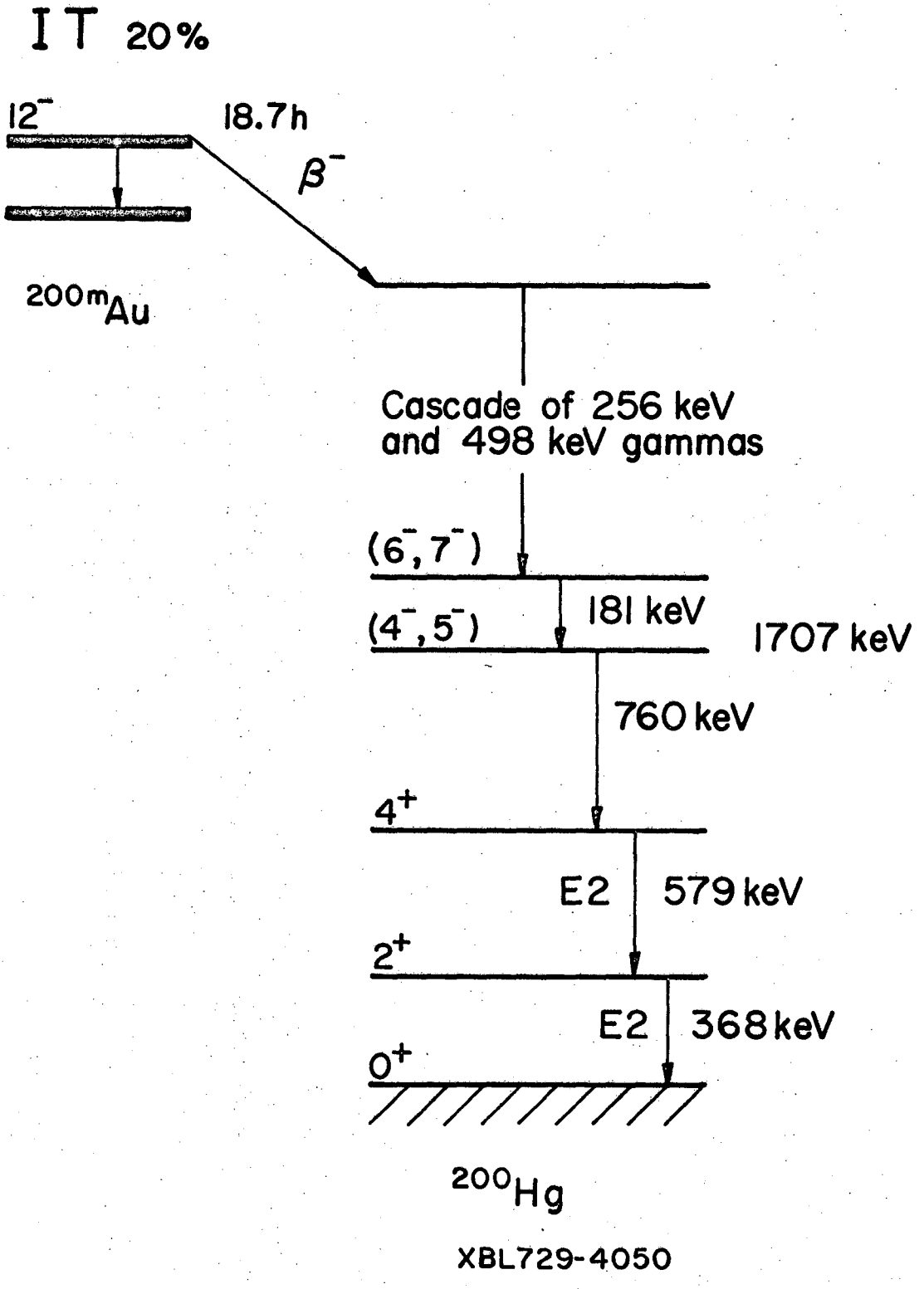


Fig. 10. Decay scheme of $^{200m}$Au.

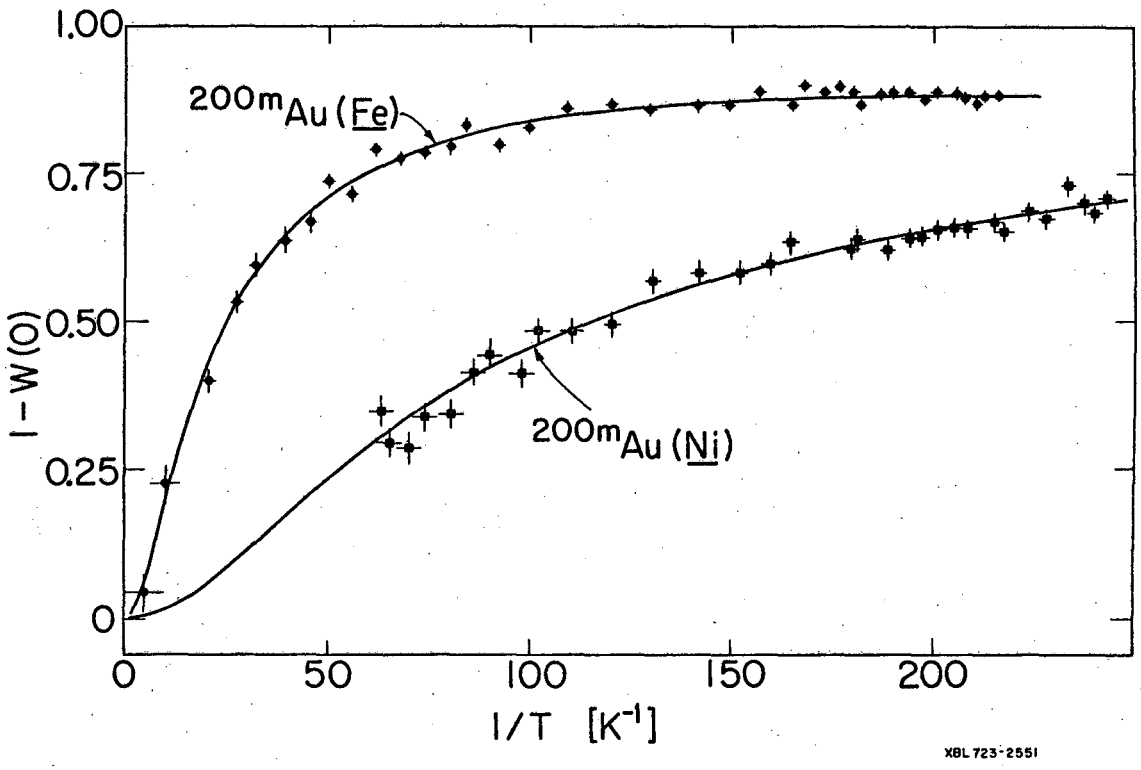


Fig. 11. The zero degree gamma ray anisotropy vs. 1/T curve for the 368 keV gamma of $^{200m}$Au in iron (the circles) and nickel (the squares). The solid curves are the results of a least squares fit of the data to the distribution function.

Table 5a. Summary of fit results for $|\mu H|$ obtained for the anisotropy curves for $^{200m}$Au(Ni) assuming various values for the spin of the isomeric state.

| I | $\|\mu H\|$ ($10^{-18}$ erg) | $(\gamma H)_{NO}/(\gamma H)_{NMR}$ |
|---|---|---|
| 11 | 7.60(30) | 1.08(4) |
| 12 | 7.65(30) | 0.995(40) |
| 13 | 7.71(30) | 0.925(40) |

Table 5b. Summary of experimental results for $^{200m}$Au

| Host | $\|\mu H\|$ ($10^{-18}$ erg) |
|---|---|
| Fe | 34.4(15) |
| Ni | 7.6(3) |

b. NMR/ON Results. For the NMR/ON experiments, the resonance frequency was estimated to be approximately 96 MHz by using the weighted average ON results for $^{200m}$Au(Ni). This value dictated the frequency range to be swept by assuming an error of approximately 10%. (The corresponding frequency in iron is 435 MHz, a value exceeding the present rf capabilities.) The summed intensities of the 498-, 580-, and 760 keV transitions were then measured as a function of applied rf frequency with a Na(I) detector placed at zero degrees relative to the polarizing field direction. The polarizing field was first turned to 4 KOe and finally to 1 KOe to remove hysteresis effects. The $H_1$ field, of strength 0.5 mOe, was applied perpendicular to the $H_o$ field but parallel to the plane of the foil. This field was frequency modulated with 100 Hz over a bandwidth of one MHz. The resonance curve observed is shown in Fig. 12. This curve is the result of four sweeps through the resonance range and was fitted with a gaussian curve plus straight line background. From this curve the resonance frequency was determined to be

$$\nu = \frac{\mu H}{Ih} = 97.7 \pm 0.2 \text{ MHz} \quad ,$$

corresponding to a

$$|\gamma H| = (6.473 \pm 0.012) \times 10^{-19} \text{ erg} \quad .$$

Using a $\nu \sim 97$ MHz and no fm, no effect was observed whereas with fm on and one MHz bandwidth sizable resonant destruction of the anisotropy occurred. Therefore, warming up due to coil resonances can be ruled out. From this measurement, the nuclear spin-lattice relaxation time was observed to be less than 10 seconds for the temperature range 4 to 10 mK.

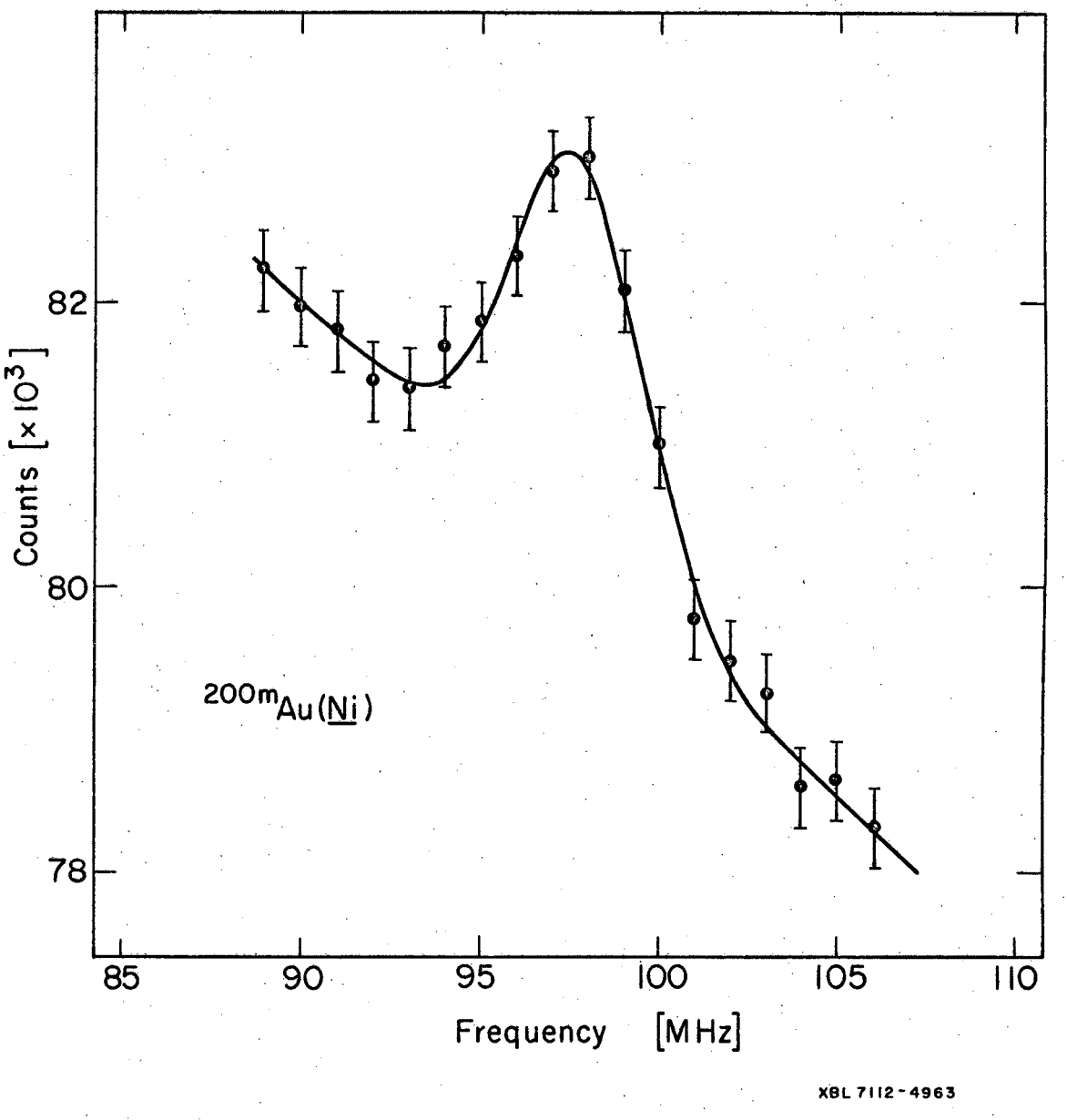


Fig. 12. The magnetic resonance curve for $^{200m}$Au oriented in nickel. The solid curve results from a gaussian plus straight line background fit to the measured intensities. The $H_1$ amplitude was 0.5 mOe, the fm frequency was 100 Hz with a bandwidth of one MHz.

With the added information from the NMR/ON results--the magnetic hyperfine splitting--and the spin established as 12, additional fits of the $^{200m}$Au(Fe) and $^{200m}$Au(Ni) data were done. The $U_k F_k$ were determined from the nickel data with $|\mu H|$ fixed from the NMR/ON results. These coefficients were similarly determined from the iron data assuming a $H_{hf} = -1169$ KOe as measured for $^{198}$Au(Fe).[42] The results for the different orientation experiments agreed within the error limits and their averaged values are presented in Table 6.

4. $^{196}$Au and $^{198}$Au

The isomeric decay of both $^{196m}$Au and $^{198m}$Au leads to ground states well suited for NMR/ON experiments. The $^{196}$Au ($t_{1/2}$ = 6.18 d) and the $^{198}$Au ($t_{1/2}$ = 2.69 d) are similar with known moments, $\mu(196) = +0.5878(14)$ nm, $\mu(198) = +0.5897(4)$ nm[37], and both have spin $2^-$. Moreover, an NMR/ON experiment on these oriented states would afford a determination of the magnetic hyperfine field, a measurement useful for the orientation experiments. For this reason, resonance experiments were done, concertedly, on $^{196}$Au(Ni) and $^{198}$Au(Ni) and concurrently with the $^{200m}$Au(Ni) experiment.

The gamma lines observed here were the 412 keV of the daughter $^{198}$Hg for $^{198}$Au and the 356 keV of the daughter $^{196}$Pt for $^{196}$Au. (See Fig. 13.) Under identical counting and rf conditions already described for $^{200m}$Au(Ni), the resonance curve given in Fig. 14 was measured. Because of the long nuclear spin-lattice relaxation time, subsequently determined

Table 6. Measured and theoretical anisotropy coefficients for five of the strongest gamma lines in the decay of $^{200m}Au$

| line (keV) | $I_i$ | L | $I_f$ | $U_2F_2$ | $U_4F_4$ | $U_2F_2$ | $U_4F_4$ |
|---|---|---|---|---|---|---|---|
| | | | | Theory | | Experiment | |
| 256 | 10 | 1 | 9 | 0.252 | 0.0 | 0.253(12) | 0.009(13) |
| | 8 | 1 | 7 | 0.252 | 0.0 | | |
| 498 | 10 | 2 | 8 | -0.360 | -0.142 | -0.342(15) | -0.130(18) |
| | 9 | 2 | 7 | -0.360 | -0.142 | | |
| 760 | 6 | 2 | 4 | -0.360 | -0.142 | -0.342(20) | -0.126(25) |
| 580 | 4 | 2 | 2 | -0.360 | -0.142 | -0.353(16) | -0.112(20) |
| 368 | 2 | 2 | 0 | -0.360 | -0.142 | -0.323(10) | -0.126(12) |

Including a correction for 20% IT in $^{200}Au$ from M. F. Martin, Nucl. Data Sheets B6, 387 (1971).

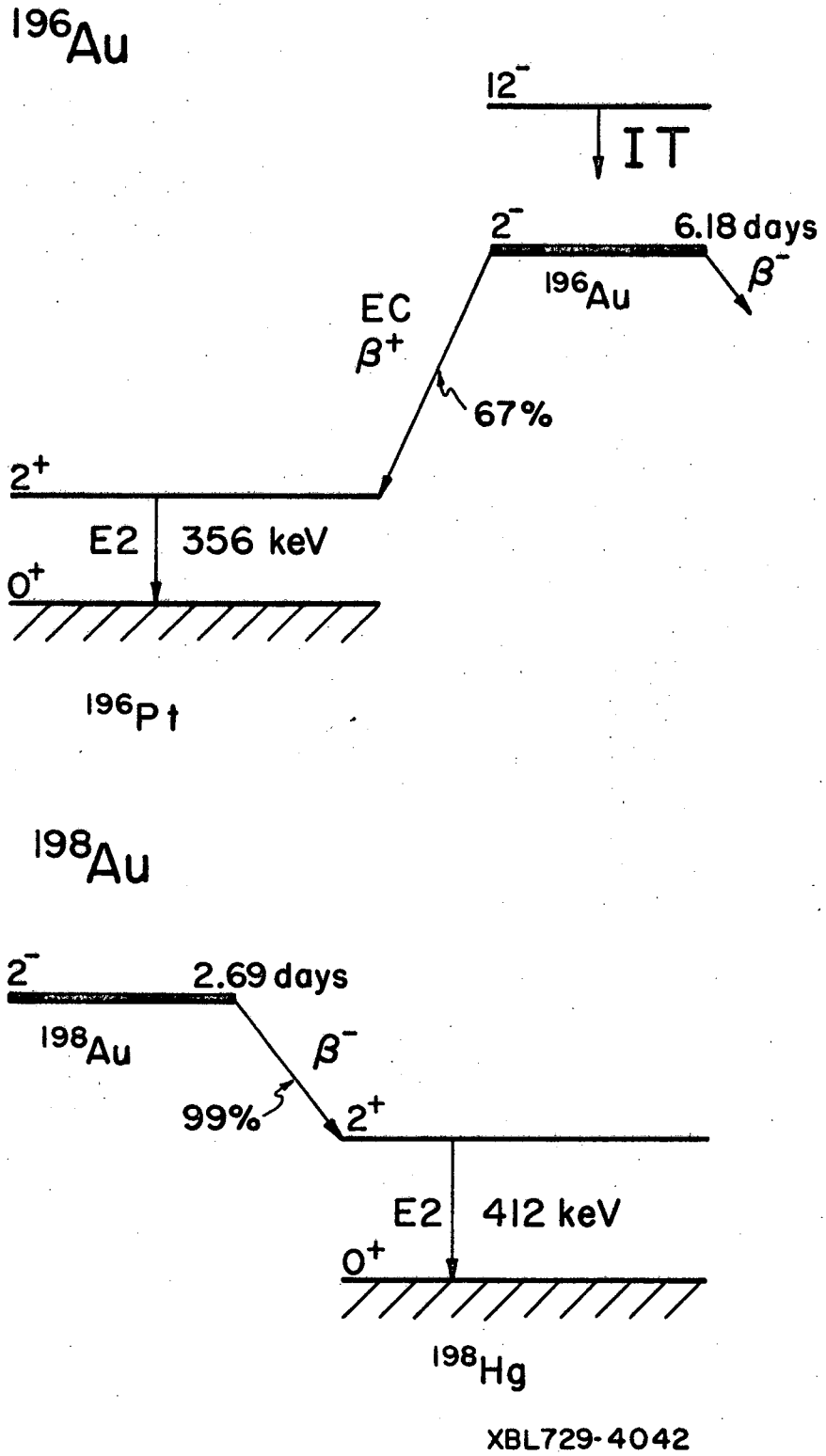


Fig. 13. Decay scheme of $^{196}$Au and $^{198}$Au.

to be $T_1' = 3 \pm 1$ min by a single exponential fit, the resonance curves measured for increasing frequency (Fig. 14 curves a) and c)) and for decreasing frequencies (same figure curves b) and d)) are shifted relative to each other and are asymmetric. This shift is apparent in spite of the 4.25 min time elapsed between adjacent points. On account of the asymmetry of the curves, the resonance frequencies were determined from the average of the leading edges to be

$^{198}$Au(Ni): $\nu = 58.5 \pm 0.4$ MHz

$^{196}$Au(Ni): $\nu = 58.3 \pm 0.4$ MHz .

A similar resonance curve was observed with $^{198}$Au activity produced differently, by alpha irradiation, and used for the $^{200m}$Au experiment. The anisotropy of the 412 keV gamma line decreased upon entering the resonance, whereas no effect was observed on the gamma originating from the $^{200m}$Au decay. Thus, foil heating due to coil resonances could be eliminated.

## II. Discussion of Results

### A. The Hyperfine Anomalies and the Magnetic Moments

The hyperfine fields of gold in iron and nickel at low temperatures are all well known: for $^{197}$Au, $H_{hf}$(Fe) = -1280(25) KOe[12] and $H_{hf}$(Ni) = (-)294(6) KOe[39] and for $^{198}$Au, $H_{hf}$(Fe) = -1169(1) KOe.[40] The isotopic variation of the iron or nickel hyperfine fields for gold has been attributed to the hyperfine anomaly known to exist for gold isotopes.[41-42] As yet, however, the hyperfine anomalies between either $^{197}$Au or $^{198}$Au and the gold isotopes studied have not been measured. For this

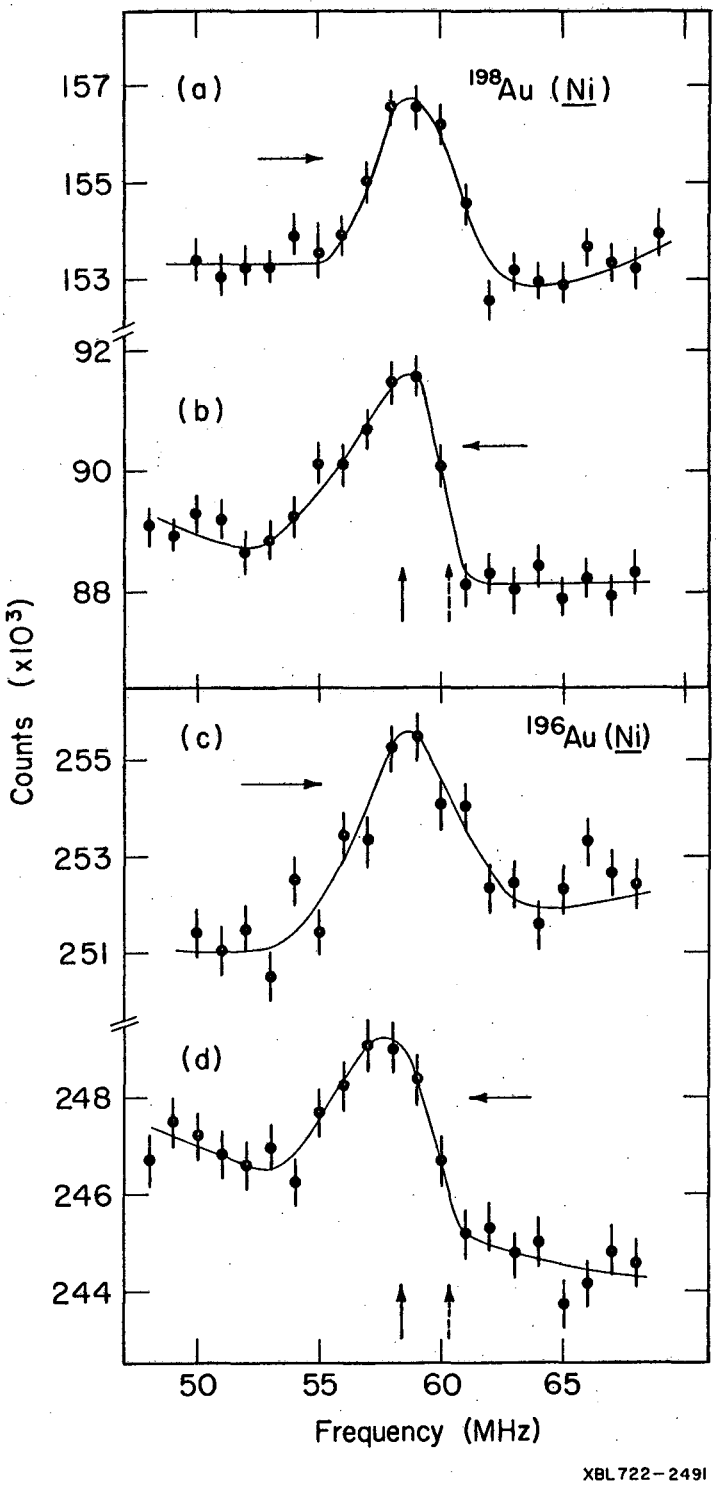


Fig. 14. The magnetic resonance curves for $^{198}$Au (a and b) and $^{196}$Au (c and d) oriented in nickel. Curves (a) and (c) refer to sweeps toward higher frequencies whereas curves (b) and (d) refer to sweeps toward lower frequencies. The solid curves result from a gaussian plus straight line background fit to the measured intensities. In both cases the $H_1$ was 0.5 mOe and the fm frequency was 100 Hz over a bandwidth of one MHz.

reason, the anomaly will be described only briefly here; however there are numerous publications on the subject.[43-47]

The hyperfine anomaly is a consequence of the break down of the Fermi-Segre[48] point dipole model of the nucleus according to which the hyperfine interaction energy of an isotope is given by

$$a_{pd} = \frac{16}{3} \pi g |\psi(0)|^2 \quad ,$$

where g is the nuclear g factor and $|\psi(0)|^2$ is the electronic density at the nucleus. The finite size of the nucleus reduces this hyperfine interaction energy relative to a point nucleus by causing both a radial variation of the electronic density in the nuclear volume and a distribution of nuclear magnetization due to the spin and orbital components of the nuclear moment. Thus the hyperfine anomaly exists only when the hfs is caused by an s (or $p_{1/2}$, for heavy nuclei) electron. Moreover, from the point nucleus approximation, the ratio of the hfs constants of two isotopes or nuclear levels 1 and 2 should equal the ratio of their respective nuclear g factors

$$(a_{pd})_1/(a_{pd})_2 = g_1/g_2 \quad .$$

But because of the finite nuclear size, the ratio of the hfs constants should differ from the g ratio by an amount ${}^1\Delta^2$.[43] Specifically, the hyperfine anomaly is defined through the following equation

$$a_1/a_2 = (g_1/g_2)(1 + {}^1\Delta^2) \quad .$$

The $^1\Delta^2$ expresses the size of the anomaly and, of course, if nuclei were point dipoles then $^1\Delta^2$ would vanish. If, for cases of interest here, $a_1$ is the total effective hyperfine interaction $(\mu H_{eff})_1$ for state one and $(\mu H_{eff})_2$ for state two, the anomaly may be expressed as

$$(\mu H_{eff})_1/(\mu H_{eff})_2 = \frac{\mu_1}{\mu_2}(1 + {}^1\Delta^2) \quad .$$

The moment ratios $\mu_1/\mu_2$ can be divided out and the hyperfine anomaly for ferromagnetic lattices can be written (Eq. (4))

$$(H_{eff})_1/(H_{eff})_2 = 1 + {}^1\Delta^2 \quad .$$

To separate out the contributions to $^1\Delta^2$ from an individual nucleus, an $\varepsilon$ is defined by

$$a = a_{pd}(1 + \varepsilon) \quad ,$$

which is the fractional reduction of the hfs relative to a point dipole for a given isotope. The anomaly then becomes

$$\begin{aligned} {}^1\Delta^2 &= (\varepsilon_1 - \varepsilon_2)/(1 + \varepsilon_2) \\ &\approx \varepsilon_1 - \varepsilon_2 \quad . \end{aligned}$$

The hyperfine anomaly results from the different effects of the hyperfine field on the spin and orbital moments of the nucleons. That the two components of the moments are differently affected can be seen through a simple analogy.[49] That is, for a proton moving in a circular orbit of radius r, its spin contributes an energy $H(r)\mu_s$, whereas the orbital

contribution is like that of a current and its energy is $-\vec{i} \times \frac{\vec{flux}}{c}$. The latter contribution depends on the average value of the $H_{hf}$ sensed through the orbit. For this reason, the $\varepsilon$ will usually be a sum of two factors

$$\varepsilon_T = \varepsilon_s + \varepsilon_\ell \quad ,$$

the fractional hfs reduction due to the finite extent of the spin $\varepsilon_s$ and orbital $\varepsilon_\ell$ magnetization distribution. There exist several models for evaluating the fractional reduction of the hfs (see Ref. 49); however, the Bohr-Weisskopf theory (BW), for the cases considered, yielded satisfactory results and the $\varepsilon$'s were determined mainly within this framework. The BW theory assumes that the nuclear charge distribution is uniform without regard to the orbits responsible for the magnetic nuclear properties. Thus, it is more applicable to nuclei of large Z where the protons can be considered as a continuous charge distribution. According to this model the fractional reduction of the hyperfine interaction due to the finite extent of spin and orbital contributions to the magnetic moment for a single isotope is (Eq. (5))

$$\varepsilon_T = -b \langle r^2/R_o^2 \rangle_{avg} \{\alpha_s + 0.62\, \alpha_\ell\} \quad .$$

Here b is a function of Z and $R_o$ values for which can be found in the literature.[44] $R_o$ is the nuclear radius and r is the electronic radius within the nucleus; the average is taken over the nuclear volume. The remaining quantities $\alpha_s$ and $\alpha_\ell$ and the $\langle r^2/R_o^2 \rangle$ are all model dependent. $\alpha_s$ and $\alpha_\ell$ are the fractional spin and orbital contributions to the magnetic moment such that

$$\alpha_s + \alpha_\ell = 1 \quad .$$

In the BW model, $\langle r^2/R_o^2 \rangle$ is set equal to 4/5; however the values of Eisinger and Jaccarino[44] were used in the present calculations. Also for the calculation of the gold hyperfine anomalies, it was assumed that the nuclear states are sufficiently described by the single particle model within which the fractional spin components of the magnetic moment are (Eq. (6))

$$\alpha_s = (g_s/g)(g - g_\ell)/(g_s - g_\ell) \quad ,$$

and

$$\alpha_\ell = 1 - \alpha_s \quad .$$

The $g_s$ is the effective spin g factor for a given case and $g_\ell$ is one and zero for proton and neutron, respectively. The other parameters used were $b = 3.47$ from Ref. 43 and $\langle r^2/R_o^2 \rangle = 0.8$ from Ref. 44.

As an example, the fractional reduction of the hyperfine interaction will be calculated for the ground state of $^{196}$Au. The ground state is a two particle state with shell model configuration $[\pi d_{3/2}, \nu p_{1/2}]2^-$. The spin and orbital components of the $d_{3/2}$ proton moment will first be calculated according to Eq. (1), giving

$$(g)_\pi = \frac{6}{5} g_\ell - \frac{1}{5} g_s \quad .$$

The effective spin $g_s$ can be calculated by taking $g = 0.0956$[37] observed for the $d_{3/2}$ proton of $^{197}$Au. This result gives $g_s = 5.52$. Similarly for the neutron (here $g_\ell = 0$), the spin component can be calculated to be

$$(g)_{\nu} = -\frac{1}{3} g_s \quad .$$

The effective spin $g_s = 2.71$ was obtained from $g = 0.9^{37}$ observed for the $p_{1/2}$ neutron in $^{197}Hg$. The proton and neutron g factors are then coupled using Eq. (2); the result is

$$(g)_{\pi-\nu} = \frac{3}{4} (g)_{\pi} + \frac{1}{4} (g)_{\nu} \quad .$$

Substituting the spin and orbital fraction of the proton and neutron moments in the above equation, one gets

$$(g)_{\pi-\nu} = (\frac{9}{10} g_{\ell} - \frac{3}{20} g_s)_{\rho} - (\frac{1}{12} g_s)_{\nu} \quad .$$

The coupled g factor was then adjusted to reproduce the experimental $g = 0.291$ for $^{196}Au^{37}$ as

$$1 = \{(\frac{9}{10} g_{\ell} - \frac{3}{20} g_s) \frac{1}{0.291}\}_{\pi} - \{(\frac{1}{12} g_s) \frac{1}{0.291}\}_{\nu}$$

$$1 = \qquad \alpha_{\pi} \qquad + \qquad \alpha_{\nu} \quad .$$

These lead to the following fractional contribution of spin and orbital moments to the magnetic moment for $^{196}Au$: $\alpha_s(\pi) = -2.84$, $\alpha_{\ell}(\pi) = +3.09$, $\alpha_s(\nu) = +0.75$. According to Eq. (5), with the stated parameters, the $\varepsilon$'s are

$$\varepsilon(\pi) = +2.5\%$$

$$\varepsilon(\nu) = -2.1\% \quad .$$

The total reduction is $\varepsilon = -0.4\%$. In a similar fashion, calculation were done for the other gold isotopes and the $\varepsilon$'s arrived at are given in Table 7 together with the experimentally observed anomalies. For $^{198}$Au the observed g factor of $^{199}$Au was used for the proton state and for $^{196m}$Au, $^{198m}$Au, and $^{200m}$Au a calculated value $g = 1.48$ for the proton state was used. Since the agreement between measured and calculated anomalies is satisfactory, the calculated values were used for correcting the reported hyperfine fields of $^{198}$Au and $^{197}$Au. Before doing so, however, a few comments can be made on the calculated fractional hyperfine interaction reduction values. Within the framework of the single particle model, states with $j = \ell - 1/2$ are favored to show larger anomalies than those with $j = \ell + 1/2$. This is particularly so for $d_{3/2}$ states; the $p_{1/2}$ and $f_{5/2}$ states show comparable anomalies but they are substantially smaller than those for the $d_{3/2}$. As seen from the Table (7), the $\varepsilon$ for $^{197}$Au, due to the $d_{3/2}$ proton, is by far the largest and for this reason causes much of the anomalies among the gold isotopes. The calculated $\varepsilon$'s for $^{198}$Au and $^{196}$Au are comparable in size, and the observed anomaly is practically zero.[41] Therefore, these states are indeed quite similar, as mentioned before.

Within this framework and assuming the hyperfine field is purely contact (discussed below), a value for the hyperfine field for each gold isotope was obtained from Eq. (4)

$$H_{hf}(A) = H^{i}_{hf}\,(1 + {}^{i}\Delta^{A}) \quad .$$

Table 7. Calculated and measured hyperfine anomalies for different Au isotopes

| A | ε (%) | $^{197}\Delta A$ Cal. | $^{197}\Delta A$ Exp. | $^{198}\Delta A$ Cal. | $^{198}\Delta A$ Exp. |
|---|---|---|---|---|---|
| 197 | 10.3 | --- | --- | -9.0 | -7.96(8)[a] |
| 198 | 0.4 | +9.9 | +8.53(8)[a] | --- | --- |
| 196 | 0.4 | +9.9 | +8.72(24)[b] | 0.0 | +0.2(3)[b] |
| 196m | -1.9 | +12.5 | | +2.3 | |
| 198m | -1.9 | +12.5 | | +2.3 | |
| 200m | -1.9 | +12.5 | | +2.3 | |
| 199 | 4.3 | + 5.8 | +3.7(2)[a] | -3.8 | -4.5(3)[a] |

Superscripts a and b refer to Refs. 42 and 41, respectively.

Here, A refers to either $^{196m}$Au, $^{198m}$Au, or $^{200m}$Au and the i to the effective hyperfine field for either $^{198}$Au(Fe) or $^{197}$Au(Fe). The nuclear moments were derived from the iron data only. The nickel data were not used because in this lattice, since saturation of the anisotropy was not reached, the $|\mu H|$ and amplitude factor parameters of the fit are more strongly correlated. The magnetic moment results for the $12^-$ isomeric gold levels with this correction together with the uncorrected moments (assuming no anomaly) are given in Table 8. The smaller of the two anomalies--that between $^{198}$Au and the $12^-$ levels--was used for this correction.

These derived moments can be compared with the theoretical moments. Assuming the $[\pi h_{11/2}, \nu i_{13/2}]12^-$ configuration, the single particle model moment is

$$\mu_{sp} = 6.0 \text{ nm} \quad .$$

The $h_{11/2}$ proton contribution to the moment was calculated from Eq. (1) and the neutron contribution was assumed to be $\mu = -1.049$ nm from the observed moment of the 13/2 state of $^{195}$Hg.[37] Following the trend of most single particle moments,[13] these values are larger than the observed ones. The single particle proton contribution

$$\mu_{sp} = 7.6 \text{ nm} \quad ,$$

is, in fact, overestimated since the nucleons do interact contrary to the basic assumption of this model. A more realistic estimate of the proton's moment is afforded by the spin polarization procedure of Arima and Horie (see Ref. 50 and Appendix I). According to the proton configuration[50]

Table 8. Summary of derived magnetic moments for the $12^-$ level of $^{196}Au$, $^{198}Au$, and $^{200}Au$

| A | $\lvert\mu H\rvert$ ($10^{-18}$ erg) | $\mu$ (nm) | $\mu$ (nm) |
|---|---|---|---|
| 196 | 30.6(12) | 5.19(20) | 5.35(20) |
| 198 | 30.4(15) | 5.15(20) | 5.29(20) |
| 200 | 34.3(15) | 5.90(40) | 6.04(40) |

$$(g_{7/2})^8(d_{5/2})^6(d_{3/2})^4(h_{11/2})^{11} \quad ,$$

a possible proton-proton interaction is

$$(h_{11/2})^{11}(h_{9/2})^0 \longrightarrow (h_{11/2})^{10}(h_{9/2})^1 \quad .$$

Considering this interaction, the proton contribution is now

$$\mu_{cm}(11/2) = 6.7 \text{ nm} \quad .$$

Coupling this moment to the neutron contribution, one gets the configuration mixed moment

$$\mu_{cm} = 5.67 \text{ nm} \quad ,$$

in good agreement with the observed value assuming a positive sign.

B. Non-Contact Contributions to the Hyperfine Field

From the known magnetic moments of $^{196}$Au and $^{198}$Au,[37] a value for the effective hyperfine field of nickel can be determined from the NMR/ON data on these isotopes. The observed moments differ only slightly, 0.33 (26%) and the anomaly is known to be practically zero.[41] This fact is born out by the essentially equal resonance frequencies found in the NMR experiments. The hyperfine field for $^{198}$Au and $^{196}$Au in nickel of

$$H_{hf} = (-)260.8(13) \text{ KOe} \quad ,$$

was derived using a mean value of the moment $\mu = 0.5897$ nm. The field value was, of course, also corrected for the one KOe polarizing field. This

hyperfine field value may be compared with the one observed from the spin echo method for $^{197}$Au(Ni) of $H_{hf}$ = -292(6) KOe.[39] (The originally quoted value of $H_{hf}$ = -294(4) was determined by using $\mu$ = 0.1439. To be consistent, this field was recalculated using $\mu$ = 0.1435 as it was used in the analysis of the atomic beam results[41] and correcting it for diamagnetism.) Using Eq. (4), the hyperfine anomaly existing between $^{197}$Au and $^{198}$Au can be calculated. The value obtained is

$$^{197}\Delta^{198}_{Ni} = (+12.2 \pm 2.3)\% \quad ,$$

which differs considerably from the anomaly observed from the atomic beam work; namely

$$^{197}\Delta^{198} = (+8.53 \pm 0.08)\%$$

Since the hyperfine anomaly exists only if the hfs results from contact type (AI·S), similar differences in anomalies measured in different chemical environments have been explained in terms of contact and non-contact contributions to the hyperfine field.[40,51,52] Here, the atomic beam measurement essentially corresponds to an isotopic variation of the hfs for the free atoms whereas the anomaly in nickel corresponds to a similar variation but for the atoms plus the lattice. So, assuming a negligibly small quadrupolar splitting of the Zeeman lines (this point will be discussed below) the effective hyperfine field of a point nucleus can be written as a sum of contact terms and non-contact terms

$$H_{hf}^{o} = H_{c}^{o} + H_{nc}^{o} \quad .$$

The contact contributions to $H_{hf}$ can result from any one of several $\vec{I}\cdot\vec{S}$ interactions (see Ref. 53) and would vary from isotope to isotope. The non-contact contributions are associated solely with the lattice and should not change with isotope. Since the anomaly results only from the contact contributions, the differently measured anomalies are related by

$$ {}^{1}\Delta^{2}_{Ni}\, H_{eff} = {}^{1}\Delta^{2}_{c}\, H_{c} \quad . $$

Insufficient data--the $\varepsilon$ for each isotope would be needed--prevent unique determination of the $H_c$ and $H_{nc}$. However, if one assumes that the main contributions to ${}^{197}\Delta^{198}$ and ${}^{197}\Delta^{196}$ arise from the $\varepsilon$ for ${}^{197}Au$, some conclusions can be reached. That is, ${}^{197}\Delta^{198} \sim \varepsilon_{197}$ and taking $H_{hf}({}^{198,196}Au)$ as the "point nucleus" field $H_{hf}{}^{o}$ (since $\varepsilon_{196} \sim \varepsilon_{198} \sim 0$), one arrives at

$$ H_c = \frac{{}^{197}\Delta^{198}_{Ni}}{{}^{197}\Delta^{198}_{c}} (-260.8)\ \text{KOe} $$

$$ = -367 \pm 70\ \text{KOe} \quad , $$

and

$$ H_{nc} = +106 \pm 70\ \text{KOe} \quad . $$

The sign and magnitude of this $H_c$ is within the systematics of $H_{hf}$ fields for trace amounts of 5d elements embedded in nickel.[54] The main contribution results from the Fermi contact term via the core polarization mechanism.

The non-contact term of $H_{hf}$ also called an orbital field[49] could be from any field that can be considered uniform over nuclear dimensions. This term can be written

$$H_{nc} = H_D + H_{dc} + H_\ell \quad .$$

The first term $H_D$ is the contribution from distributions of magnetic dipoles of less than cubic symmetry. Taking the z direction as the axis of symmetry this term can be written

$$H_D = -\mu_s \langle 3\cos^2\theta - 1 \rangle_{avg} / \langle r^3 \rangle_{avg}$$

$$= -\mu_B g \quad ,$$

where $\mu_s$ is the net spin moment, $\mu_B$ is the Bohr magneton and $g = \partial^2 V/\partial z^2$ is the field gradient. This term is often small.[51] The $H_{dc}$ term is the externally applied d. c. field as with normal NMR or, to be discussed later, brute force polarization. The $H_\ell$ field results from electron orbital momentum states with $\ell \neq 0$ and with an orbital moment

$$H_\ell = 2\mu_\ell / \langle r^3 \rangle_{avg} \quad .$$

The orbital field contribution to $H_{hf}$ can be large ($\sim 10^6$ Oe)[55], particularly for rare earth elements. In the transition series, however, it is often, though not necessarily, quenched: $\langle L_z \rangle = 0$.[55] From recent results, however, it seems likely that the main component of $H_{nc}$ is the orbital field due to the orbital momentum of the 5d gold electrons.[56] That is, the $5d_{3/2} - 5d_{5/2}$ free atom spin-orbit splitting in this region is 1.5 to 2 eV while one can

take as the crystal field coupling strength the width of the 5d band in metallic gold, 5 eV. With the crystal field coupling strength being almost of order the spin-orbit coupling and since the 5d spins are polarized through the exchange field and consequently contribute to $H_c$ via spin-exchange polarization of inner s electrons, one does not expect complete quenching of the orbital momentum. The positive sign of $H_{nc}$ would indicate that the orbital and spin moments of the 5d gold electrons are polarized parallel. The magnitude of the non-contact field is of the order of the non-contact fields found for other gold[40] and iridium isotopes.[51] However, as mentioned before, the orbital fields are generally much larger. Therefore, one can only assume that the orbital momentum is only fractionally unquenched.

As pointed out by Stone,[57] hyperfine anomalies derived from Eq. (4) when the $H_{eff}$'s are measured by nuclear orientation may be misleading if there is significant quadrupolar splitting of the Zeeman lines. In ON the pure Zeeman interaction leads to 2I + 1 evenly spaced energy levels unequally populated. A quadrupolar perturbation of the Zeeman lines would result in unevenly spaced energy levels with still, however, unequal populations. Randomization of the unevenly spaced levels by a rf field would lead to a frequency shift, large for large spins, relative to the pure Zeeman line and the $H_{eff}$ thereby determined would be in error. As yet, no such shifts have been observed; they would clearly depend on the quadrupole coupling constant in a given lattice. This coupling constant is known for neither $^{196}$Au nor $^{198}$Au in nickel. It is expected to be small since the quadrupole moments should be small.[37]

Furthermore, according to Stone's calculations, the shifts should be small for spins this size. It seems reasonable then that the anomaly measured in nickel is in fact good within the errors quoted.

In Table 9 the magnetic moments of the $12^-$ gold levels are given. In this case, however, the hyperfine field in iron was corrected for non-contact contributions according to

$$H_{hf}(A) = H_c^{\,i}\,(1 + {}^{i}\Delta^{A}) + H_{nc} \quad .$$

A value for $H_{nc}$ of +270 KOe was taken from the work of Stone[40] for iron. For these results the largest deviation between calculated and measured hyperfine anomalies including the correction for the non-contact contributions was taken as the error. All of the measured moments support the $[\pi h_{11/2}, \nu i_{13/2}]12^-$ assignment which gives $\mu = 5.67$ nm. The $^{196m}$Au and $^{198m}$Au moments agree more with each other, however, than with the $^{200m}$Au moment. The $^{200m}$Au moment differs by more than 10% from the $^{196m}$Au moment. The difference may be due to a different neutron moment contribution to the $i_{13/2}$ neutron of this state. A similar behavior has been observed for the 13/2 neutron state of $^{195}$Pt where the moment differs by more than 0.4 nm[58] from known moments for corresponding Hg isotopes.

## C. The Decay Scheme of $^{200m}$Au

As mentioned earlier, anisotropies were observed for five--256-, 368-, 498-, 580-, and 760 keV--of the six gamma lines of $^{200m}$Au. Using gamma ray anisotropy data, proposed energy level schemes of isotopes can be supported;

Table 9. Summary of derived magnetic moments corrected for non-contact contribution to the hyperfine field for the $12^-$ level of $^{196}Au$, $^{198}Au$, $^{200}Au$.

| A | $\mu$ (nm) |
|---|---|
| 196 | 5.35(20) |
| 198 | 5.55(34) |
| 200 | 6.10(20) |

however, because of the insensitivity of the magnitude of $U_k F_k$ coefficients to small differences in assumed angular momenta--spin or multipole order--the level scheme itself cannot unambiguously be elucidated. In this light, the anisotropy data for $^{200m}$Au will be discussed in accord with the latest proposed level scheme, indicated in Fig. 10, by Ton et al.[59] Table 6 summarizes the anisotropy results together with the calculated coefficients. The observed results were determined from a fit of the data to $W(\theta)$ with $|\mu H|$ and $I = 12$ held constant, from the resonance experiments, and the coefficients as free parameters.

The 368-, 580-, and 760 keV Transitions

A multipolarity of E2, with $I_i - I_f = 2$, is established for the 368 and 580 keV transitions.[60] The 580 keV transition accompanies the de-excitation of the $4^+$ state to the $2^+$ state which in turn de-excites to the $0^+$ ground state by emitting the 368 keV gamma. The magnitude and sign (Fig. 2) of the measured anisotropies agree with the E2 assignment. The 760 keV transition is known to follow the decay of the 1.07 ns level at 1.7 MeV from $\gamma$-$\gamma$ and $\gamma$-$e^-$ coincidence experiments.[59] Further, Ton et al. assumed by analogy with other even mass isotopes in this Z region that the level that de-excites by the 760 keV line had either spin $4^-$ or $5^-$. However, the sign of the observed $U_2F_2$ and $U_4F_4$ coefficients favors a spin 6; spin $4^-$ or $5^-$ leads to a positive anisotropy. Comparison with other even mass Hg isotopes[61] suggests a positive parity for this state.

The 256- and 498 keV Transitions

The 256 keV and 498 keV transitions precede the 1.07 ns level, although their relative order has not been established. The positive

anisotropy data for the 256 keV strongly suggests a dipole character, $I_i - I_f = 1$, for this transition. Taking into account the relative gamma intensities of the cascading transitions, its multipole character is likely E1. Similarly, the negative anisotropy of the 498 keV line suggests a predominant E2 character. Since no spins are known for the levels above the 1.7 MeV state, no very definite statements can be made. The measured magnitude of the coefficients are consistent with either a state of spin 10 or 8 de-exciting to a state of 9 or 7 emitting the 256 keV (E1) gamma ray. Likewise, it can only be said that the 498 keV line, probably E2, de-excites from a state of spin 10 or 9 to one of spin 8 or 7 since the observed coefficients are negative. At present though, there are insufficient data to further interpret the $U_k F_k$ coefficients for the 256- and 498 keV transitions.

## MAGNETIC RESONANCE ON $^{195m}$Pt ORIENTED IN IRON

There exist also in this Z region many one particle high spin states. The even-odd mass isotopes, of which $^{195}$Pt and $^{197m}$Hg are examples, generally have spins of I = 13/2 arising from the single $i_{13/2}$ neutron whereas the odd-even mass isotopes, e.g. $^{197m}$Au and $^{195m}$Au, have spins of 11/2 from the single $h_{11/2}$ proton. During the course of this work all of the above mentioned isotopes were studied with, however, inconclusive results due to uncertainties in internal fields, mixing ratios and nuclear spin-lattice relaxation times. One successful case, though, was the 4.1 d isomer of $^{195}$Pt. Since this is a neutron state, the magnetic moment is expected to be small, but with the large induced hyperfine field for Pt(Fe)[12], sizable anisotropies were expected.

### I. Experimental

#### A. Activity Production and Preparation

The $^{195}$Pt activity was produced by thermal neutron irradiation, by a flux of $2.5 \times 10^{15}$ n/cm$^2$-s, of 57% enriched $^{194}$Pt foils. Because of the small thermal neutron cross section, the irradiation times varied from one week for the orientation experiments to two weeks for the resonance work. Foils for the orientation experiment were made by melting a portion of the target with a $^{60}$Co(Fe) foil under $H_2$ gas. The final concentrations were typically $\leq 1$ at. % platinum in iron. Alternate cold rolling and annealing yielded foils of about 0.005 inch thickness. These foils were then attached to the copper fin of the cooling apparatus described in Chapter 4. Here, as before, the polarizing field was 4 KOe.

Major contaminants from the neutron irradiation would be $^{197}$Au and $^{199}$Au from the beta decay of $^{197}$Pt and $^{199}$Pt, respectively. For increased specific activity the gold was separated from the platinum by HCl-ethyl acetate extraction[29] for the resonance foils. The target was dissolved in aqua regia, evaporated to dryness and taken up with 6M HCl followed by ethyl acetate-HCl extraction. The platinum rich phase is the aqueous phase which was evaporated to dryness. Platinum activity, in the form of platinum black, was obtained by adding dilute HCl and Mg powder. Subsequently, the platinum black was dried and melted with high purity iron. As with the orientation foils, foils of thickness about 20000 Å were made by rolling and annealing. Copper was vapor deposited onto the thin foils to facilitate soldering to the copper fin.

## B. Results

The isomeric decay of the 13/2 state of platinum occurs through several gamma transitions (Fig. 15), the most intense ones being the 129 keV and 99 keV transitions. Anisotropy data were accumulated and processed as previously described for these two lines and the $^{60}$Co lines. In this case temperatures in the 6 mK range were reached. A least squares fit of the anisotropies to the distribution function led to a weighted average value for the magnetic hyperfine interaction constant of

$$|\mu H| = 3.873 \pm 0.030 \times 10^{-18} \text{ erg} \quad ,$$

from the 129 keV anisotropy data. An amplitude factor/mixing ratio and $|\mu H|$ were the free parameters for this fit. In the analysis of the

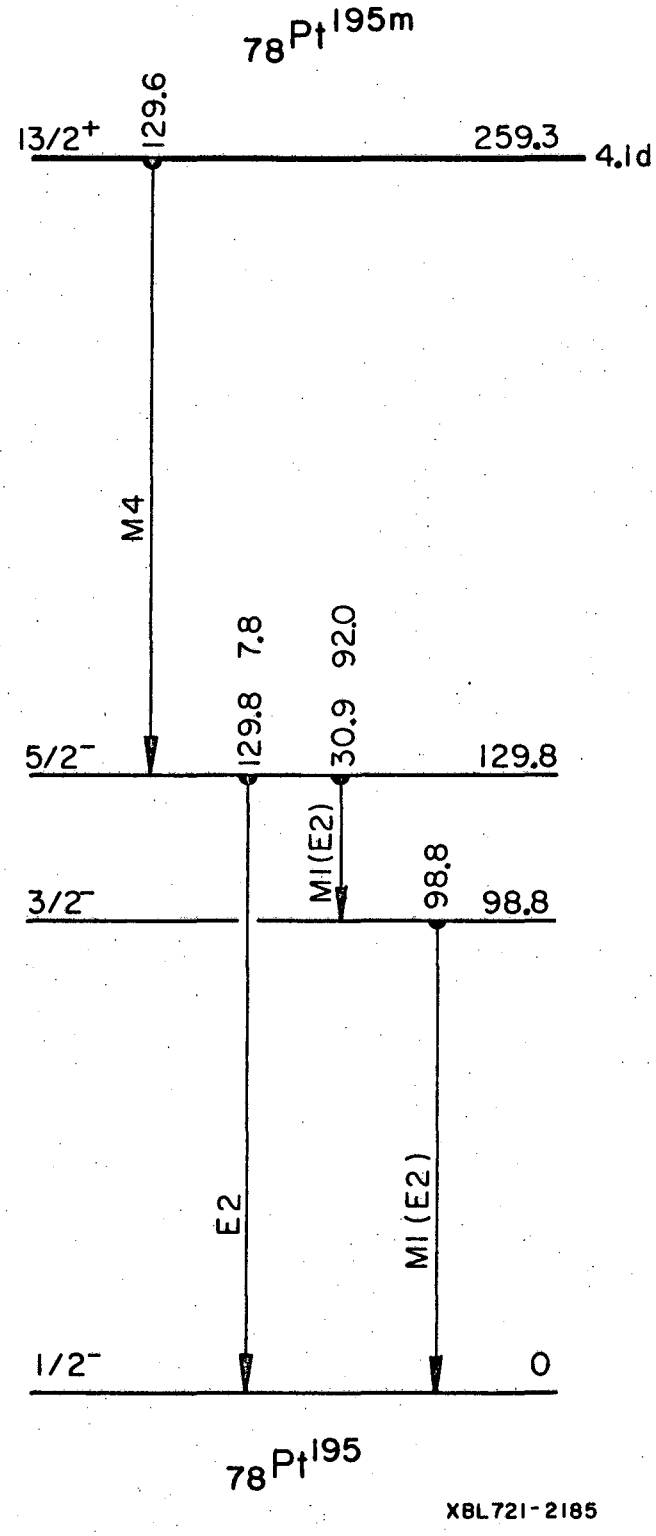


Fig. 15. Decay scheme of $^{195m}Pt$.

129 keV gamma ray, the influence of the 129.6 keV M4 transition was taken into account. For this purpose, the branching ratios used were those of Schöneberg,[62] the conversion coefficient $\alpha = 1.76 \pm 0.19$ for the 129.8 keV was from Ref. 63, and the theoretical conversion coefficient of 1230 for the 129.6 keV was taken from Ref. 64. From these values, the ratio of the gamma intensity of the M4 transition to that of the E2 transition at 129 keV was calculated to be 0.029.

The insensitivity of $|\mu H|$ to assumed spins of this size obtained from anisotropy fits is again demonstrated in Column 2 of Table 10. The anisotropy of the 129 keV was fitted using $|\mu H|$ as a single parameter and assuming various spins. The resulting $|\mu H|$'s are independent of the assumed spin within the error limits--again demonstrating that only a value of the magnetic moment can be obtained from the anisotropy curves.

The E2/M1 mixing ratio for the 99 keV transition obtained from the orientation work is

$$\delta = -0.14 \pm 0.03 \quad .$$

Figure 16 shows the zero degree anisotropy data for a) the 99 keV transition and b) the 129 keV line.

For the resonance experiment the intensities of the 99 keV, 129 keV, and 158 keV gamma rays of $^{199}$Au were separately measured with the 4-Channel Multi-Scalar at zero degrees with Na(I) detectors as a function of the applied rf frequency. Figure 17 shows the fitted resonance curve for the 99 keV gamma corresponding to a resonance frequency of

$$\nu = 89.5 \pm 0.5 \text{ MHz} \quad .$$

Table 10. Results of a one parameter fit of the anisotropy curve for the 129 keV γ line of $^{195m}$Pt(Fe) for various values of the spin I of the isomeric state.

| I | $\lvert\mu H\rvert$ ($10^{-18}$ erg) | $(\gamma H)_{ON}/(\gamma H)_{NMR}$ |
|---|---|---|
| 9/2 | 3.872 ± 0.031 | 1.451 ± 0.020 |
| 11/2 | 3.867 ± 0.030 | 1.186 ± 0.016 |
| 13/2 | 3.873 ± 0.030 | 1.005 ± 0.013 |
| 15/2 | 3.882 ± 0.030 | 0.873 ± 0.012 |
| 17/2 | 3.892 ± 0.030 | 0.772 ± 0.010 |

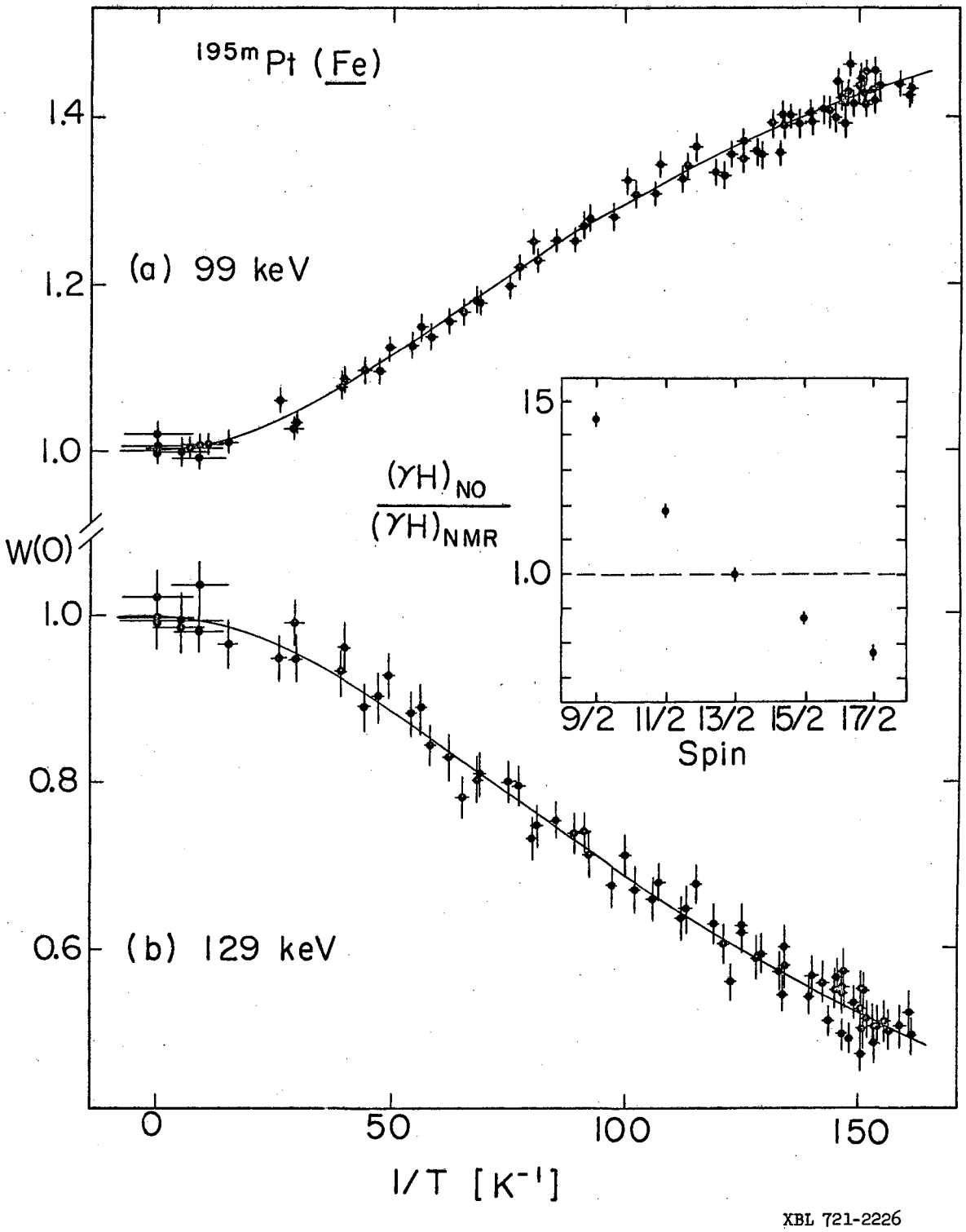


Fig. 16. The zero degree gamma ray anisotropy vs. 1/T curves for (a) the 99 keV gamma and (b) the 129 keV gamma of $^{195m}$Pt oriented in iron. The solid curves are the results of a theoretical fit of the data to the distribution function. The insert is a plot of the ratio $|\gamma H|_{ON}$ and $|\gamma H|_{NMR}$ versus assumed spin for the isomeric level of $^{195}$Pt.

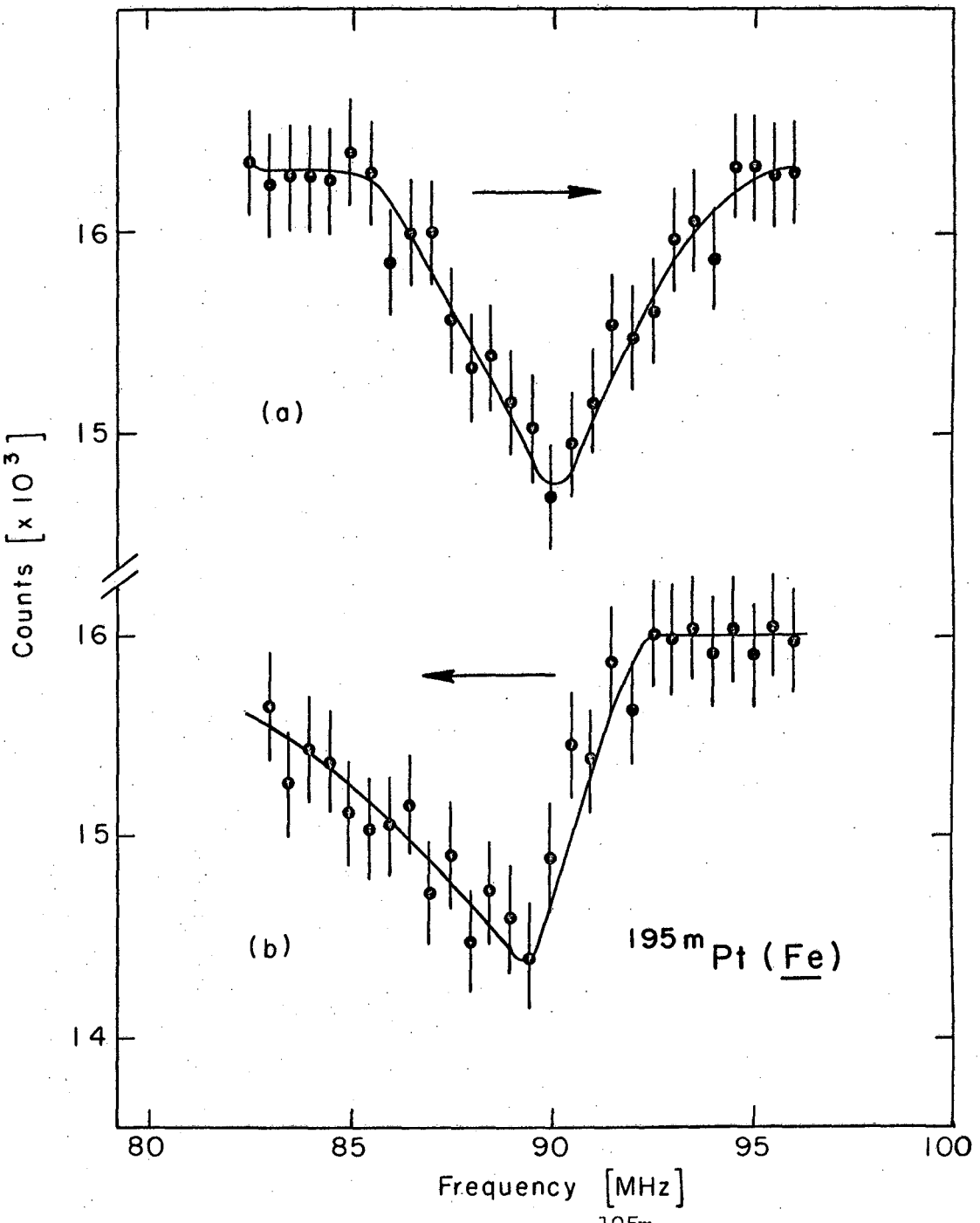


Fig. 17. The magnetic resonance curves for $^{195m}$Pt oriented in iron. Curve (a) refers to upward sweeps and curve (b) refers to downward sweeps in frequencies. The solid curves are the results of a gaussian plus straight line fit to the measured intensity of the 99 keV gamma. The $H_1$ amplitude was 0.8 mOe and the fm frequency was 100 Hz over a bandwidth of one MHz. Each point corresponds to 0.5 MHz.

In this case, the rf amplitude was 0.8 mOe with a modulation frequency of 100 Hz over a bandwidth of one MHz. The step width is 0.5 MHz per point of 3.5 min time interval. The sloping background is due to rf heating and the relative shifts of the curves measured for increasing vs. decreasing frequencies are due to the long nuclear spin-lattice relaxation time $T_1'$. A single exponential fit[11] gave $T_1' = 10 \pm 1$ min at an inverse temperature of $1/T = 150 \pm 5\ K^{-1}$. (See Fig. 18.) A similar resonance curve was observed for the 129 keV gamma ray. The 158 keV gamma ray of $^{199}$Au showed no effect, thus eliminating the possibility of sample heating from coil resonances. This possibility was further excluded by passing over the resonance region without frequency modulation, under which conditions no effect was observed.

The assigned 13/2 spin for this state was verified through agreement of the $(\gamma H)_{ON}/(\gamma H)_{NMR}$ ratio for only a spin of 13/2. The sensitivity of this method is demonstrated by a plot of this ratio versus assumed spins given in the insert of Fig. 16 and Column 3 of Table 10. As alluded to before, the sensitivity increases with decreasing spin value.

The E2/M1 mixing ratio of the 99 keV transition was again determined by using $\delta$ as a single free parameter with $|\mu H|$ fixed from the resonance results. The fit of the anisotropy vs. 1/T now gives

$$\delta^* = -(0.16 \pm 0.02) \quad ,$$

in agreement with the mixing ratio determined from the orientation results. The absolute value of $\delta$ is in good agreement with previous measurements,[66,67] but the negative sign is opposite to the one given in Ref. 67.

---

*In the definition of Biedenharn and Rose, Ref. 65.

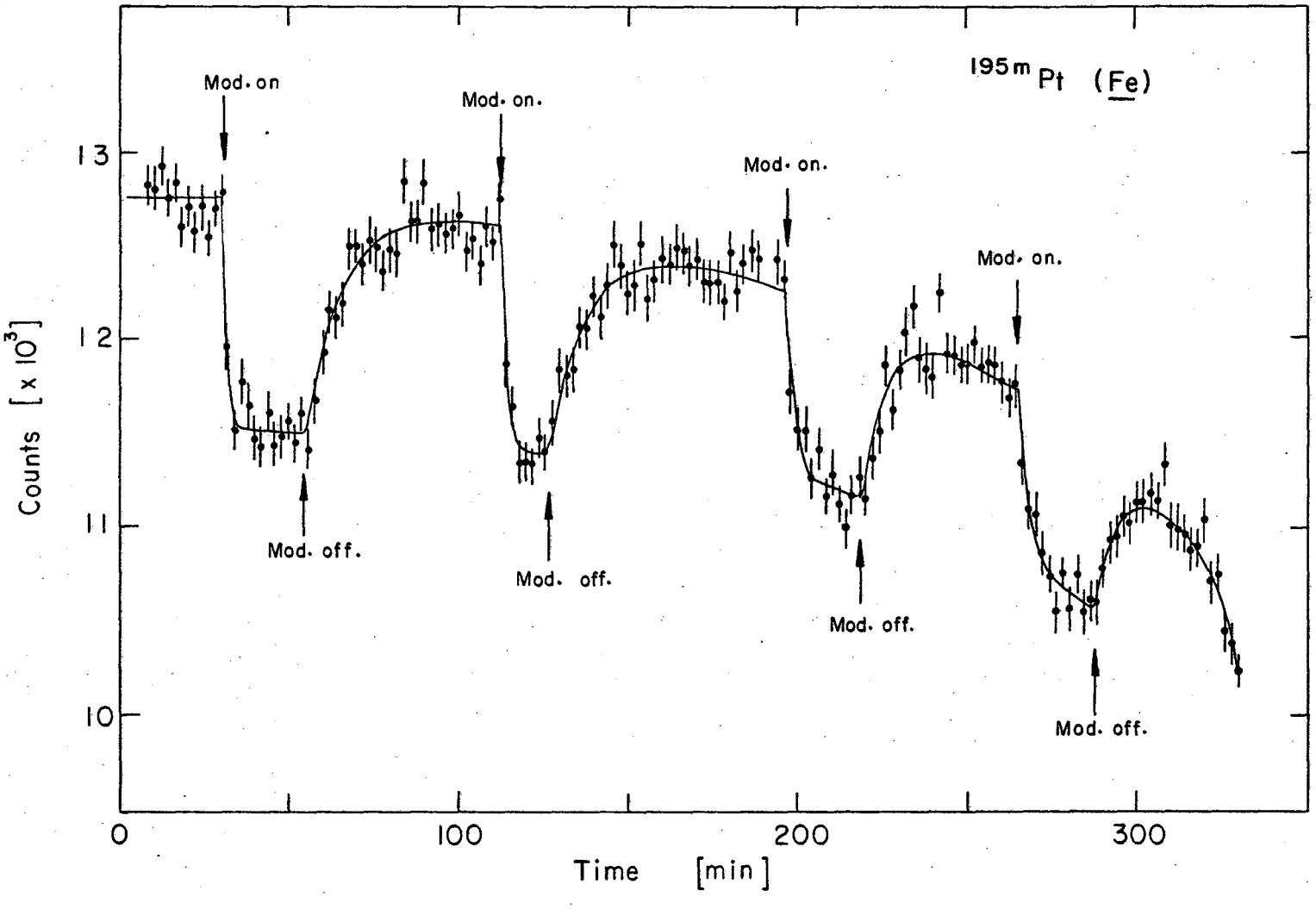


XBL7112-4941

Fig. 18. The nuclear spin-lattice relaxation time curves observed for $^{195m}$Pt in iron. These data results from the intensity measurements of the 99 keV gamma under conditions of fm on with frequency of 100 Hz over a bandwidth of one MHz, $H_1$ amplitude of 0.8 mOe and $\nu$ = 89 MHz and fm off. The solid curve is a fit of the intensities to a single exponential plus hyperbolic background.

II. Discussion

For a derivation of the magnetic moment of the $13/2^+$ state, the hyperfine field $H_{hf}(T = 0) = -1280 \pm 26$ KOe observed for the $1/2^-$ ground state of $^{195}$Pt in iron was used.[39] This leads to

$$\mu = \pm 0.597 \pm 0.015 \text{ nm} \quad .$$

The negative sign is assumed from systematics. A correction for a possible hyperfine anomaly between the isomeric and ground levels has not been applied. In the neighboring odd mercury isotopes $^{195}$Hg and $^{197}$Hg, however, the anomalies between the 13/2 and 1/2 states have been measured: $^{195m}\Delta^{195} = +0.91 \pm 0.02\%$ and $^{197m}\Delta^{197} = +0.97 \pm 0.07\%$.[68] A hyperfine anomaly of this size can also be expected between the analogous states of $^{195}$Pt. For this reason, the quoted value for the moment should perhaps be decreased by 1%.

The result for the spin of the isomeric state confirms the spin assignment made on the basis of the M4-multipolarity of the 129 keV isomeric transition.[69] For $^{195m}$Pt a neutron configuration $(i_{13/2})^{13}(f_{5/2})^4$ outside of the N = 82 core and filled $f_{7/2}$ and $h_{9/2}$ neutron shells are expected since the $p_{3/2}$, $p_{1/2}$, $f_{5/2}$, and $i_{13/2}$ levels are very close in energy; hence, the neutron pairs are expected to fill the states of higher angular momentum first due to the relative pairing energies. This neutron configuration is also suggested from a calculation of $\mu_{cm}$. Of the two possible neutron configurations which would lead to configuration mixing

1) $[82]\ (f_{7/2})^8(h_{9/2})^{10}(i_{13/2})^{13}(p_{3/2})^4$

2) $[82]\ (f_{7/2})^8(h_{9/2})^{10}(i_{13/2})^{13}(f_{5/2})^4$ ,

only the second one leads to neutron-neutron-proton interaction corrections to the single particle moment giving a moment μ of -0.64 nm in agreement with the observed one.

The measured moment may be compared with moments of other $13/2^+$ neutron states in neighboring even-odd nuclei:[68,70] $^{195}$Hg(μ = -1.0280(2) nm), $^{197}$Hg(μ = -1.0112(3) nm), $^{193}$Hg(μ = -1.0416(3) nm), and $^{205}$Pb(μ = -0.975(39) nm). In going from Pt to Hg, where the proton $d_{3/2}$ shell is being filled, the effect of the two additional protons on the magnetic moment is obviously quite drastic and much larger than expected on the basis of the single particle moment with configuration mixing. For the Hg isotopes the magnetic moments of the $13/2^+$ states have been interpreted assuming mixed neutron configurations with fewer than 13 neutrons in the $i_{13/2}$ shell. This interpretation is in agreement with the small spectroscopic factor (S = 7.4) for the $13/2^+$ state derived from (d,p)-stripping and (d,t)-pick-up reactions on $^{198}$Hg and $^{200}$Hg, respectively.[60] The question, however, of whether such a difference in the neutron configurations can explain the pronounced differences in the magnetic moments of the 13/2 state of $^{195}$Pt and the even-odd Hg isotopes cannot be clarified at the present time, since too little is known about the wavefunctions of these states.

## BRUTE FORCE POLARIZATION OF $^{93m}$Mo

The 21/2 isomeric state of $^{93}$Mo[71,72] presented an ideal case for brute force polarization. This 6.9 h lived level is a three particle state of two protons and a neutron with shell model configuration $[\pi(g_{9/2} - g_{7/2})^2, \nu d_{5/2}]21/2$. The two protons and the neutron are expected to yield a very large nuclear moment within shell model considerations. The $^{93m}$Mo was oriented in niobium and subsequently in iron, in which lattice a resonance experiment was done. The details of these experiments follow.

### I. Experimental

#### A. Activity Production and Chemistry

Targets for both the brute force and iron orientation were produced from naturally occurring $^{92}$Nb metal ($\sim$ 100% natural abundance) foils of thicknesses 15 - 10 mg/cm$^2$ by either a (p,n)-reaction or a (d,2n)-reaction. The former, and less efficient, reaction required 18 MeV protons for 60 μA hrs and the latter required 13 MeV deuterons for 30 μA hrs at the LBL 88" Cyclotron. The deuteron irradiation populated exclusively the 21/2 level whereas the proton irradiation also produced a longer lived isotope with two gamma lines at $\sim$ 840 keV and 450 keV.

The $^{93m}$Mo(Nb) foils for the brute force polarization were made by simply cutting an area with the appropriate activity from the bombarded target. Since soft solder does not tin niobium metal, a layer of copper was vapor deposited onto the foils as described in Chapter 4.

The $^{93m}$Mo(Fe) foils for ON experiments were made by melting a piece of the active niobium foil with a 99.999% iron foil, a typical concentration being 0.6 at. % Nb(Fe). The $^{93m}$Mo(Fe) foil was then melted with a $^{60}$Co(Fe) foil and, to insure a homogeneous mixture, the melting was repeated at least three times. Thereafter, the foil was rolled into the shape of a disc approximately 0.004 inch thick and annealed. The NMR/ON foil was identically prepared except that no thermometer was added and the final thickness was about 10000 Å.

## B. Brute Force Apparatus Description

The brute force apparatus was designed to provide high field-high homogeneity NMR experiments on oriented nuclei (see Fig. 19); the components are discussed below.

### 1. The Superconducting Magnets and Their Brute Force Operation

The specifications for the superconducting polarizing and cooling magnets are given in Table 11 and Table 12, respectively. To minimize the effect of the high field polarizing magnet at the site of the cooling salt, the distance between the two was such that at 50 KOe the fringe field would be less than the internal dipolar field of CMN. A distance > 15 inches was arrived at from the approximate expression for the axial field variation outside of a solenoid

$$H_z = H_o/2 \{\cos \beta - \cos \alpha\}$$

where $\alpha$ and $\beta$ are angles about the solenoid's center line from the upper and lower ends respectively. The actual separation is 18 inches. The

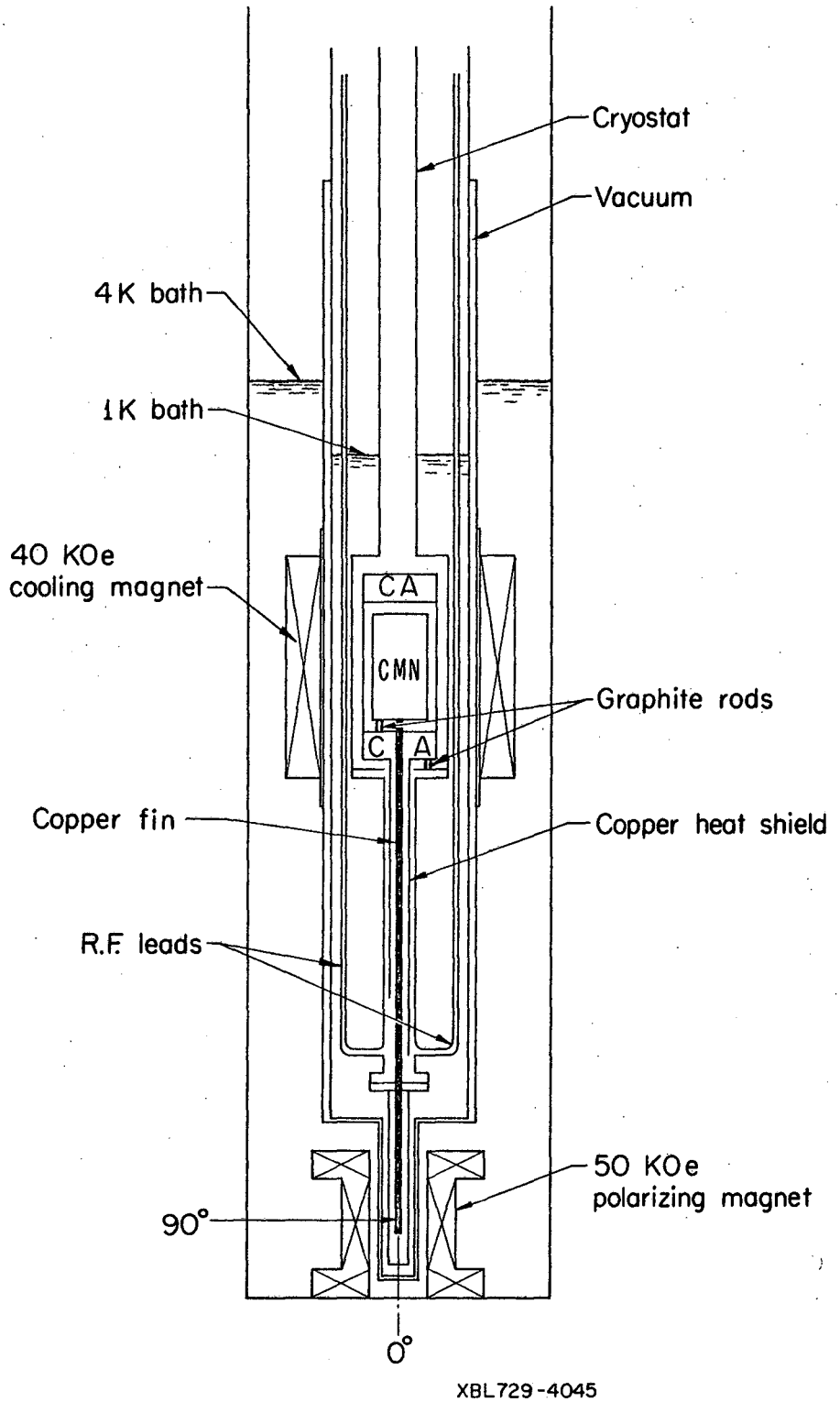


Fig. 19. The magnetic cooling apparatus used for the brute force polarization of $^{93m}$Mo in niobium.

Table 11. List of polarizing solenoid specifications

I. Geometry of a sixth order solenoid with ear thickness twice that of the body
   A. Length of 10.062 inches
   B. Inner diameter of bore form of 2.125 inches

II. Coil constant of 534.3 gauss/ampere*
   A. Transition current of 95 amperes
   B. Critical charge rate of > 0.5 volts

III. Superconducting wire
   A. 12.5/20 NbTi superconductor
   B. Winding length of 8.39 inches
   C. Number of layers
      1. 22 for body
      2. 44 for ears

IV. Room temperature resistance of 18 ohms and LN temperature resistance of 12 ohms

V. Persistent mode switch
   A. Pure NbTi wire of 0.015 inch diameter
   B. Maximum current capacity of 100 amperes
   C. Heater switch resistance of 35 ohms

*Measured with gaussmeter of accuracy 0.1%.

Table 12. List of cooling solenoid specifications

I. Geometry of a straight solenoid

   A. Length of 14 inches

   B. Inner diameter of bore form of 5.25 inches

II. Calculated coil constant of 236 gauss/ampere

   A. Transition current $I_c$ of 190 amperes

   B. $I_c$ insensitive to charge rate

III. Superconducting wire

   A. 15/30 NbTi

   B. Winding length of 10.375 inches

IV. Room temperature resistance of 155 ohms and LN temperature resistance of 18 ohms.

V. One eighth inch thick Mu metal bore form

polarizing field was reduced in this manner rather than by using magnetic compensating coils because the effect of field compensation on the homogeneity would have been uncertain. In addition, the polarizing field was operated in the persistent mode (see Appendix IV for comments). In a separate experiment, mentioned below, no measurable field decay occurred over a 12 hour period. The current for this magnet was measured by a digital millivoltmeter (Data Technology Corp.) which allowed 1/100 millivolt readings.

For orientation in ferromagnetic lattices, the cooling magnet typically operates at a field of 40 KOe and after demagnetizing the polarizing field is charged to 4 KOe. This procedure, however, does not work at all for brute force orientation because of severe eddy current heating of the copper fin. In a separate experiment using $^{60}$Co(Fe) and after demagnetizing, the polarizing field was charged to 4 KOe and the temperature reached was 1/T = 190. Thereafter, the field was charged at different rates and fields with the result of an increase in temperature of about 2 millidegree K for an average charge rate of less than 2 KOe/min. For this reason, another method had to be found. The method finally adopted involved concurrent operation of both cooling and polarizing solenoids each at operating field strengths. The procedure, which worked well, is outlined below.

1) Before magnetization and pumping of the 1 K bath, the polarizing magnet was charged (at < 0.5 volts) to a field of about 45 KOe.

2) With the polarity of the cooling magnet opposite to that of the polarizing magnet, magnetization and pumping proceeded as usual (see Ref. 32). The cooling magnet operating field was 30 KOe.

3) After both magnets were at their maximum operating values for about thirty minutes, the polarizing magnet was placed in persistent mode.

To prevent damaging the persistent mode switch and the magnet in the event of mishaps, the switch should perhaps remain normal until demagnetization is complete. This can be done but with an appreciable increase in liquid helium boil-off.

As mentioned earlier, the polarizing magnet was designed to have a high field homogeneity, although to no advantage in the present orientation experiment. The homogeneity (or spatial variation of the field over a one $cm^3$ sample probe) was determined by a home made NMR probe tuned to 40 MHz. The sample consisted of the protons of $H_2O$ doped with $CuSO_4$ to reduce the relaxation time; its approximate volume was one $cm^3$. Using a magnetic field of H = 9340(10) Oe the homogeneity was determined to be better than $1/10^5$ over a 1/2 inch axial distance. The measured field variation itself is given in the Appendix IV for future use. One should be aware, however, that the values given are valid only if coil deterioration has not occurred through electrical shorts.

2. The Salt Pill

The salt pill had the same functional design as the one described in Chapter 4. For the top CA guard pill and CMN salts, the containers were made from 0.005 inch thick electrolytic grade copper, and the bottom CA guard salt was made from 0.010 inch thick mylar. The CMN cylinder of diameter 2.625 inches and height 7 inches contained about 400 $cm^3$ of cooling salt slurry in contact with 18 copper fins for indirect cooling of the sample.

The top CA pill with about 100 $cm^3$ of salt provided the heat shield for the CMN, and the bottom CA pill (about 100 $cm^3$) served as a one degree heat sink. Thermal insulation between the CMN and bottom CA container and between the bottom CA container and the cryostat was provided by pitch-bonded graphite rods and fibreglass. The thermal link between the cooling salt and the sample site was provided by a 24 inch long silver soldered copper stalk (1/4 × 1/8 × 1/8 inch) the top of which diverged into fins giving a contact area of about 1800 $cm^2$. This stalk had a heat shield in contact with CA. A relaxation process was observed at the start of an experiment through the gradual growth of the anisotropy. (Typically for a ferromagnetic polarization, it would take about 15 minutes for the anisotropy to level off.) The relaxation most likely reflects the heat removal due to eddy current heating from the magnet as opposed to a thermal relaxing of the stalk since for the brute force no drastic relaxation was observed. Once cold, the pill would remain so for about nine hours.

3. Cryostat

The pill container of the cryostat was made from a 0.065 inch thick 3.5 inch O.D. copper tube. The joints were either silver soldered or PbSn (50-50% by weight) soldered with no apparent superconducting effects on the salt pill from the latter solder which is superconducting. The pumping tube was a 1.5 inch O.D. stainless steel tube. The tail of the cryostat was attached by means of a Varian flange. To insure against superleaks, the copper gaskets were indium coated by soldering.

4. The 4 K Dewar

The 4 K liquid helium dewar stands 72 inches high and has no liquid nitrogen heat shield. Instead of the 77 K heat shield, thirty layers of 0.00025 inch thick aluminized mylar interwoven with nylon net served to insulate against room temperature radiation. The outer wall of this dewar consists of a 0.094 inch thick stainless steel cylinder 10 inches in diameter and the inner wall has a 0.016 inch thickness and a 8.5 inch inner diameter. The dewar's liquid helium volume, when the apparatus is completely assembled, is about 35 liters. At liquid helium temperatures, the operating pressure for the dewar is typically $1 \times 10^{-6}$ mm. Its boil-off rate during magnetization is 0.7 liters/h, if thermal equilibrium is reached. Because of the proximity of the cooling magnet to the top of the 4 K bath, two liquid helium refills ($\sim$ 6 liters each) are often required before demagnetization. These refills, of course, include a safety level of 6 inches of helium above the magnet; one refill might suffice though. It is, however, very essential in using this dewar that thermal equilibrium be established. With the 500 liter liquid helium dewar (Cryogenic Engineering Company) the 4 K bath can be filled within 45 minutes, but this is far too rapid to insure thermal equilibrium and a better filling schedule would be one and one half to two hours.

5. The 1 K Dewar

The inner wall of this 1 K dewar consists of a 0.035 inch thick stainless steel tube 4-1/2 inches in outer diameter; the bottom end is tapered to an ID of about 1-1/2 inches. The outer wall of this dewar is made of copper to provide a better 4 K heat shield. The copper shield

covers two thirds of the total height of the inner wall and is made from a 0.065 inch wall 5 inches in OD tube. The outer wall is also tapered, but to two inches to fit into the polarizing magnet. During 77 K pre-cooling, no liquid nitrogen is placed in the 1 K bath but rather about 30 μ of helium gas is introduced into its vacuum jacket. Subsequent evacuation, at the start of liquid helium transfer, proceeds rapidly (within 45 minutes) to an operation pressure of $< 10^{-7}$ mm.

6. Vacuum Pumps

Continuous pumping of the 1 K and 4 K dewars are provided by oil diffusion pumps described elsewhere.[30] A 160 liter/second Consolidated Vacuum oil diffusion pump serves to evacuate the cryostat. For pumping on the one degree bath a KMBV 1250 Kinney pump was used.

## C. Electronics

The electronics for the $^{93m}$Mo(Nb) and $^{93m}$Mo(Fe) experiments were the same as those for the gold experiment described in Chapter 4.

## D. Data Taking and Processing

In the orientation experiments for $^{93m}$Mo(Fe), a 4 KOe field was applied parallel to the plane of the foil. Fifteen minute full spectrum counts--the 263-, 675-, and 1479 keV gammas of $^{93m}$Mo and the $^{60}$Co gamma lines--were taken continuously with two Ge(Li) detectors at zero and ninety degree angles. These data were stored on magnetic tape by use of a PDP-7 computer as already described. A 44.3 KOe polarizing field was used for the $^{93m}$Mo(Nb) orientation with only one Ge(Li) detector at zero

degrees. Continuous fifteen minute full spectrum counts were also taken for this experiment and the data similarly stored.

For the resonance work, data were accumulated as described in Chapter 4 with a Na(I) detector at zero degrees. In this case, however, a window was set on the energy range 230 keV to 1490 keV since there were no contaminant gamma lines. The applied $H_1$ = 0.5 mOe was frequency modulated at 100 Hz over a bandwidth of one MHz.

The data processing was described in Chapter 4.

## E. Results

### 1. Polarization of $^{93m}$Mo in Niobium and Iron

The $^{93m}$Mo(Nb) anisotropy results are summarized in Table 13. The zero degree anisotropies for the 263- and 1479 keV gammas for the brute force experiment were fitted using a single free parameter, $|\mu H|$, without an amplitude factor. This procedure was necessary because saturation of the anisotropies was not reached. The temperatures were determined from a $^{60}$Co(Fe) foil soldered adjacent to the $^{93m}$Mo(Nb) foil. The thermometer anisotropies were corrected for the 44.3 KOe external field. The average of the magnetic hyperfine interaction constant from the 263 keV and 1479 keV gammas is

$$|\mu H| = (1.73 \pm 0.06) \times 10^{-18} \text{ erg} \quad .$$

Figures 20 and 21 show the corresponding anisotropies for the 263- and 1479 keV transitions respectively as a function of 1/T for a 44.3 KOe field.

The results of a simultaneous fit of the zero and ninety degree data for the $^{93m}$Mo(Fe) orientations are given in Table 14 for all three

Table 13. Summary of experimental results for $^{93m}$Mo(Nb)

| γ (keV) | $\lvert\mu H\rvert$ ($10^{-18}$ erg) |
|---|---|
| 263 | 1.64 ± 0.06 |
| 1479 | 1.82 ± 0.08 |

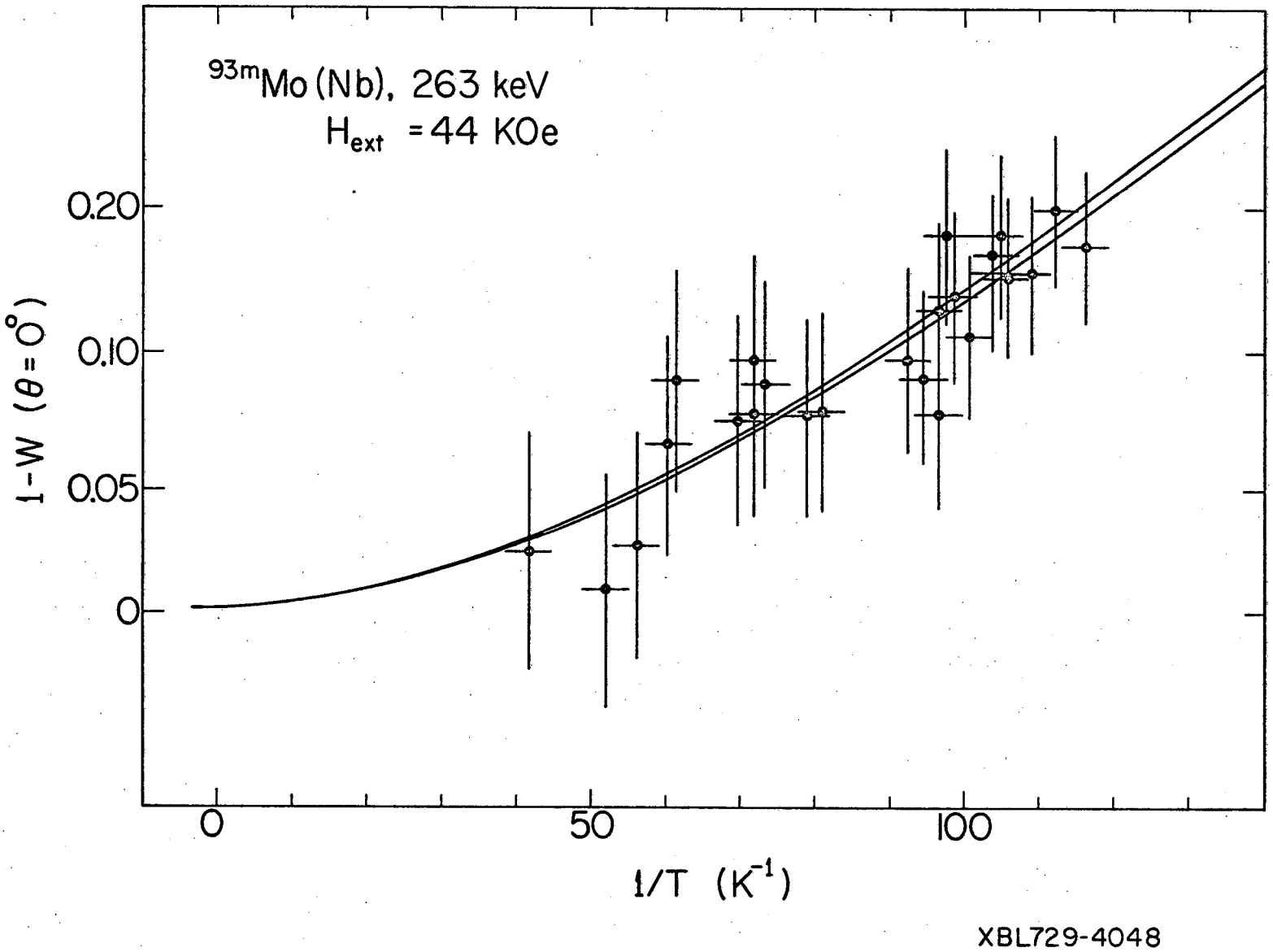


Fig. 20. The zero degree anisotropy vs. 1/T curve for the 263 keV gamma of $^{93m}$Mo oriented in niobium. The solid curve is a single parameter fit of the anisotropy of the distribution function.

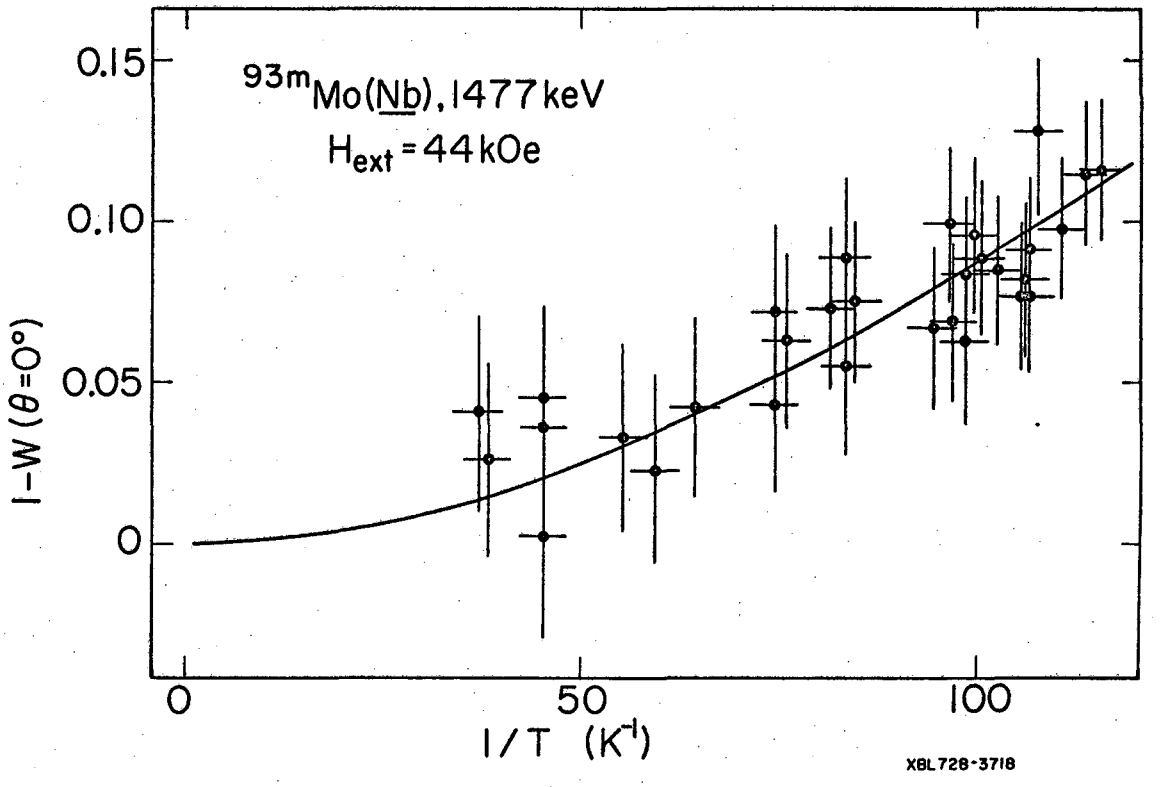


Fig. 21. The zero degree anisotropy vs. 1/T curve for the 1479 keV gamma of $^{93m}$Mo oriented in niobium. The solid curve is a single free parameter fit of the anisotropy to the distribution function.

Table 14. Summary of experimental results for $^{93m}$Mo(Fe)

| $\gamma$ (keV) | $\lvert\mu H\rvert$ ($10^{-18}$ erg) | $\delta$ |
|---|---|---|
| 263 | 12.24(19) | 0.177(6) |
| 685 | 11.89(36) | 0.188(39) |
| 1479 | 12.11(39) | 0.199(38) |

transitions. Here, the decay scheme is well known (see Fig. 22), so the $U_k F_k$ (k = 2,4) coefficients are calculable. (A program named UCO, which can calculate any $U_k$ coefficient, was written to calculate $U_4(21/2, 13/2, 4, 4)$.) Therefore $|\mu H|$ and an amplitude factor are the only free parameters needed. The weighted average of

$$|\mu H| = (12.15 \pm 0.15) \times 10^{-18} \text{ erg} \quad ,$$

here obtained agrees within the errors with the weighted average of

$$|\mu H| = (12.08 \pm 0.16) \times 10^{-18} \text{ erg} \quad ,$$

from a single spectrum fit of the data. The amplitude factors $\delta$ are all the same within error limits and suggest about only 97% magnetization of the foil. That is, the explicit form of $\delta$ appears in the fit as $1/(1 + \delta^2)$, and it should be zero provided there are no multipole admixtures in the transitions. The $W(\theta)$ vs. $1/T$ simultaneous fits of the zero and ninety degree data for the 263 keV (a), the 675 keV (b), and the 1479 keV (c) gammas are shown in Fig. 23.

2. NMR/ON on $^{93m}$Mo(Fe)

Searching in the frequency range suggested by the iron anisotropy results and with rf conditions given in the Experimental Section, the resonance frequency was found at

$$\nu = 170.5 \pm 0.4 \text{ MHz} \quad .$$

Figure 24 shows the gaussian plus straight line fit of the curve where each point corresponds to one megacycle. The best fit value of the HWHM is 1.09 MHz. This resonance frequency gives a magnetic hyperfine splitting of

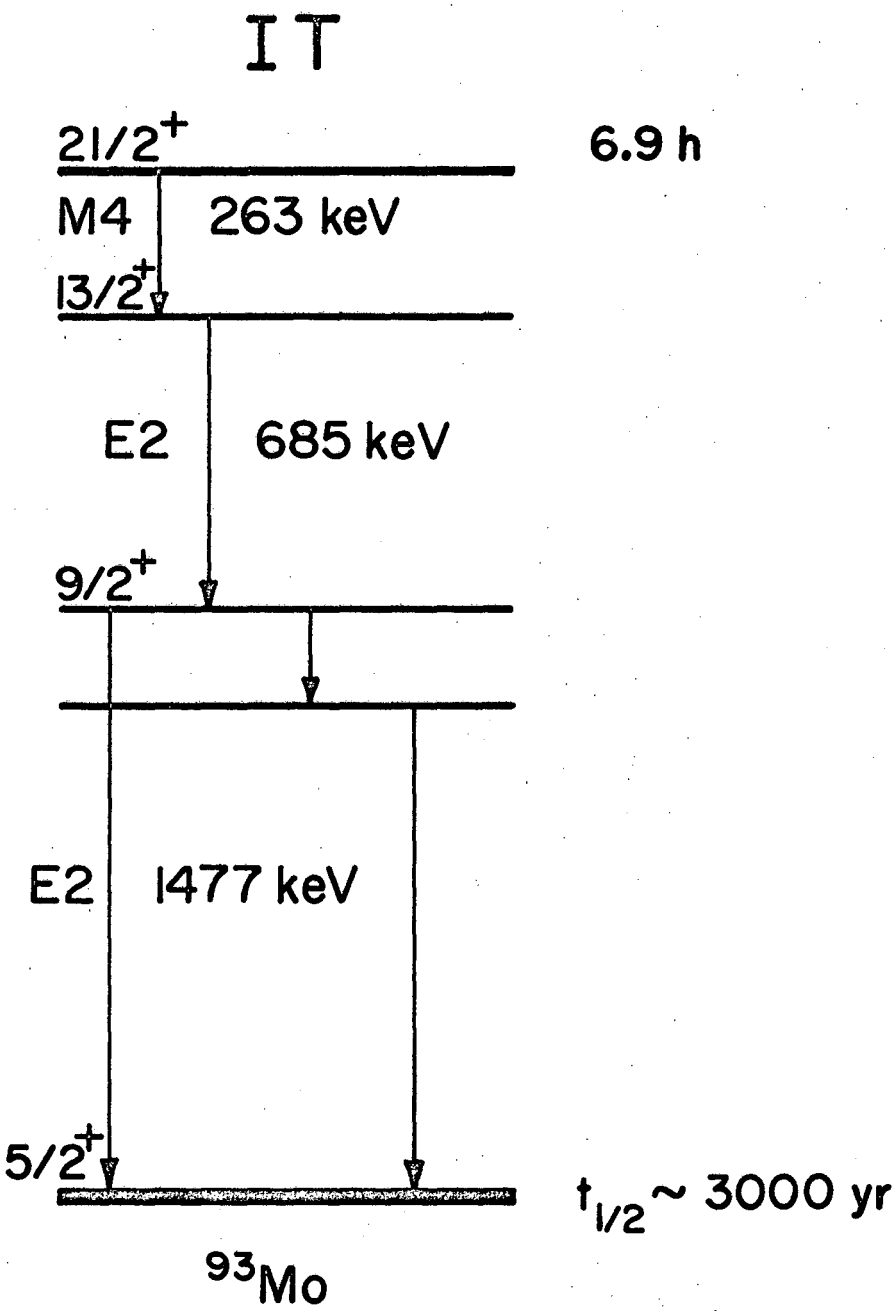


Fig. 22. Decay scheme of $^{93m}$Mo.

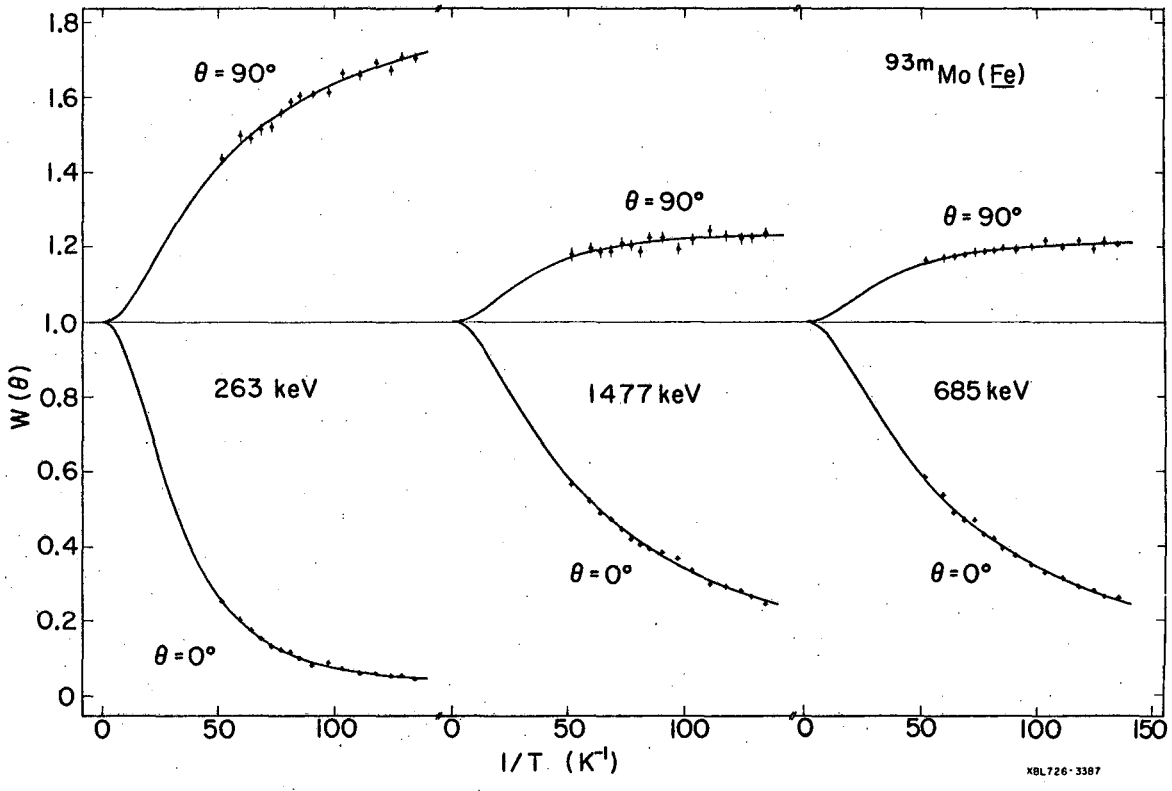


Fig. 23. Temperature dependences of the 263-, 1479-, and 685 keV gamma-ray anisotropies of $^{93m}$Mo oriented in iron. The solid curves are the results of a simultaneous fit of the zero and ninety degree data to the distribution function.

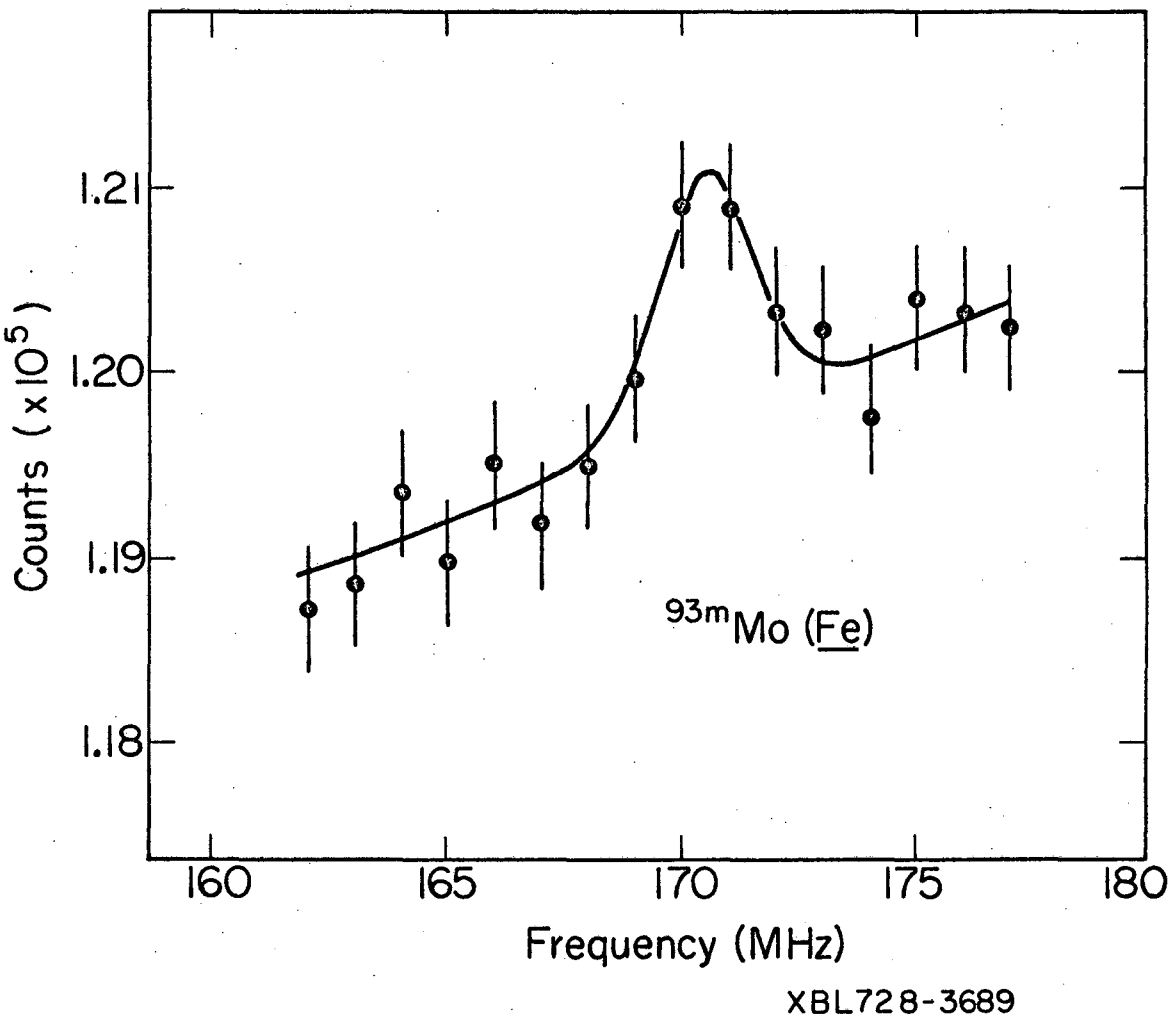


Fig. 24. Resonance curve for the $^{93m}$Mo in iron. The solid curve is a gaussian plus straight line background fit to the summed measured measured intensities of the 263-, 685-, and 1479 keV gammas. The HWHM is about 1 MHz. The $H_1$ amplitude was 0.5 mOe and the fm frequency was 100 Hz over a one MHz bandwidth.

$$|\gamma H| = (1.1294 \pm 0.0026) \times 10^{-18} \text{ erg} \quad .$$

Agreement between the ratio of $|\gamma H|_{ON}$ to $|\gamma H|_{NMR}$ is reached only for a spin of 21/2, the assigned spin. Table 15 summarizes the results of this ratio for various assumed spins. As in the case of $^{200m}$Au for which I = 12, the error reflects the lower sensitivity of this method for large spin values.

II. Discussion

Taking $H_{hf} = 252 \pm 5$ KOe[12] for the hyperfine field of molybdenum in iron, one gets a magnetic moment for the 21/2 level of $^{93}$Mo from the anisotropy data of

$$\mu = \pm(9.55 \pm 0.31) \text{ nm} \quad ,$$

where the weighted average of the simultaneous fit data was used. This value agrees with the one determined from the NMR/ON results

$$\mu = \pm(9.21 \pm 0.20) \text{ nm} \quad .$$

The sign of the moment, most likely positive, cannot however be determined from these experiments since even powers of $P_k(\cos \theta)$ are observed.

In spite of the fact that the hyperfine field was measured for the ground state of $^{95}$Mo, little or no corrections are expected due to a hyperfine anomaly. For this element (Z = 42), the anomaly should be very small (< 1%) since it increases as $Z^2$; e.g., for the classic hyperfine anomaly case, $^{85}$Rb and $^{87}$Rb, $^{85}\Delta^{87} = 0.3513$.[44] Nonetheless, an analysis of the $^{95}$Mo and its excited state was carried out, the results of which are

Table 15. Summary of results of the $(\gamma H)_{NO}/(\gamma H)_{NMR}$ ratio with various assumed spins for $^{93m}Mo(\underline{Fe})$

| I | $(\gamma H)_{NO}/(\gamma H)_{NMR}$ |
|---|---|
| 23/2 | 0.946 ± 0.014 |
| 21/2 | 1.036 ± 0.016 |
| 19/2 | 1.145 ± 0.017 |

$$^{95}\Delta^{93m} = -0.16\% \quad ,$$

with

$$\epsilon_{93m} = -0.36\% \quad ,$$

and

$$\epsilon_{95} = -0.52\% \quad .$$

Here, the effective spins of each of the three nucleons were derived as

$$(\nu d_{5/2}): g_s = -1.82 \text{ with } \mu(5/2\ \nu) = -0.913 \text{ nm} \quad [37]$$

$$(\pi g_{7/2}): g_s = +3.31 \text{ with } \mu(7/2\ \pi) = +2.6 \text{ nm} \quad [37]$$

and

$$(\pi g_{9/2}): g_s = 12.32 \text{ with } \mu(9/2\ \pi) = +6.16 \text{ nm} \quad [37]$$

from $^{95}$Mo, $^{99}$Tc, and $^{93}$Nb, in that order. These particles were then coupled through two successive uses of Eq. (2): first, the two protons were coupled such that g = 1.36 measured for $^{90m}$Zr, I = 8,[37] and second, the two-proton state was coupled to the neutron adjusted to give g = 0.94 calculated for $^{93m}$Mo from the single particle model. An anomaly this size would not significantly alter the moment results, aside from the fact that the calculated anomalies are generally larger than the experimental ones.

The $^{93m}$Mo isomer has been described as a case of "core isomerism"[73] where the isomerism is ascribed to an excitation of the even-even core

to a high spin state, presumably 8. This most likely proceeds by breaking up a $g_{9/2}$ pair of protons with one of the protons going into the $g_{7/2}$ state. The odd neutron probably remains in the $d_{5/2}$ state during this transition. The total excitation energy of this state of 2.4 MeV supports this assumption since it is roughly the sum of the energy due to the breaking up of a $g_{9/2}$ proton pair (1 to 2 MeV) and the flipping of spin $g_{9/2} \rightarrow g_{7/2}$ (spin-orbit energy $\sim$ 1.5 MeV). Furthermore, from the calculated single particle moment of

$$\mu_{sp} = 9.97 \quad ,$$

assuming a shell model configuration of $[\pi(g_{9/2} - g_{7/2})^2, \nu d_{5/2}]21/2$, one sees that there is qualitative agreement with the observed one. For this calculation the moment of $\mu$ = 10.89 nm[37] of the $8^+$ state of $^{90m}Zr$ was taken as the $g_{9/2} - g_{7/2}$ proton pair contribution and $\mu$ = -0.913 nm[37] of $^{95}Mo$ as the neutron contribution. The agreement between the observed and calculated moments together with the measured spin supports the shell model configuration for this isomer.

Since the applied magnetic field for the brute force is known, $H_{ext}$ = 44.32 ± 0.05 KOe, a value for the magnetic moment can be determined directly

$$\mu = 7.76 \pm 0.25 \text{ nm} \quad .$$

This moment is outside of the error limits of the previously reported moment for the $^{93m}Mo(\underline{Fe})$ experiment. It seems unlikely that the difference results from the 21/2 "single level anomaly" or $\varepsilon_{93m}$; in fact, a calculation supports this. As earlier mentioned, a brute force

polarization provides a method for studying the fractional reduction of the hyperfine interaction of an isotope or level. This can be seen as follows. In an environment, say a ferromagnet, where the hfs results in part from an $A\vec{I}\cdot\vec{S}$ interaction, the effect of the hyperfine anomaly on the hfs constant $a_1$ can be written

$$a_1 = a_{pd}(1 + \epsilon_i) \quad ,$$

where i refers to a single level. For a brute force polarization, however, the externally applied magnetic field is uniform over the nuclear volume and the only contact interactions present are the negligible contributions arising from spin paramagnetism. Casting this problem in terms of a hfs constant $a_2$ for this case, one can write

$$a_2 = a_{pd} \quad ,$$

and the ratio of the constants gives

$$a_1/a_2 = 1 + \epsilon_i \quad .$$

For a ferromagnetic and brute force polarization the a's are

$$a_1 = \mu_i H_{hf} \quad ,$$

and

$$a_2 = \mu_i H_{dc} \quad ,$$

respectively. If R equals the ratio of the hyperfine field to the external field, the relationship

$$\frac{a_1}{a_2} = R(1 + \varepsilon_i) \quad ,$$

must hold if the level has an anomaly, which is from the above equation (Eq. (6))

$$\varepsilon_i = \left(\frac{a_1}{a_2}\right) R^{-1} - 1 \quad .$$

This result should hold in general and implies a unique method for measuring the single-level hyperfine anomalies. Using Eq. (6), one finds

$$\varepsilon_{93m} = 0.22 \quad ,$$

in disagreement with the calculated $\varepsilon_{93m}$.

The difference perhaps may be due to quadrupolar splitting of the Zeeman lines. Other molybdenum isotopes, $^{97}$Mo and $^{95}$Mo, do have quadrupole moments,[37] and the $^{93m}$Mo is also expected to have one. Any quadrupolar splitting would make a greater perturbation in the brute force results, since the magnetic hyperfine interaction is smaller, than in the iron orientation work. The result would be that the assumed pure Zeeman Hamiltonian would no longer completely describe the interactions and a quadrupolar interaction would have to be added. The quadrupolar effects cannot at present be estimated because of a lack of quadrupole moment and field gradient data.

(For a critique on brute force polarization see Appendix II.)

## MAGNETIC RESONANCE ON ORIENTED $^{101m}$Rh

Though not necessarily a high spin state, another isotope, $^{101m}$Rh, studied proved interesting from the point of the induced hyperfine fields at this impurity site. The 9/2 spin isomer of $^{101}$Rh has a 4.5 d halflife and from systematics should arise from a $g_{9/2}$ proton state. As predicted earlier,[74] this element as a solute in nickel may be a localized moment case. Nuclear orientation experiments were done on this isotope in iron and nickel and a resonance was detected in nickel.

### I. Experimental

#### A. Activity Production and Chemistry

The $^{101m}$Rh activity was produced by a (d,2n)-reaction, deuteron energy of 25 MeV, on a ruthenium metal target. Foils for most of the experiments were prepared from a 99.999% single crystal; however, a few foils were prepared from less pure ruthenium. The carrier free $^{101m}$Rh activity was obtained by the standard ruthenium-rhodium separation[75] which takes about one and one half man days. A few conveniently efficient modifications[76] have been made and, for this reason, the chemistry will be treated more thoroughly. The targets are prepared from naturally occurring ruthenium with no noticeable active contaminants. The requisite steps in the separation follow.

1) Fuse the ruthenium-rhodium target with $Na_2O_2$ in a nickel crucible at 350 C for one and one half hours.

2) Dissolve the residue (predominantly a mixture of Rh, Ru, and Ni, from the crucible) in hot aqua regia. Centrifuge out the insolubles and keep the supernate.

3) Add $H_2SO_4$ and a saturated solution of $KBrO_3$ to the supernate of #2 and heat to $\sim$ 100 C. The Ru is distilled out in this process.

4) Make the solution, now containing mainly Ni and Rh cations, basic with 6 M NaOH. In this step, the Rh is almost quantitatively co-precipitated ($\sim$ 95%) as an hydroxide with the Ni(OH).

5) Wash with $H_2O$ and dissolve the ppt in dilute $HNO_3$. Add 5 mg of $Fe^{3+}$ to precipitate $Fe(OH)_3$ by adding $NH_4OH$. Here, the Rh carries quantitatively on the $Fe(OH)_3$ ppt and the nickel amine complex remains in solution.

6) Dissolve the iron-rhodium hydroxides in 6 N HCl and solvent extract the rhodium from the iron with ethyl ether.
Generally, since most commercially available ethyl ethers contain iron,[76] the rhodium rich aqueous phase was further separated from iron by using a Dowex 1 anion exchange column equilibrated at pH = 8. The rhodium passes through the column whereas the iron remains. The separated rhodium was subsequently electroplated onto a high purity iron or nickel foil. These foils were thereafter melted together with either a $^{60}Co$ in iron or nickel foil in $H_2$ gas. Alternate rolling and annealing of these foils would yield $\sim$ 0.004 inch thick orientation and $\sim$ 10000 Å resonance foils.

The foils were attached to the copper fin of the magnetic cooling apparatus described in Chapter 4 and cooled to temperatures of about 4 mK. In the orientation experiment, full spectrum data were taken as already mentioned for the two most intense $^{101m}Rh$ gamma lines, the 306.7 keV and 544 keV. The energy level scheme is given in Fig. 25.

## B. Results

The results of the iron and nickel experiments are summarized in Table 16 for both transitions and for both zero and ninety degree data.

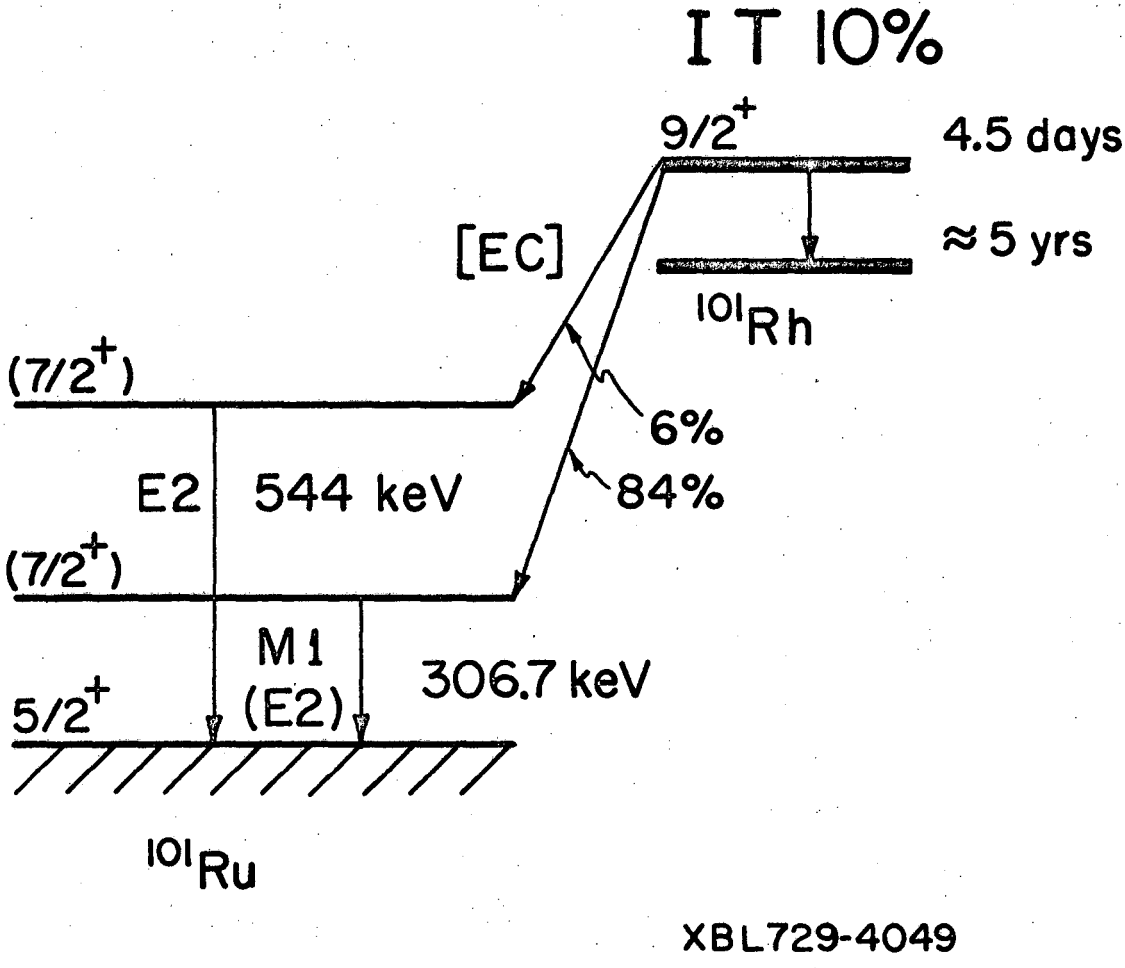


Fig. 25. Decay scheme for $^{101m}$Rh.

Table 16. Summary of experimental results for $^{101m}Rh$

| Host | θ | γ-line (keV) | $\lvert\mu H\rvert$ ($10^{-18}$ erg) |
|---|---|---|---|
| Fe | 0° | 306.7 | 12.04(37) |
| Fe | 90° | 306.7 | 14.65(75) |
| Fe | 0° | 544. | 12.86(150) |
| Ni | 0° | 306.7 | 6.14(17) |
| Ni | 90° | 306.7 | 6.39(28) |
| Ni | 0° | 544. | 7.51(106) |

Like other fits, these results follow from a two free parameter fit, $|\mu H|$ and $\delta$, of single spectrum data to $W(\theta)$ vs. 1/T. The low intensity of the 544 keV did not allow analyses of the ninety degree data. The average of the hyperfine interaction constant for the iron lattice is

$$|\mu H| = (12.56 \pm 0.32) \times 10^{-18} \text{ erg} \quad ,$$

and

$$|\mu H| = (6.21 \pm 0.22) \times 10^{-18} \text{ erg} \quad ,$$

for the nickel lattice. Figures 26 and 27 show the anisotropy vs. 1/T curves for the 306.7 keV transition in iron and nickel, respectively; Figs. 28 and 29 show the same for the 544 keV.

Figure 30 shows the fitted observed resonance curve for $^{101m}$Rh(Ni). Here, the radiofrequency conditions were $H_1$ = 0.8 mOe, fm frequency of 100 Hz and bandwidth of 1 MHz; each point corresponds to one MHz. The fit gives for the resonance frequency

$$\nu = 206.5 \pm 0.2 \text{ MHz} \quad ,$$

from which the magnetic hyperfine interaction in nickel is

$$|\mu H| = (6.14 \pm 0.01) \times 10^{-18} \text{ erg} \quad .$$

This value is in good agreement with the nickel nuclear orientation work, which was used to direct the resonance search. Thus the 9/2 spin assignment is confirmed.

From the average of $|\mu H|$ for the iron data plus errors, the frequency range of 380 MHz to 433 MHz was searched for the resonance. In a subsequent

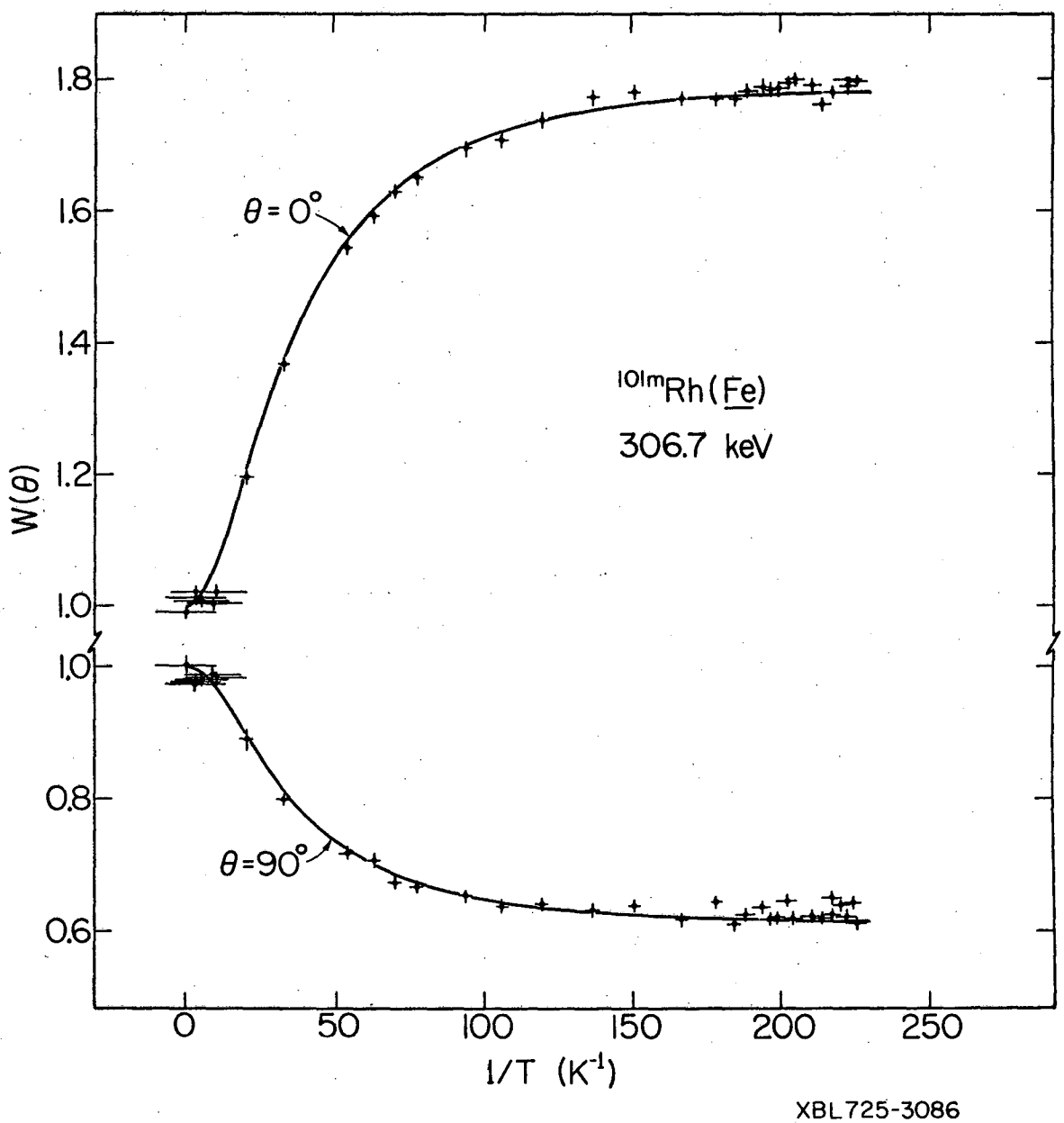


Fig. 26. The temperature dependence of the anisotropy of the 306.7 keV gamma of $^{101m}$Rh oriented in iron. The solid curves are the results of a simultaneous fit of the zero and ninety degree data to the distribution function.

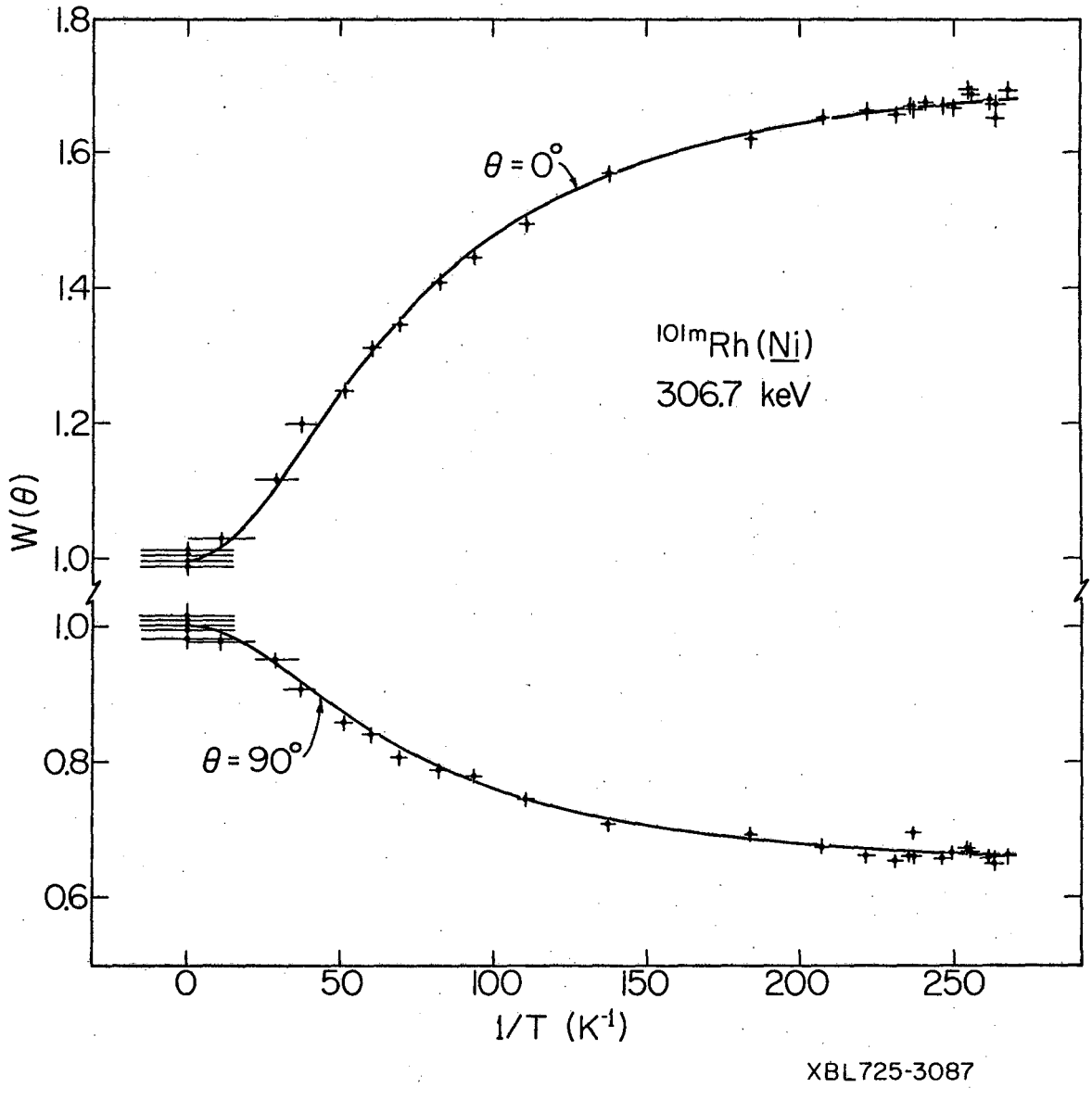


Fig. 27. The temperature dependence of the anisotropy of the 306.7 keV gamma of $^{101m}$Rh oriented in nickel. The solid curves are the results of a simultaneous fit of the zero and ninety degree data to the distribution function.

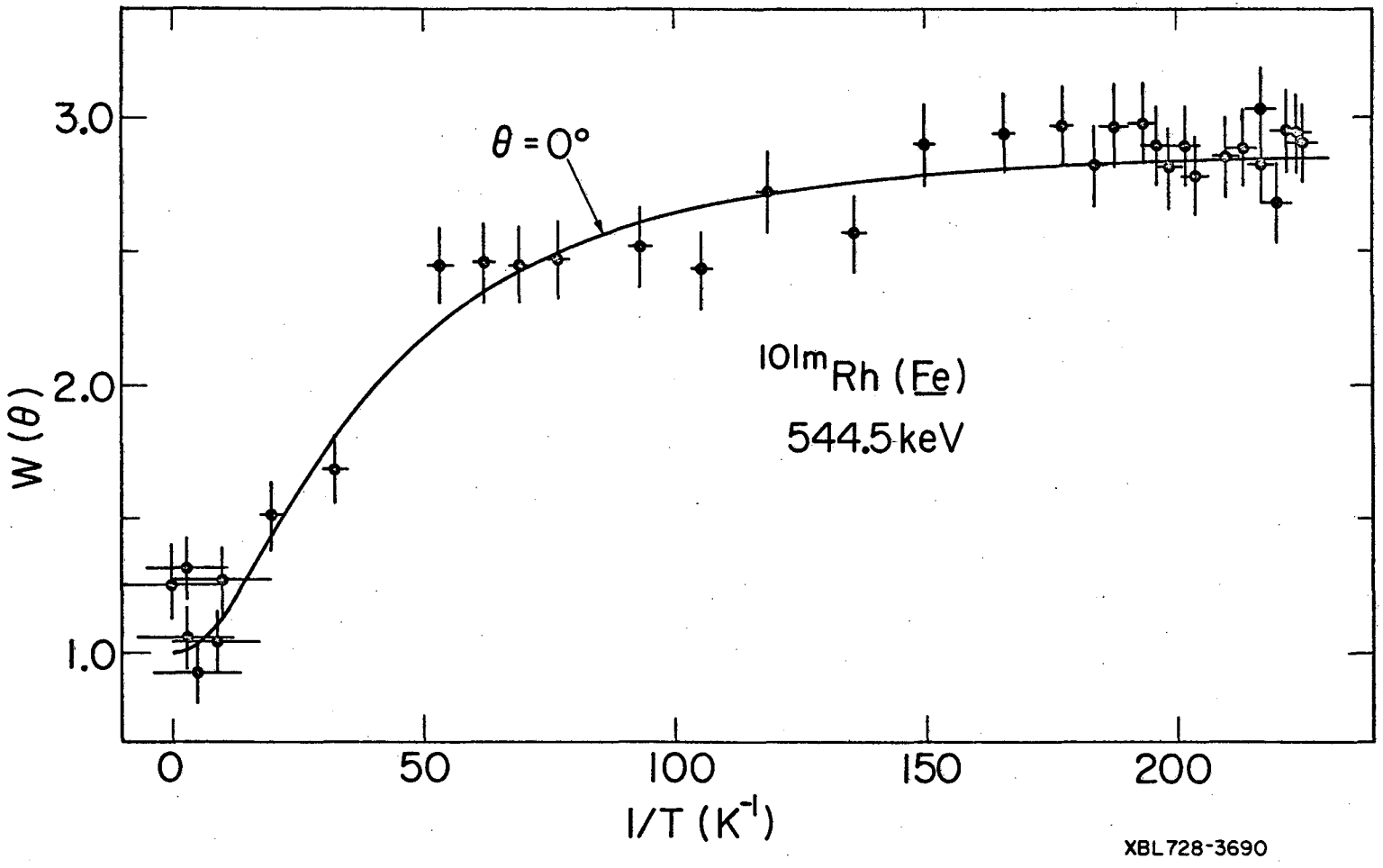


Fig. 28. The temperature dependence of the anisotropy of the 544 keV gamma of $^{101m}$Rh in iron. The solid curves are the results of a simultaneous fit of the zero and ninety degree data to the distribution function.

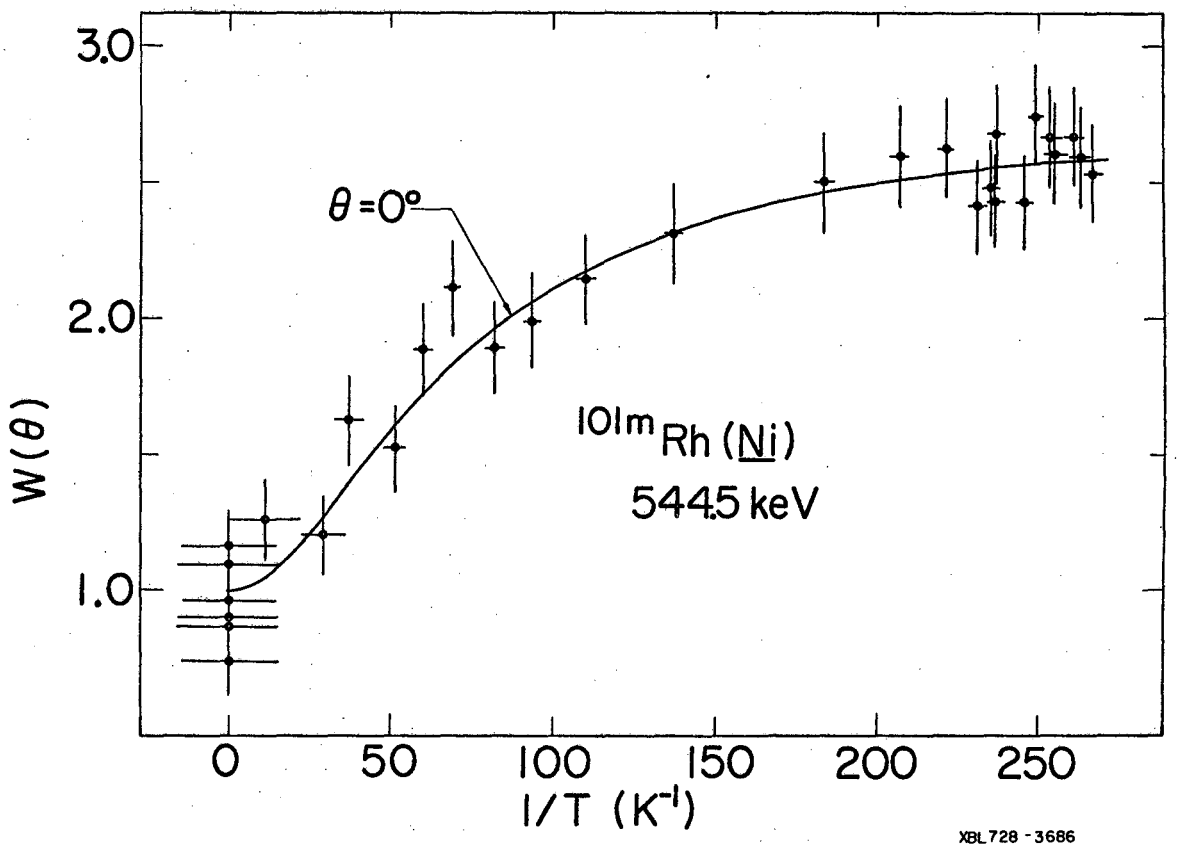


Fig. 29. The temperature dependence of the anisotropy of the 544 keV gamma of $^{101m}$Rh oriented in nickel. The solid curves are the results of a simultaneous fit of the zero and ninety degree data to the distribution function.

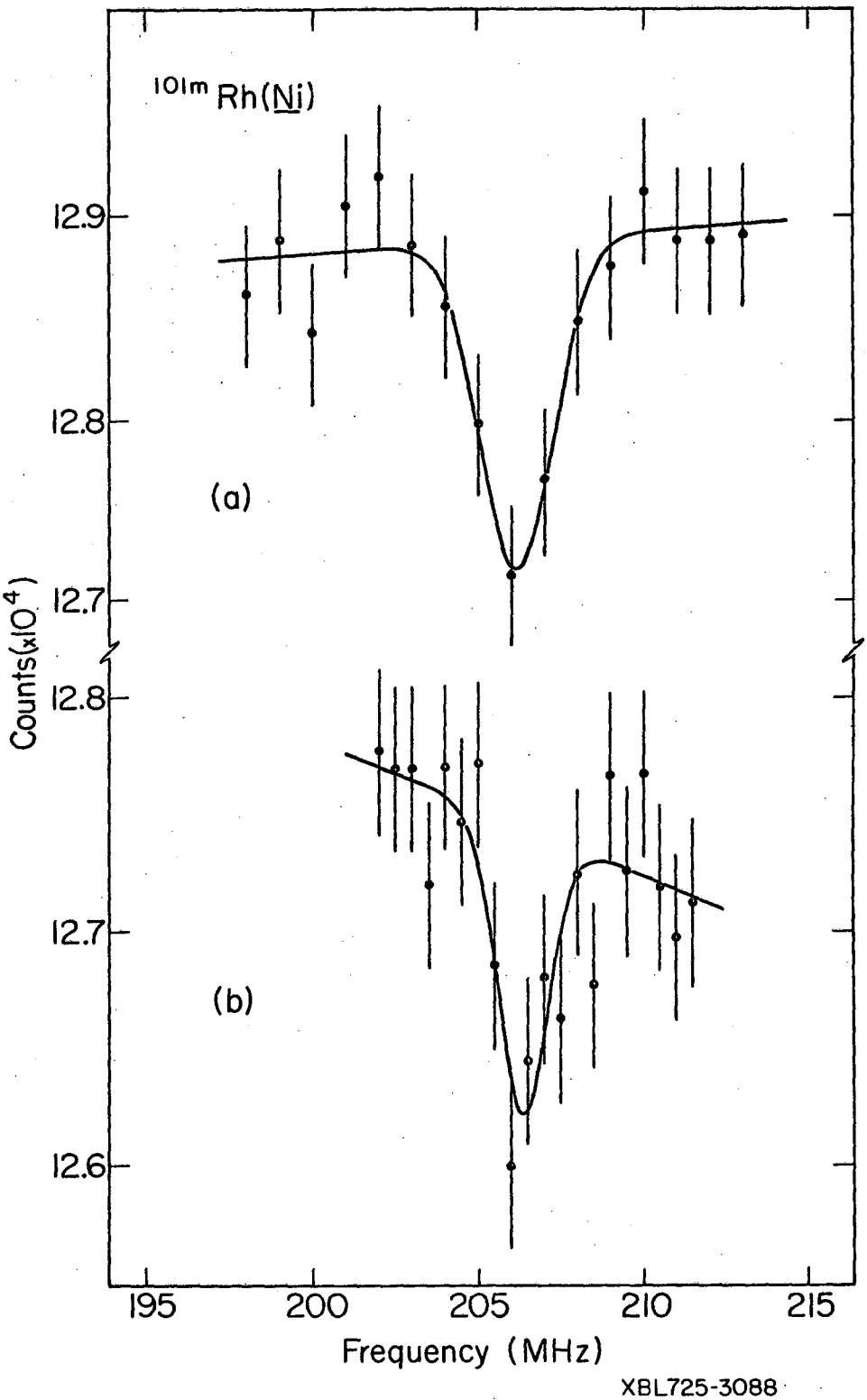


Fig. 30. The resonance curve for $^{101m}$Rh in nickel. The curve (a) refers to upward sweeps in frequencies and the curve (b) refers to downward sweeps. The solid curves result from gaussian plus straight line background fits to the measured 306.7 keV gamma intensities. The $H_1$ was 0.8 mOe and the fm frequency was 100 Hz over a bandwidth of one MHz.

experiment, this range was widened appreciably still without success. The reason for not finding the resonance may well be due to the very fast nuclear spin-lattice relaxation times observed for some local moment cases.[77] Experiments would suggest that the Rh(Fe) system involves local moments.[78]

II. Discussion

As reported some time ago,[79] elements in this region of the periodic chart show induced hyperfine fields larger in magnitude than can be explained within the framework of the conduction electron polarization theory. Moreover, the induced internal fields were, in some cases, found to follow magnetization curves differing appreciably from similar curves for the ferromagnet alone.[79] This behavior was explained by Jaccarino et al.[80] as resulting from localized magnetic moments at solute sites arising from unpaired solute d electrons and contributing to the hyperfine field. Later, work by Shirley et al.[74] further substantiated the local moment contributions to the hyperfine field. The anisotropy results for the rhodium in nickel when interpreted with the existing room temperature field suggest similar local moment behavior for this system.

There also exists strong evidence[78] for local moment behavior in the Rh(Fe) system; however, a T = 0 K extrapolation for the internal field which is -559.6(16) KOe[12] does exist for this system. Correcting the $H_{hf}$ for the applied d.c. field and using the average of the values of the hyperfine interaction constants, one gets a value for the magnetic moment of the 9/2 state of $^{101m}Rh$

$$\mu = \pm(4.25 \pm 0.33) \text{ nm} \quad .$$

Disconcertingly, this value is less than expected on both theoretical and experimental grounds. Assuming this state to arise from a proton $[\pi g_{9/2}]_{9/2}$ the single particle model gives

$$\mu_{sp} = 6.7 \text{ nm} \quad ,$$

and the corresponding configuration mixed moment is

$$\mu_{cm} = 6.19 \text{ nm} \quad .$$

For this state only two possible interactions can affect the corrected moment: the proton-proton interaction $\pi(g_{9/2})^5\pi(g_{7/2})^0 \rightarrow \pi(g_{9/2})^4\pi(g_{7/2})^1$ and the proton-neutron interaction $\nu(g_{9/2})^{10}\pi(g_{9/2})^5\nu(g_{7/2})^6 \rightarrow \nu(g_{9/2})^9 \pi(g_{9/2})^5\nu(g_{7/2})^7$. This configuration mixed moment is in agreement with the neighboring 93 keV level of $^{103}$Rh where $\mu = 6.21 \pm 0.09$ nm.[81] The reason for this unexpectedly low moment cannot be ascribed to an anomaly between the $^{100}$Rh, for which the field was measured, and $^{101m}$Rh states. A calculated anomaly, $^{100}\Delta^{101m} = -0.3\%$, does not significantly alter the internal field value. For this calculation, a coupled neutron and proton configuration of $[\pi(g_{9/2})^5, \nu\{(d_{5/2})^{s-n}(s^n_{1/2})\}_{5/2}]2^+$ (Ref. 82) was assumed for the 74.8 keV level of $^{100}$Rh. It was assumed, as in the work of Matthias et al.,[83] that the neutron contribution was the same as that for the $d_{5/2}$ groundstate in $^{99}$Ru, g = -0.25. An "interpolated" g = +1.25 from the observed values in $^{93}$Nb of g = +1.37, $^{99}$Tc of g = +1.26 and $^{109}$In of g = +1.23 (Ref. 37) was selected as the $g_{9/2}$ proton contribution.

The coupled proton and neutron moment was adjusted to reproduce the observed g = +2.13 (Ref. 37) for this level. A g factor of 1.25 was assumed for the $g_{9/2}$ proton state of $^{101m}$Rh. As for $^{93m}$Mo, a small anomaly is expected.

Although not systematically studied, measured hyperfine fields at different temperatures point to a possible local moment behavior for the Rh(Ni) system also; i.e., $H_{hf}$ (T = 473 K) = (-) 164 KOe and $H_{hf}$ (T = 298 K) = (-) 207 KOe.[84] In view of the strong temperature variation of the rhodium hyperfine field in nickel, an estimate of the field at below helium temperatures can be obtained from the present work. Using the observed moment of 4.25 nm from the iron orientation data, one gets a value for the internal field of nickel

$$H(T \sim 0) = \nu Ih/\mu$$
$$= 272.1 \text{ KOe} \quad ,$$

from the NMR/ON magnetic hyperfine splitting results. This result leads to a (room temperature)/(below liquid helium temperature) ratio for the induced nickel fields of

$$\frac{H_{hf}(T \sim 298 \text{ K})}{H_{hf}(T \sim 0 \text{ K})} = 0.78 \quad .$$

This ratio is similar to the known ratio of the local moment case of Ru(Ni)[79]

$$\frac{H_{hf}(T = 298 \text{ K})}{H_{hf}(T = 0 \text{ K})} = 0.80 \quad .$$

That the ratio is significantly less than unity adds support to the expected local moment behavior of this system. In addition, the ratio of the hyperfine interaction constants from the anisotropy data for iron and nickel

$$|\mu H|_{Fe}/|\mu H|_{Ni} \cong 2 \quad ,$$

does not give the expected $\sim$ 3 to 1 ratio[85] for the induced hyperfine fields in iron and nickel. This relationship, however, follows from the effective electronic spin moments at solute sites for iron and nickel $\mu_{Fe}/\mu_{Ni} = 2.2/0.6$ and is roughly valid only for non-localized moment cases. There still remains, though, a determination of the liquid helium temperature field for the Rh(Ni) system.

On the other hand, if one assumes the room temperature field for rhodium in nickel to be applicable at 0 K, the moment is

$$\mu = \pm(6.07 \pm 0.18) \text{ nm} \quad .$$

This value is in good agreement with the calculated configuration mixed moment and neighboring $g_{9/2}$ proton-state moments, assuming the positive sign. Nevertheless, there is not, at present, enough information to clarify the $^{101m}$Rh(Fe) and $^{101m}$Rh(Ni) results.

## Appendix I. CONFIGURATION MIXED MAGNETIC MOMENTS

In the derivation of the single particle magnetic moment, pure eigenstates were assumed. This assumption, though, is not experimentally verified. A realistic correction to the single particle model moment follows from the spin polarization method of Arima and Horie. They assume a ground configuration with small amplitudes of other admixed configurations. Those configurations which contribute to the deviations of the magnetic moment from the single particle moment by their mixing differ by a single particle type. The effects of polarization on the magnetic moment depends on the configuration of the closed shells, which can be partially aligned through spin dependent interactions with the extra nucleon. A brief description of their formalism follows and details can be found in Ref. 52.

The type of configuration mixing responsible for the deviations resembles the intermediate coupling in which the $\ell$ orbits are unchanged and the mixing is caused by the decoupling of individual j orbits by the action of the central orbit-orbit forces. The total admixed configuration can be written

$$|JM\rangle = |n\ell j;\ JM\rangle + \sum_{\substack{p \\ j_p \neq j}} \alpha_p |n\ell j_p;\ JM\rangle \quad .$$

The first term is the zero order wave function; $j_p$ is the orbit of the odd nucleons and p is an odd number. The mixing amplitude is given from first order perturbation theory as

$$\alpha_p = - \langle p | \sum_{i>j} V_{ij} | o \rangle / \Delta E \quad .$$

This amplitude factor is assumed small ($\alpha_p \sim 0.1$) and the moment is given by

$$\mu = \langle JM | \mu_z | JM \rangle$$

$$= \mu_{oo} + 2 \sum_p \alpha_p \mu_{op} \quad ,$$

to first order in $\alpha_p$. The first term is just the single particle moment for odd mass nuclei. The cross term $\mu_{op}$ is the correction to $\mu_{oo}$. This term is only non-zero for states $|p\rangle$ in which only one j value differs from those of $|o\rangle$. For the pairs of states $|o\rangle$ and $|p\rangle$ there are three types of for odd nuclei:

a) $|o\rangle \equiv (\ell + \frac{1}{2})^n$; $|p\rangle \equiv (\ell + \frac{1}{2})^{n-1}(\ell - \frac{1}{2})^1$

b) $|o\rangle \equiv (\ell + \frac{1}{2})^{2\ell+2}(\ell - \frac{1}{2})^n$; $|p\rangle \equiv (\ell + \frac{1}{2})^{2\ell+1}(\ell - \frac{1}{2})^{n+1}$

c) $|o\rangle \equiv (\ell + \frac{1}{2})^{n_1}(\ell \pm \frac{1}{2})^n$; $|p\rangle \equiv (\ell + \frac{1}{2})^{n_1-1}(\ell - \frac{1}{2})^1(\ell \pm \frac{1}{2})^k$ .

The pairs a), b), and c) correspond to states with $J = \ell + \frac{1}{2}$, $J = \ell - \frac{1}{2}$, and $J = \ell \pm \frac{1}{2}$, in that order. The terms in parentheses are the j values; n is an odd integer and $n_1$ is an even integer. For cases a) and b) the correction to the single particle moment is

$$\delta\mu = (g_s - g_\ell)\, A\, (\ell,\ell',k)\, \varepsilon_s(\ell\ell')/\Delta E_\ell \quad .$$

The $\varepsilon_s$ is the singlet interaction strength parameter, $A(\ell, J, k)$ is a function of $\ell$ and J. The spin orbit splitting energy is $\Delta E_\ell$. A similar correction for case c is

$$\delta\mu = (g_s - g_\ell)\, B\,(\ell,\ell',J) \times \begin{cases} \varepsilon_s(\ell\ell')/\Delta E_\ell \\ \varepsilon_t(\ell\ell')/\Delta_\ell \end{cases} .$$

Here, $\varepsilon_t$ is the triplet interaction strength accounting for unlike nucleons (proton-neutron) interactions; $B(\ell\ell'J)$ is a function of $\ell$, $\ell'$ and J.

## Appendix II. CRITIQUE OF BRUTE FORCE POLARIZATION

The present brute force polarization experiment on $^{93m}$Mo(Nb) was exploratory in nature with the main objective of laying a foundation for future brute force work. Nonetheless, it is felt that the magnetic moment results are good in that the differences in moments from the iron polarization are not due mainly to the foreseen difficulties of this method mentioned below. That is, at the present experimental stage, a brute force orientation where the gamma ray anisotropy is observed suffers on two main accounts:

1) thermometry

2) external field measurement.

Since the conventional $\gamma$-ray thermometers require ferromagnetic lattices, the thermometer must be external to the brute force sample. This can be a serious problem if there exist thermal gradients between the sample and the thermometer and may lead to meaningless temperature measurements since the thermal gradients would lead to a distribution of the $B_k$'s. The most likely solution to this problem would be to use an internal thermometer. The local moment cases, e.g., $^{54}$Mn in the noble metal host, may have some use for this purpose and the nuclei to be oriented can be embedded in the host. This method, however, will have very limited use since the external field and temperature must be such that the Kondo state still exists. Therefore it seems that the state of thermometry in brute force orientation experiments now is very much where it was for orientation experiments, say, several years ago; i.e., in need of a standard internal thermometer.

The thermometry considerations, though, become less important if a magnetic resonance experiment is done on the oriented system. The value

of the externally applied field must (should) still be known (measured) with very little uncertainty for each experiment, however. The coil constant deteriorates most through magnet transitions where turn to turn shorts or layer to layer shorts develop. The latter short can be very serious. (In a prior experiment, it was found that the coil constant had changed by 20% through layer to layer shorts.) For this reason, the coil constant should be measured frequently and preferably during an experiment as with conventional NMR.

## Appendix III. THE PERSISTENT MODE SWITCH

Within the past several years, the technology for making reliable persistent mode switches has advanced significantly. At present, three of the existing magnetic cooling apparatuses have polarizing magnets which operate in this mode. Figure 31 gives a schematic of the magnet and switch circuitry. For the sake of future use, a few comments will now be given on their constructions first and operation last.

1) The persistent joints are all spot welded

2) The superconducting wire is 0.0125 inch pure NbTi. For stability, the superconductor is non-inductively wound--two layers with equal number of turns but oppositely wound.

3) The heater for the superconductor consist of two layers of non-inductively wound copper. Generally, six to nine volts applied to the heater are required to drive the superconductor normal.

4) For greater stability the switch is placed such that the magnet's fringe field has a minimal effect.

Although the switches may differ in dimension, points 1 through 4 will be common to their design. Moreover, voltage lead taps are necessary. With these leads and using the Harrison 6260A dc power supply (Hewlett Packard) in the remote sensing mode, the voltage drop across the magnet only, exclusive of the leads, determine the charge rate. The voltage across the magnet must be zero--a vanishingly small voltage will keep sections of the switch normal--before the persistent mode can be established.

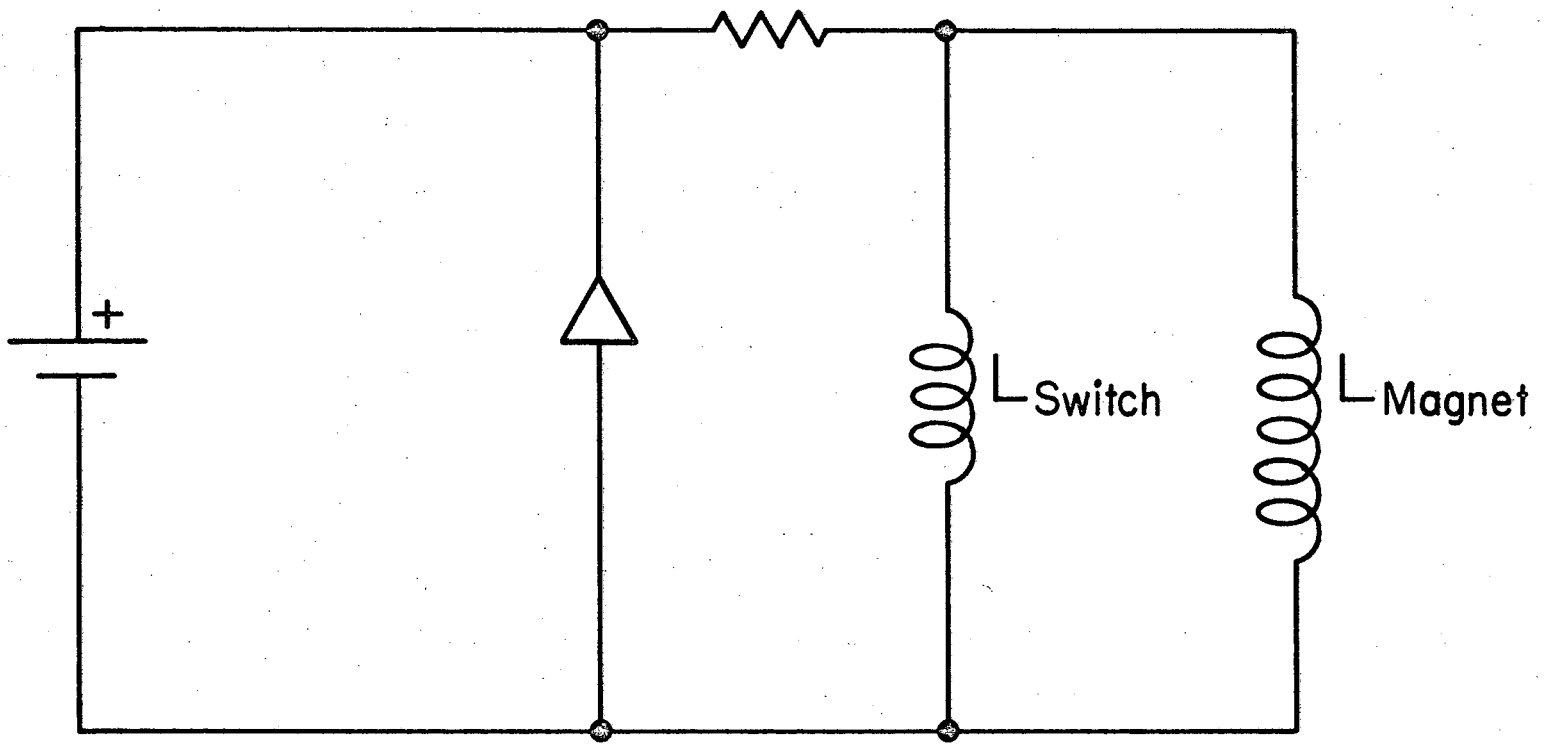


Fig. 31. A schematic of the persistent mode switch (indicated by $L_{switch}$) and the magnet (indicated by $L_{magnet}$) circuitry.

## Appendix IV. MEASURED FIELD VARIATION OF THE BRUTE FORCE SIXTH ORDER SOLENOID

At the geometric center of the solenoid 5 3/32 inches, Z = 0

| Z (inches) | $\lvert H_{resonance} - H \rvert$ (gauss) |
|---|---|
| | Upward Movement |
| 1/8 | 0.24 |
| 1/4 | 0.49 |
| 3/8 | 0.73 |
| 1/2 | 0.98 |
| 5/8 | 1.03 |
| 3/4 | 1.23 |
| 7/8 | 1.96 |
| | Downward Movement |
| 1/8 | 0.44 |
| 1/4 | 0.51 |
| 3/8 | 0.73 |
| 1/2 | 1.23 |
| 5/8 | 1.23 |
| 3/4 | 1.27 |
| 7/8 | 1.27 |
| 1 | 0.73 |

## Appendix V. LITHIUM DRIFTED GERMANIUM DETECTORS SPECIFICATIONS

UCLRL # 112-6 Coax

I. Crystal

A. Length of 45 mm

B. Diameter of 33 mm

C. Diffusion depth of 0.017 inches

II. Maximum voltage of +1750 volts

UCLRL # 32-B Coax

I. Crystal

A. Length of 50 mm

B. Diameter of 32 mm

C. Diffusion depth range of 0.025 to 0.040 inches

II. Maximum voltage of +1400 volts

UCLRL # 3572-C Coax

I. Crystal

A. Length of 50 mm

B. Diameter of 34 mm

C. Diffusion depth range of 0.025 to 0.040 inches

II. Maximum voltage of ±1600 volts

ACKNOWLEDGMENTS

As with any research project, the scientific and technical resources of many individuals are required and the collective efforts towards the completion of this work of the many LBL personnel is deeply acknowledged. It is a pleasure, though, to acknowledge individually many of the persons who were instrumental to the success of my graduate career both academically and socially.

Firstmost, I would like to express many thanks to my research director Professor D. A. Shirley who played an integral part to my success by his guidance and many stimulating discussions.

Secondly, I acknowledge the post-docs, H.-E. Mahnke and G. Kaindl, who co-authored much of this work, for the many useful discussions, scientific and otherwise.

I also acknowledge Drs. W. D. Brewer, J. A. Barclay, and J. J. Huntzicker who were my forebearers in nuclear orientation at LBL and who initiated me to much of the methodology of this field.

I express sincere thanks for the assistance of Mrs. W. Heppler who played an important part in the chemical preparations and who was such an unfailingly kind person, D. N. Voronin who assisted a great deal in assembling and maintaining the brute force apparatus and V. Walton who wound the magnets for this work.

I also acknowledge my fellow students, particularly Art Soinski, Dan Salomon, and Bill Davis, for the many interesting discussions, moral support and fun during these sometimes trying graduate years.

I express many deep thanks to Misses B. W. Yancey, B. D. McGhee, R. E. Mason, and Mrs. L. Hill who fostered many of the more pleasantly

motivating moments while here at Berkeley; I singularly thank Miss R. E. Mason whose warmth and companionship during this writing will never be forgotton.

Finally, I express sincere thanks to my parents who through their meager means are heavily responsible for my success.

The financial support of the Atomic Energy Commission is greatly appreciated.

REFERENCES

1. C. J. Gorter, Physica 14, 504 (1948).

2. M. E. Rose, Phys. Rev. 75, 213 (1949).

3. B. Bleaney, Proc. Phys. Soc. Lond. A64, 315 (1951).

4. R. V. Pound, Phys. Rev. 76, 1410 (1949).

5. B. N. Samoilov, V. V. Sklyarevskii, and E. P. Stepanov, Soviet Phys.--JETP 36, 488 (1959).

6. C. J. Gorter, Phys. Z. 35, 923 (1934).

7. D. A. Shirley, Ann. Rev. Nucl. Sci. 16, 89 (1966).

8. E. Matthias and R. J. Holliday, Phys. Rev. Letters 17, 897 (1966).

9. N. Bloembergen and G. M. Temmer, Phys. Rev. 89, 883 (1953).

10. W. D. Brewer, D. A. Shirley, and J. E. Templeton, Phys. Letters 27A, 81 (1968).

11. F. Bacon, J. A. Barcley, W. D. Brewer, D. A. Shirley, and J. E. Templeton, Phys. Rev. B5, 2397 (1971).

12. T. A. Koster and D. A. Shirley, in Hyperfine Interactions in Excited Nuclei, ed. by G. Goldring and R. Kalish (Gordon and Breach, New York, 1971) p. 1239.

13. J. P. Elliott and A. M. Lane, in Encyclopedia of Physics XXXIX, ed. by S. Flugge (Springer-Verlag, Berlin, 1957) p. 241.

14. M. A. Preston, Physics of the Nucleus (Addison-Wesley Publishing Co., Palo Alto, 1962).

15. A. Bohr and B. R. Mottelson, Nuclear Structure, Vol. 1 (Benjamin, New York, 1969).

16. R. J. Blin-Stoyle and M. A. Grace, in Encyclopedia of Physics XLII, ed. by S. Flugge (Springer-Verlag, Berlin, 1957) p. 556.

17. M. Ferentz and N. Rosenzweig, Table of F. Coefficients, Argonne National Laboratory Report ANL-5324 (1955).

18. D. A. Camp and A. L. Van Lehn, Nucl. Instr. Methods 76, 192 (1969).

19. H. I. West, Lawrence Radiation Laboratory Report UCRL-5451 (1959), unpublished.

20. P. M. Berglund, H. K. Collan, G. J. Ehnholm, R. G. Gylling, and O. V. Lounasmas, J. Low Temp. Phys. 6, 357 (1972).

21. D. A. Shirley, in Hyperfine Interactions and Nuclear Radiations, ed. by E. Matthias and D. A. Shirley (North-Holland, Amsterdam, 1968) Ch. X.

22. D. A. Shirley, in Colloque Ampere XV (North-Holland, Amsterdam, 1969) p. 81.

23. A. Abragam and R. V. Pound, Phys. Rev. 92, 943 (1953).

24. C. P. Slichter, Principles of Magnetic Resonance (Harper Row, New York, 1963).

25. H. Frauenfelder and R. M. Steffen, Alpha, Beta, and Gamma Ray Spectroscopy, Vol. 2, ed. by K. Seigbahn (North-Holland, Amsterdam, 1966).

26. E. Matthias, B. Olsen, D. A. Shirley, and J. E. Templeton, Phys. Rev. A4, 1626 (1971).

27. A. M. Portis, Phys. Rev. 91, 1071 (1953).

28. These programs were written by G. Kaindl and H. -E. Mahnke.

29. J. F. Emery and G. W. Leddicotte, Nuclear Science Series, NAS-NS 3060, p. 19 (1961).

30. J. A. Barclay, D. Phil. Thesis, Lawrence Radiation Laboratory Report UCRL-18986 (1969) unpublished.

31. J. D. Jackson, Classical Electrodynamics (John Wiley and Sons, Inc., New York, 1962).

32. W. D. Brewer, D. Phil. Thesis, Lawrence Radiation Laboratory Report UCRL-19533 (1969) unpublished.

33. C. Kittel, Introduction to Solid State Physics (J. Wiley and Sons, New York, 1953).

34. J. J. Huntzicker, D. Phil. Thesis, Lawrence Radiation Laboratory Report UCRL-18476 (1968) unpublished.

35. A. H. Wapstra, P. F. A. Goudsmit, J. F. W. Jansen, J. Koijn, K. E. G. Lobner, G. J. Nijgh, and S. A. deWit, Nucl. Phys. A93, 527 (1967).

36. J. C. Cunnane and P. J. Daly, private communication.

37. V. A. Shirley, in Hyperfine Interactions in Excited Nuclei 4, ed. by G. Goldring and R. Kalish (Gordon and Breach, New York, 1971) p. 1255.

38. K. Sakai and P. J. Daly, Nucl. Phys. A118, 361 (1968).

39. M. Kontani and J. Itoh, J. Phys. Soc. Japan 22, 345 (1967).

40. R. A. Fox and N. J. Stone, Phys. Letters 29A, 341 (1969).

41. S. G. Schmelling, V. F. Ehlers, and H. A. Shugart, Phys. Rev. C2, 225 (1970).

42. P. A. Van der Bout, V. J. Ehlers, W. A. Nierenberg, and H. A. Shugart, Phys. Rev. 158, 1078 (1967).

43. A. Bohr and V. F. Weisskopf, Phys. Rev. 77, 94 (1949).

44. J. Eisinger and V. Jaccarino, Rev. Mod. Phys. 30, 528 (1958).

45. H. H. Stroke, R. J. Blin-Stoyle, and V. Jaccarino, Phys. Rev. 123, 1326 (1961).

46. A. Bohr, Phys. Rev. 81, 331 (1951).

47. R. A. Sorenson, Am. J. Phys. 35, 1078 (1967).

48. E. Fermi and E. G. Segre, Z. Physik 82, 729 (1933).

49. G. J. Perlow, in Hyperfine Interactions in Excited Nuclei 2, ed. by G. Goldring and R. Kalish (Gordon and Breach, New York, 1971) p. 651.

50. A. Arima and H. Horie, Progr. Theoret. Phys. 12, 623 (1954).

51. G. J. Perlow, W. Henning, D. Olsen, and G. L. Goodman, Phys. Rev. Letters 23, 680 (1969).

52. F. E. Wagner and W. Potzel, in Hyperfine Interactions in Excited Nuclei 2, ed. by G. Goldring and R. Kalish (Gordon and Breach, New York, 1971) p. 681.

53. W. Marshall, Phys. Rev. 110, 1280 (1958).

54. D. A. Shirley and G. A. Westenbarger, Phys. Rev. 138, 170 (1965).

55. R. E. Watson and A. J. Freeman, in Hyperfine Interactions, ed. by A. J. Freeman and R. B. Frankel (Academic Press, New York, 1967) p. 53.

56. D. A. Shirley, private communication.

57. N. J. Stone, in Hyperfine Interactions in Excited Nuclei 2, ed. by G. Goldring and R. Kalish (Gordon and Breach, New York, 1971) p. 237.

58. F. Bacon, G. Kaindl, H. -E. Mahnke, and D. A. Shirley, Phys. Rev. Letters 28, 720 (1972).

59. H. Ton, G. H. Dulfer, J. Brasz, R. Kroondijk, and J. Blok, Nucl. Phys. A153, 129 (1970).

60. M. F. Martin, Nucl. Data Sheets B6, 387 (1971).

61. R. F. Petry, R. A. Naumann, and J. S. Evans, Phys. Rev. 174, 1441 (1968).

62. R. Schöneberg, D. Gfoller, and A. Flammersfeld, Z. Physik 203, 453 (1967).

63. T. Fink and Benczer-Koller, Nucl. Phys. A138, 337 (1969).

64. R. S. Hager and E. C. Seltzer, Nucl. Data Tables A4, 1 (1968); O. Dragoun, Z. Plajner, and F. Schmtzler, Nucl. Data Tables A9, 119 (1971).

65. L. C. Biedenharn and M. E. Rose, Rev. Mod. Phys. 25, 729 (1953).

66. B. Ahlesten and A. Backlin, Nucl. Phys. A154, 303 (1970); L. Grodzins, R. R. Borchers, and G. B. Hagemann, Nucl. Phys. 88, 474 (1966).

67. D. Ashery, A. E. Blaugrund, and R. Kalish, Nucl. Phys. 76, 336 (1966).

68. P. A. Moskowitz, C. H. Lin, G. Fulop, and H. H. Stroke, Phys. Rev. C4, 620 (1971).

69. Nucl. Data Sheets NRC 61-4-94.

70. K. H. Maier, J. R. Leigh, and R. M. Diamond, Nucl. Phys. A176, 497 (1971).

71. D. E. Alburger and S. Thulin, Phys. Rev. 89, 1146 (1953).

72. S. I. H. Naqvi, I. F. Bubb, and J. L. Wolfson, Phys. Rev. C3, 412 (1970).

73. M. Goldhaber, Phys. Rev. 89, 1146 (1953).

74. E. Matthias, S. S. Rosenblum, and D. A. Shirley, Lawrence Radiation Laboratory Report UCRL-16324 (1965).

75. G. R. Choppin, Nuclear Science Series, NAS-NS 3008, p. 26 (1960).

76. W. E. Heppler and T. A. Koster, private communication.

77. J. Flouquet, Phys. Rev. Letters 25, 288 (1970).

78. E. Matthias, D. A. Shirley, N. Edelstein, H. J. Körner, and B. A. Olsen, in Hyperfine Structure and Nuclear Radiation, ed. by E. Matthias and D. A. Shirley (North-Holland Publishing Co., Amsterdam, 1968) p. 878.

79. D. A. Shirley, S. S. Rosenblum, and E. Matthias, Phys. Rev. 170, 363 (1968).

80. V. Jaccarino, L. R. Walker, and G. K. Wertheim, Phys. Rev. Letters 13, 752 (1964).

81. I. Lindgren, Arkiv Fysik 29, 553 (1965).

82. J. S. Evans and R. A. Naumann, Phys. Rev. 138, 1017 (1965).

83. E. Matthias, D. A. Shirley, J. S. Evans, and R. A. Naumann, Phys. Rev. 140, 264 (1965).

84. S. Koicki, T. A. Koster, R. Pollak, D. Quitmann, and D. A. Shirley, Phys. Letters 32B, 351 (1970).

85. A. E. Balabanov and N. N. Delyagin, Soviet Physics--JETP 27, 752 (1968).

*TECHNICAL INFORMATION DIVISION*
*LAWRENCE BERKELEY LABORATORY*
*UNIVERSITY OF CALIFORNIA*
*BERKELEY, CALIFORNIA 94720*